UNIVERSITY OF NAIROBI

SYNTHESIS & CHARACTERIZATION OF POLYMER-LAYERED SILICATE NANOCOMPOSITES AND THEIR EVALUATION AS SORBENTS FOR LEAD AND CADMIUM IN WATER POLLUTION REMEDIATION

BY

JOHN NDUNG'U MMBAGA

REG. NO. I56/80870/2012

THESIS SUBMITTED IN PARTIAL FULFILLMENT OF THE REQUIREMENTS OF THE DEGREE OF MASTERS OF SCIENCE IN ENVIRONMENTAL CHEMISTRY OF THE UNIVERSITY OF NAIROBI

2018

DECLARATION

This thesis is the original work of the author except where due references are made. It has not been submitted partially or wholly for the award of degree to this or any other institution of learning.

JOHN NDUNG'U MMBAGA

I56/80870/2012

This thesis has been submitted for examination with our approval as the University supervisors.

DR. DAMARIS N. MBUI

DEPARTMENT OF CHEMISTRY

UNIVERSITY OF NAIROBI

DR. DICKSON M. ANDALA

DEPARTMENT OF CHEMISTRY

MULTI-MEDIA UNIVERSITY

DR. DEBORAH A. ABONG'O

DEPARTMENT OF CHEMISTRY

UNIVERSITY OF NAIROBI

DEDICATION

This work is dedicated to:

My beloved wife Anne Mmbaga and my son Jerome Baraka for their love, inspiration, encouragement and unending support in the duration of this study;

My mother, the late Grace Wanjiku Mmbaga for sacrificially laying an educational foundation for me in spite of long term ailment;

My father, the late Daniel Luvembe Mmbaga for inspiring me to be a reader even at a very young age;

My grandmother, the late Joyce Wanjiru Mbotte for her encouragement to pursue further studies

ACKNOWLEDGEMENTS

I would like to thank my God and Savior for his grace and the gift of life. I would like to appreciate my supervisors Dr. Damaris Mbui, Dr. Dickson Andala and Dr. Deborah Abong'o for their guidance, support and mentorship while undertaking this project. I would like to appreciate Dr. Damaris Mbui for her thoughts and guidance in shaping the concept of this research project. I also thank Dr. Deborah Abong'o for her insights towards the final paper.

Special appreciation goes to Dr. Dickson Andala for his advice, assistance in acquiring reagents and for facilitating the Powder X-Ray Diffraction and Scanning Electron Microscope analyses from the Botswana Institute of Technology, Research & Innovation (BITRI) and University of the Free State, South Africa respectively.

I thank the National Research Fund (NRF) for their financial assistance during the course of the research.

I am also very grateful to Dr. Vincent Madadi & Mr. Enock Osoro of the Pesticides and POPs lab, Chemistry department (UoN) for allowing me to use the mass balance and the orbital shaker in my experiments. I am also very grateful to Mr. Charles Mirikau for allowing me to use the Fourier Transform Infrared Spectrometer (FTIR) at the Chemistry Department (UoN) and Mr. Eric Kimega for allowing me to use the pH metre at the Physical Chemistry labs (UoN).

I would like to appreciate Mr. Joram W. Katweo and Mr. Murithi of the Ministry of Mining (GoK) for their assistance while using the Atomic Absorption Spectrophotometer (AAS) and the materials pulverizer.

Special appreciation goes to my dear wife Anne Mmbaga for her encouragement, understanding and support during the course of the project and my studies.

ABSTRACT

Zeolites employ the principle of surface adsorption of toxic heavy metals in remediation of polluted water. However, at nanoscale, they tend to aggregate which reduces their effectiveness in adsorption. Incorporating suitable polymers like cellulose into their crystal lattice can improve their adsorption capacity by reducing the aggregation effect. The general objective of this study is to assess the capacity of fabricated cellulose-zeolite nanocomposites to remove lead and cadmium ions from spiked water samples. The composites were synthesized through melt blending and solution mixing. After mixing and annealing at 160^{o}C, a composite lump was obtained which was pulverized to 150µm mesh-size. Scanning Electron Microscopy, Energy Dispersive X-Ray Spectroscopy, Fourrier Transform Infrared Spectroscopy and Powder X-Ray Diffraction Crystallography were used to assess the morphology, elemental composition, bonding and crystallinity of the nanocomposites respectively. Fourrier Transform Infrared Spectroscopy showed evidence of bonding between the residual silanol groups of the zeolite and hydroxyl groups of the cellulose chain. Scanning Electron Microscopy showed that porosity in the nanocomposites increased with increase in the zeolite loading. Powder X-Ray Diffraction Spectroscopy showed a highly crystalline spectrum for the pristine zeolite. However the zeolite peaks reduced with the increase in the ratio of cellulose. Also, with nanocomposite formation, there was a reduction of the 2 theta values to lower angles due to intercalation and an increase in the d-spacing. Cadmium and lead metal solutions were used to assess the viability of the composites in water remediation. It was noted that a maximum of 98.87% of Lead ions were adsorbed using 20% zeolite nanocomposite while 85.30% of Cadmium ions were adsorbed using 40% zeolite nanocomposites. The time-dependent adsorption experiments for both heavy metals in solution favoured a pseudo second order kinetic model. Contact time experiments were conducted for 5, 10, 20, 40 and 75 minutes. Lead ion uptake took place at an optimum pH range of 7. Maximum cadmium removal took place at a pH of 10 because of precipitation of its metal hydroxide. Thermodynamic parameters were determined for both metal ions over 298, 323 and 343K. The enthalpy of adsorption (ΔH_{Ads}) for Lead and Cadmium ions was 37.87kJ mol^{-1} and 41.43kJ mol^{-1}, respectively. The adsorption entropic parameters (ΔS_{Ads}) for both Lead and Cadmium were 150.65Jmol^{-1}K^{-1} and 142.40Jmol^{-1}K^{-1}, respectively. Regeneration studies for repeated adsorption by the nanocomposites were also carried out. Lead adsorption reduced from 91.47% for the first adsorption to 46.67% for the second adsorption while Cadmium adsorption reduced from 67.70% to 35.50%. The Langmuir Isotherm showed the best fit for both metals with R^2 values of 0.985

and 0.996 for Lead and Cadmium ions respectively. The zeolite-cellulose acetate nanocomposites can be applied in metal removal from water and could be up-scaled and commercialized into membrane or granular based domestic water purification platforms.

TABLE OF CONTENTS

DECLARATION ii
DEDICATION iii
ACKNOWLEDGEMENTS iv
ABSTRACT v
TABLE OF CONTENTS 1
LIST OF FIGURES 5
LIST OF TABLES 9
LIST OF APPENDICES 10
ABBREVIATIONS AND ACRONYMS 11
CHAPTER 1 14
INTRODUCTION 14
1.1 Background Information 14
1.2 Statement of the problem 15
1.3 Objectives of the study 15
1.3.1 General Objective 15
1.3.2 Specific objectives 15
1.4 Justification of the study 15
1.5 Significance of the study 16
CHAPTER 2 17
LITERATURE REVIEW 17
2.1 Introduction 17
2.2 Water Pollution 18
2.3 Heavy metal toxicity 19
2.3.1 Lead (Pb) 20
2.3.2 Cadmium (Cd) 20
2.4 Water Treatment Methods. 21
2.5 Adsorption 22
2.5.1 pH 25
2.5.2 Temperature 27
2.5.3 Contact time 28

2.5.4 Metallic ion concentration 29
2.5.5 Adsorbent mass 29
2.5.6 Regeneration of adsorbent 30
2.6 Adsorption Isotherms 30
2.6.1 Langmuir Adsorption Isotherm 31
2.6.2 Freundlich Adsorption Isotherm 31
2.6.3 Tempkin Adsorption Isotherm 32
2.6.4 Dubinin- Radushkevich (DR) Adsorption Isotherm 32
2.6.5 Flory-Huggins Adsorption Isotherm 32
2.7 Zeolites 33
2.7.1 Occurrence and characteristics 33
2.7.2 Removal of pollutants using zeolites. 35
2.7.3 Electro-kinetic (Zeta) potential 35
2.7.4 Surface Area Determination 37
2.8 Nanocomposites 38
2.8.1 Polymer Layered Silicate Nanocomposites (PLSNs) 39
2.8.2 Polymer Layered Silicate Nanocomposite Synthesis methods 40
2.8.3 Polymer Layered Silicate Nanocomposite characterization methods 43
2.8.4 Polymer Layered Silicate Nanocomposite properties 44
2.8.5 Polymer Layered Silicate Nanocomposite applications 45
2.9 Instrumental Analysis 45
2.9.1 Atomic Absorption Spectroscopy (AAS) 46
2.9.2 Fourier Transform Infra-Red (FTIR) Spectroscopy 47
2.9.3 Powder X-Ray Diffraction (XRD) Crystallography 48
2.9.4 Scanning Electron Microscopy & Energy Dispersive X-Ray (SEM/ EDX) Analysis 50
CHAPTER 3 52
MATERIALS & METHODS 52
3.1 List of Apparatus, Instruments & Reagents 52
3.1.1 Equipment and apparatus 52
3.1.2 Chemicals and reagents 52
3.2 Synthesis of Cellulose Acetate/ Zeolite Nanocomposites. 52
3.3 Physical Characterization of Nanocomposites 53

3.3.1 FTIR Analysis 53
3.3.2 Powder X-Ray diffraction crystallography 54
3.3.3 Scanning Electron Microscopic Analysis 54
3.4 Atomic Absorption Spectroscopy Measurements 54
3.5 Batch adsorption experiments 55
3.5.1 Varying zeolite loading 56
3.5.2 Varying contact time 56
3.5.3 Varying adsorbent mass 56
3.5.4 Varying metallic ions concentration 57
3.5.5 pH adjustment measurements 57
3.5.6 Varying temperature 57
3.5.7 Regeneration by acid conditioning 57
3.6 Statistical data analysis 58
CHAPTER 4 59
RESULTS AND DISCUSSION 59
4.1 Synthesis of Nanocomposites 59
4.2 Fourier- Transform Infra-Red (FTIR) Spectroscopy 59
4.3 Powder X-Ray Diffraction Crystallography (XRD) 64
4.4 Scanning Electron Microscopy & Energy Dispersive X-Ray Spectroscopy (SEM/ EDX) 72
4.5 Batch Adsorption Experiments 77
4.5.1 Effect of zeolite loading on adsorption 77
4.4.2 Effect of contact time on adsorption 78
4.4.3 Effect of the adsorbent mass on adsorption 81
4.4.4 Effect of varying metallic ion concentration on adsorption 82
4.4.5 Effect of pH on adsorption. 84
4.4.6 Effect of temperature on adsorption 86
4.4.7 Effect of regeneration by acid conditioning 88
4.5 Adsorption Isotherms 89
4.5.1 Langmuir Adsorption Isotherm. 89
4.5.2 Freundlich Adsorption Isotherm 91
4.5.3 Tempkin Adsorption Isotherm 93
4.5.4 Dubinin- Radushkevich Adsorption Isotherm 94

4.5.5 Flory- Huggins Adsorption Isotherm 96
CHAPTER 5 99
CONCLUSIONS AND RECOMMENDATIONS 99
5.1 Conclusions 99
5.2 Recommendations 100
REFERENCES 101
Internet references 132
APPENDICES 134
Appendix 1: Effect of varying zeolite ratios on adsorption 134
Appendix 2: Effect of contact time on adsorption 136
Appendix 3: Kinetic data for adsorption experiments 138
Appendix 4: Effect of nanocomposite mass on adsorption 141
Appendix 5: Effect of metal ion concentration on adsorption 143
Appendix 6: Effect of pH on the adsorption 145
Appendix 7: Effect of temperature on metal ion adsorption 147
Appendix 8: Effect of Acid conditioning in regeneration of nanocomposites for reuse 149

LIST OF FIGURES

Figure 2.1: The tetrahedral structure of zeolites ……..…….……..4

Figure 2.2: A pictorial representation of adsorption ……10

Figure 2.3: Chemisorption and Physisorption depicted by the Lennard- Jones Potential well.....11

Figure 2.4: pH speciation diagram for Lead ……...……..12

Figure 2.5: pH speciation diagram for Cadmium ……..……..…..13

Figure 2.6: Precipitation of different metals at different pH ……13

Figure 2.7: A plot showing the adsorption of Cadmium onto zeolites ……...……..16

Figure 2.8: Zeolite structure depicting the molecular channels ……...…….21

Figure 2.9: Relationship between ionic radii and their adsorption coefficient on zeolites …...…22

Figure 2.10: Pictorial representation of determination of the zeta potential …….23

Figure 2.11: Graphical presentation of aggregation of zeolite nanoparticles…….....….23

Figure 2.12: Effect of pH on the zeta potential of zeolites ……..…….24

Figure 2.13: Structure of Cellulose Acetate ……..26

Figure 2.14: Multi step process for polymer dissolution in an organic solvent.……27

Figure 2.15: Depiction of intercalated and exfoliated nanocomposites ……..……..31

Figure 2.16: Excitation of energy of an atom's electron for AAS measurement……. ….33

Figure 2.17: IR activity using a carbon dioxide molecule …….……...35

Figure 2.18: Working principle of an X-Ray Diffraction crystallographer …….…….35

Figure 2.19: Miller indices showing different crystal lattice orientations …….……...36

Figure 2.20: Bragg's Law depicted with incident ray A approaching at angle Θ ……37

Figure 2.21: Secondary electrons, backscattered electrons and X- Ray fluorescence...……38

Figure 3.1: Batch Orbital Shaker ……..……42

Figure 3.2: Atomic Absorption Spectrophotometer..……57

Figure 4.1: Nanocomposite lump before annealing ……..46

Figure 4.1: Nanocomposites after annealing, drying and pulverizing…….……..46

Figure 4.3(a): FTIR Spectra for Cellulose Acetate …….……...……...47

Figure 4.3(b): FTIR spectrum for 10% zeolite loaded nanocomposites ……...……47

Figure 4.3(c): FTIR spectrum for 20% zeolite loaded nanocomposites ……...……48

Figure 4.3(d): FTIR spectrum for 30% zeolite loaded nanocomposites ……...……48

Figure 4.3(e): FTIR Spectrum for zeolite ……...……..49

Figure 4.4: XRD Spectrum for pristine zeolite ……...……..52

Figure 4.5(a): XRD spectrum for 10% zeolite loading……...……...54

Figure 4.5(b): XRD spectrum for 20% zeolite loading …….…….55

Figure 4.5(c): XRD spectrum for 30% zeolite loading……..56

Figure 4.6: XRD Spectra comparing the peaks of pristine zeolite and 20% zeolite- loaded nanocomposites ……57

Figure 4.7: SEM Micrograph showing polymer surface loaded with 10% zeolite……59

Figure 4.8: SEM Micrograph showing polymer loaded with 40% zeolite with microporous structure ……..…59

Figure 4.9: SEM micrograph for pristine zeolite……60

Figure 4.10: EDX graph for pristine zeolite ……..60

Figure 4.11: SEM micrograph for 40% zeolite nanocomposite…….....61

Figure 4.12: EDX graph for 40% zeolite nanocomposite…..……..61

Figure 4.13: SEM micrograph for 20% zeolite nanocomposite ……62

Figure 4.14: EDX graph for 20% zeolite nanocomposite ……..……62

Figure 4.15: SEM micrograph for 10% zeolite nanocomposite….……..……..63

Figure 4.16: EDX graph for 20% zeolite nanocomposite ……..….63

Figure 4.17: Metallic adsorption onto nanocomposites with different zeolite loading……..…64

Figure 4.18: Percentage metallic adsorption onto nanocomposites against time….…….65

Figure 4.19: Pseudo First Order Kinetic Model for the Lead adsorption onto nanocomposites ……66

Figure 4.20: Pseudo Second Order Kinetic model of Lead adsorption onto nanocomposites……66

Figure 4.21: Pseudo First Order Kinetic model for Cadmium adsorption onto nanocomposites…67

Figure 4.22: Pseudo Second Order Kinetic model for the adsorption of Cadmium onto nanocomposites……..67

Figure 4.23: Percentage adsorption of metallic ions onto nanocomposites of different masses ……68

Figure 4.24: Mass of adsorbents vs adsorption capacity for metallic ions onto nanocomposites ……...….69

Figure 4.25: Percentage adsorption of different concentrations of metallic ions onto nanocomposites…… ….70

Figure 4.26: Adsorption capacity of nanocomposite vs concentration of metal ions ..……71

Figure 4.27: Effect of pH on the adsorption of Lead and Cadmium ions onto nanocomposites ……...….72

Figure 4.28: Percentage adsorption of metallic ions onto nanocomposites at different temperatures ……..……..….73

Figure 4.29: Van't Hoff Thermodynamic plot for Lead adsorption onto nanocomposites ……...74

Figure 4.30: Van't Hoff Thermodynamic plot for Cadmium adsorption onto nanocomposites....74

Figure 4.31: Comparison of the regenerative adsorption of Lead and Cadmium onto nanocomposites ……...…..75

Figure 4.32: Langmuir Isotherm for Lead adsorption onto nanocomposites……...……77

Figure 4.33: Langmuir Isotherm for Cadmium adsorption onto nanocomposites ……77

Figure 4.34: Freundlich Isotherm for Lead adsorption onto the nanocomposite.…….….79

Figure 4.35: Freundlich Isotherm for the adsorption of Cadmium onto the nanocomposites.....79

Figure 4.36: Tempkin Isotherm for the adsorption of Lead onto nanocomposites.……..…..80

Figure 4.37: Tempkin Isotherm for the adsorption of Cadmium onto nanocomposites …….…..81

Figure 4.38: Dubinin Radushkevich Isotherm for Lead adsorption onto nanocomposites. ….... ..82

Figure 4.39: Dubinin Radushkevich Isotherm for Cadmium adsorption onto nanocomposites…82

Figure 4.40: Flory- Huggins Isotherm for Lead adsorption onto nanocomposites.……...84

Figure 4.41: Flory- Huggins Isotherm for Cadmium adsorption onto nanocomposites……..…..84

LIST OF TABLES

Table 2.1: Effect of enthalpy on polymer intercalation into silicate……..……...29

Table 3.1: Working parameters for Atomic Absorption Spectrophotometer……..…40

Table 4.1: FTIR characterization of zeolites……..50

Table 4.2: FTIR characterization of cellulose acetate…….....51

Table 4.3: XRD d-spacing and 2-theta Data……..……..……..58

Table 4.4: Rate constant values for kinetic models…….68

Table 4.5: Thermodynamic parameters for adsorption……..74

Table 4.6: Langmuir isotherm parameters for adsorption……..78

Table 4.7: Freundlich isotherm parameters for adsorption…….80

Table 4.8: Tempkin isotherm parameters for adsorption……81

Table 4.9: Dubinin- Radushkevich isotherm parameters for adsorption……83

Table 4.10: Flory- Huggins isotherm parameters for adsorption……84

LIST OF APPENDICES

Appendix 1: Effect of varying zeolite ratio on adsorption……..121

Appendix 2: Effect of contact time on adsorption……..123

Appendix 3: Kinetic data for adsorption experiments……..…125

Appendix 4: Effect of adsorbent mass concentration on adsorption……..…….128

Appendix 5: Effect of metal ion concentration on adsorption…….....130

Appendix 6: Effect of pH on adsorption……..…132

Appendix 7: Effect of temperature on metal ion adsorption……..…..134

Appendix 8: Effect of acid conditioning in regenerating nanocomposites for reuse……...136

ABBREVIATIONS AND ACRONYMS

AAS : Atomic Absorption Spectrophotometer

A_{cs}: Adsorbate cross- sectional area

AgNPs: Silver Nanoparticles

A_T: Tempkin Isotherm Equilibrium Binding Constant (L/mg)

BET: Brunnauer Emmett Teller

b_T: Tempkin Isotherm constant

CA: Cellulose Acetate

CA/Z: Cellulose Acetate/ Zeolite nanocomposite

C_e: Amount of adsorbate in solution at equilibrium (mg/L)

C. N. T: Carbon Nanotubes

D_o: Fick's law temperature independent pre-exponent (m^2/s)

D: Fick's law diffusion coefficient (m^2/s)

DSC: Differential Scanning Colorimetry

DNA: Deoxyribonucleic Acid

E: Dubinin- Radushkevich Isotherm mean free energy of adsorption ($kJ\ mol^{-1}$)

EBPR: Enhanced Biological Phosphate Removal

FTIR: Fourrier Transform Infrared

ΔG^o: Standard Gibbs Energy

ΔH^o: Standard Enthalpy Change

IARC: International Agency for Research on Cancer

IQ: Intelligence Quotient

IR: Infrared

IUPAC: International Union of Pure and Applied Chemists

K_d: Adsorption equilibrium coefficient (L/g)

K_F: Freundlich Isotherm constant

K_{FH}: Flory- Huggins Isotherm Equilibrium constant

K_L: Langmuir Isotherm constant

mV: millivolt

n_{FH}: Flory- Huggins Isotherm model exponent

N: Avogadro's number ($6.023* 10^{23}$)

OSPAR: Oslo/ Paris Agreement

Pb^{2+}: Lead ions

PLSN: Polymer Layered Silicate Nanocomposite

P/P_o: BET relative partial pressure of gas

Q_d: Fick's law activation energy for diffusion (J mol^{-1})

q_e: Amount of adsorbate on the adsorbate at equilibrium (mg/g)

q_t: Amount of ions adsorbed at equilibrium time t

R: Universal Gas Constant (8.314 J/mol.K)

r: Lennard Jones distance between particles

r_m: Lennard Jones distance between particles at which there is minimum potential

ΔS^o: Standard Entropy Change

SEM: Scanning Electron Microscope

S_t: BET total surface area of the adsorbent

t: equilibrium time

TGA: Thermo-gravimetric Analysis

UNEP: United Nations Environment Programme

USEPA: United States Environment Protection Agency

UV: Ultra- Violet

V_{LJ}: Lennard Jones Potential

V_m: Langmuir Maximum monolayer coverage capacity

WHO: World Health Organization

W_m: Weight of the monolayer of the adsorbate

XRD: X- Ray Diffraction

CHAPTER 1
INTRODUCTION

1.1 Background Information

Water, being a finite resource, covers 70% of the earth's surface. However, only 3% of the global water reserves are fresh (Guto, 2012). Water scarcity due to lack of fresh water resources can be depicted by Kenya's fresh water supply dilemma which stands at 647 cm^3 per person compared to the global benchmark of 1000 cm^3 per person. It is further expected to drop to 235 cm^3 by the year 2025 (WHO, 2008a). Some of the contributing factors to water scarcity include altered weather patterns, over use of water, water pollution and population pressure (www.worldwildlife.org, 2013).

Heavy metals as pollutants contribute to a growing list of environmental (Callender, 2004; Roy, 2010) and health (Musarrat *et al*., 2011; Prabhakar *et al*., 2012) problems together with other water pollutants such as drugs, cosmetics, pesticides, industrial chemicals etc. Human activities such as coal production & usage, metal smelters, fertilizer usage, pesticide usage, waste incinerators, mining and urban run-offs contribute significantly to global heavy metal pollution of water resources (Friedman *et al*., 1993; Lindqvist, 1995; Nagajyoti *et al*., 2010). Toxic heavy metals, being bio-accumulants, are non-biodegradable in nature. Their discharge into fresh water bodies therefore poses a serious pollution problem which drastically compromises water quality (Ogoyi *et al.*, 2011). Their presence in drinking water even in extremely small concentrations could lead to their bio-accumulation through food chains. Lead ions may lead to health effects such as poor child mental development while cadmium ions may lead to kidney damage and cancer (Roberts, 1999; WHO, 2011).

Even though heavy metal removal could be done using metallic hydroxide treatment (Doye & Duchesne, 2003; Moreno *et al.*, 2001), low reaction rates and formation of large amounts of waste materials (Lottermoser, 2003; Ziemkiewicz *et al.*, 2003) make this method very costly and environmentally hostile. Zeolites, being available adsorbents are increasingly emerging as materials of choice in specifically targeting aqueous heavy metals because of their unique adsorption and ion-exchange properties (Colella, 1999).

1.2 Statement of the problem

Toxic heavy metal pollutants such as cadmium, mercury, lead, chromium (VI) and metalloid arsenic contribute to increased water scarcity (Lopez, 2009). In the past, various heavy metal adsorbents such as chitosan, zeolites, clay and fly-ash have been used. However, zeolites have generated increased interests due to the high ion exchange capabilities and their affinity for divalent adsorbates such as lead and cadmium (Babel & Kurniawan, 2003). At nano-scale, zeolites are even more effective in heavy metal adsorption due to their large surface areas and sizes improving access to their micro-channels. However, employment of nanoscale zeolites in adsorption may lead to particle aggregation due to low surface charges or zeta potential when subjected to different electrolytic conditions (Obare & Meyer, 2004; Curkovic *et al*., 1996; Mthombo *et al*., 2011). Fabrication of nano- optimized zeolites therefore presents an opportunity for employing zeolites for water remediation purposes.

1.3 Objectives of the study

1.3.1 General Objective

To assess the potential of fabricated cellulose-zeolite nanocomposites in the targeted sorption of Pb (II) & Cd (II) from water samples.

1.3.2 Specific objectives

i. To fabricate cellulose acetate/ zeolite nanocomposites using a combination of solution and melt blending methods.

ii. To characterize the nanocomposites using FTIR, XRD, SEM & EDX methods to elucidate the material bonding, crystallinity and surface morphology.

iii. To apply cellulose acetate/ zeolite nanocomposites in the removal of Lead & Cadmium from synthetic water samples.

iv. To investigate the regeneration and recyclability of the nanocomposites.

1.4 Justification of the study

Since water pollution is an increasing concern in many nations, advances in research has led to development of environmentally friendly methods of water purification such as usage of silver nanoparticles (AgNPs), dendrimers, graphene, carbon nano-tubes (CNTs), metal oxide nanoparticles (TiO_2 & ZnO), zero-valent Iron (Fe^0), bentonites, clays and zeolites due to the superior cation exchange (Xiaolei *et al*, 2013; Savage & Diallo, 2005). Even though substantial research has been done in the field of polymer- based composites, few researches have been carried

out using zeolites as the filler material (Pehlivan *et al.*, 2005). Incorporating a suitable polymer such as cellulose into the zeolite matrix would result into a composite material with remarkably improved physico-chemical properties (Mthombo *et al.*, 2011, 2009; Mishra, 2013) capable of being employed in more efficient adsorption studies.

1.5 Significance of the study

Polymer- silicate nanocomposites are a unique breed of organic-inorganic materials due to their employment in various applications such as cosmetics, toxic gas adsorbents, drug delivery vehicles and wastewater effluent treatment (Patel *et al.*, 2006). These nanocomposites could be synthesized by adjusting the interaction enthalpies of the constituent components using heat or solvents (Fischer, 2003). Since nanocomposites have a larger accessible surface area and a high affinity for aqueous heavy metals, their usage in adsorption processes (Mishra, 2015). In this study, Zeolite/ Cellulose Acetate nanocomposites were fabricated through a combination of solution and melt blending methods and were assessed for their adsorption capacity for heavy metals from synthetic water samples for application in water treatment and purification.

CHAPTER 2

LITERATURE REVIEW

2.1 Introduction

Water free from environmental pollutants and pathogens is important to human health (Savage & Diallo, 2005). Introduction of impurities in water resources through point and non-point sources is referred to as water pollution. These impurities include nitrates, phosphorus, pathogens, arsenic and selected heavy metals (www.epa.gov).

Several water treatment methods are employed in purification of drinking water: chemical flocculants such as aluminum sulfate could be used in the removal of suspended solids such as clay, silt, food wastes and fecal matter which contribute to water turbidity (Edzwald, 2011); ion exchange resins could be used for the removal of ions such as calcium and magnesium in the process of water softening (Zagorodni, 2007); also adsorbents such as zeolites, bentonites and various clays could be employed heavy metal pollution remediation through ion exchange mechanisms.

Zeolites are naturally formed through alternation of volcanic rocks with water (Almaraz *et al.*, 2003). Several types of naturally occurring zeolites exists which include analcime, chabazite, clinoptilolite, erionite, faujasite, heulandite, laumontite, mordenite, and phillipsite (Hay & Sheppard, 2001). Zeolites can also be derived from agricultural wastes such as rice husk ash (Prasetyoko *et al.*, 2006). Today, both natural and synthetic zeolites (A-type, X-type and Y-type) are used in industry for water purification, gas separations, as catalysts, detergents as well as in nuclear processing (Abd-el Rahman *et al.*, 2006). They possess cation- exchange ability due to net local charges on their crystalline surfaces generated by isomorphic substitution of Si^{4+} ions with Al^{3+} ions (Figure 2.1) which are counter-balanced by metal cations such as Na^{+}, Ca^{2+} and K^{+}

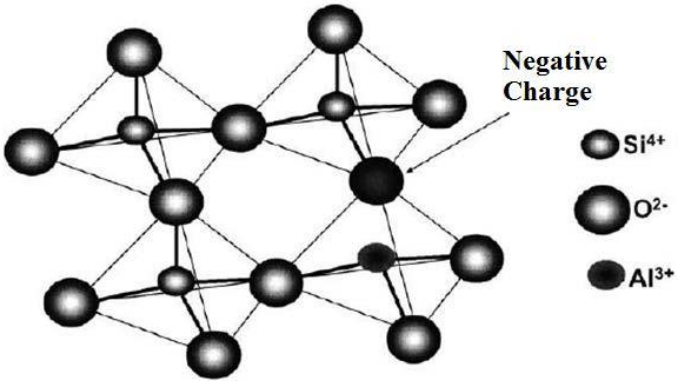

Figure 2.1: Tetrahedral structure of zeolites (Burcin *et al.*, 2013)

A specific number of water molecules co-ordinate to these metallic cations interacting weakly with the lattice (Theng, 1974; Rozic *et al.*, 2000). Because their effectiveness is surface- dependent, nano-scaled zeolites have greater ion- exchange potency than those at micro or macro scale because of a higher surface area to volume ratio (Curkovic *et al.*, 2006). Nano-materials are materials with a measurement of less than 100nm in at least one dimension which can be exploited for applications in water treatment (Xiaolei *et al.*, 2013). Many nanomaterials are subjects of research to determine their effectiveness in water treatment applications because their high surface area to volume ratio increases their reactivity, contact and adsorption of pollutants (Cloete, 2010; Karn *et al*., 2009; Xiaolei *et al*., 2013). Nanomaterials can also include nanocomposites which are formed by blending of two or more materials with differing physico-chemical properties with distinguishable interfaces at nanoscale (Mishra, 2015). In polymer-layered silicate nanocomposites, the inorganic and organic phases are separated at nanoscale. These nanomaterials have unique properties not possessed by their individual parent materials at macro or micro scale (Mishra, 2015; Okada *et al.*, 1990; Gianellis, 1996; Gianellis *et al.*, 1999; le Baron *et al.*, 1999; Vaia *et al.*, 1999; Biswas & Sinha, 2001). The zeolite nano- pore structure can be characterized into either macro-pores which have a dimension of 500Å (50nm), meso-pores having a dimension between 20- 500 Å (2-50nm) and micro-pores with a dimension of upto 20 Å (2nm) (Viswanadham *et al.*, 2009).

2.2 Water Pollution

Water pollution is a human or naturally induced phenomenon that alters the physico-chemical or biological nature of water resulting into health problems for ecosystem (Carr and Neary 2008; UNEP, 2010). Because a number of pollutants or contaminant might be found in a water resource, their combined synergistic effects could be more profound than the cumulative effect of one contaminant (Millennium Ecosystem Assessment, 2005).

Nutrient pollution, responsible for the increased levels of nitrates and phosphates in water, could result into increased photosynthesis leading to algal bloom and growth of highly vascular plants like water hyacinths (UNEP, 2010; Millennium Ecosystem Assessment, 2005; Nechifor *et al*, 2015). Sedimentation is a naturally occurring process which provides sediments and organic matter in aquatic ecosystems. However, in many regions, the rate, timing and volume of sedimentation has been affected by human activity resulting into a higher discharge than usual into water bodies

(UNEP, 2010; Carr & Neary, 2008). Sediments in rivers and lakes could adsorb pollutants such as heavy metals temporarily reducing their concentration in the water column before releasing them back into water after agitation (Douben and Koeman, 1989; Mohapatra, 1988). Thermal pollution hampers the natural water temperature cycles altering aquatic life impairing reproduction of aquatic species and reducing oxygen concentration in the water column (UNEP, 2010; Carr & Neary, 2008). Increased aquatic temperatures increase the metabolic rates of aquatic species leading to higher food consumption. It also increases solubility of toxic substances like heavy metals (Sokolova & Lannig, 2008; Goel, 2006). Aquatic acidification resulting from acid rain increases the levels of carbonate in water which forms strong bonds with divalent and trivalent metal ions. This could increase the concentration of heavy metals in water (Xiangfeng *et al.*, 2015). Pathogenic pollution of water is also a subject of great concern especially in regions facing acute water scarcity. These free-living pathogens, like some *Vibrio spp, E.Coli spp, Salmonella spp, Cryptosporidium spp, Giardia spp, Rotavirus spp, Adenovirus spp,* Guinea worm, and others pose health risks such as bloody diarrhea, meningitis, amoebisis etc. (WHO, 2008). Endocrine disruptors, are a new class of emerging water contaminants, whose consequences towards human health, water quality and the environment are still not fully understood (UNEP, 2010). Most of them are additives in cosmetics, pesticides, disinfectants, plastic manufacturing, and pharmaceuticals like birth control pills. These chemicals inhibit hormonal activity in the body in humans directly exposed to them especially during the formative years. Their effects can be life-long and irreversible (Colborn, 1993). Toxic heavy metal pollution involves contamination of water resources with metals such as lead, cadmium, mercury, chromium (VI) and arsenic. They originate from human activities such as mining, smelting, coal burning, fertilizer & pesticide manufacture and usage (Eick *et al.*, 1999).

2.3 Heavy metal toxicity.

Toxic heavy metals are elements with density higher than that of water noted for their potential toxicity within environmental contexts (Srivastava & Goyal, 2010). The term is often used to refer to cadmium, lead, mercury, chromium (VI) and arsenic (Braithwaite & Rabone, 1985). Toxic heavy metal exposure pathways have five components: a contamination source such as an industry; an environmental transport medium such as water or ambient air; an exposure point such as inhaling, ingesting or dermal exposure; an exposure route such as absorption by the digestive tract, lungs; and an exposed population living in a continuously polluted environment (WHO, 2010).

Toxic heavy metals target biomolecules such as proteins, enzymes and DNA by interacting with their terminal amino-acid sulfhydryl groups or DNA nucleotide bases through molecular mimicry leading to a disruption of their metabolic activity (Bralley & Lord, 2001). Heavy metal concentrations in environmental media can be determined using Atomic Absorption Spectroscopy (AAS) (Garcia & Baez, 2012) or Inductive Coupled Plasma (ICP) spectroscopy method (Ahan *et al.*, 2007).

2.3.1 Lead (Pb)

Lead poisoning contributes to about 0.6% of the global disease burden with exposure mainly occurring through air, food, paints and water. The WHO maximum allowable limits for lead concentration in water is 0.01mg/l. However, much lower concentrations have been observed to compromise the immune, reproductive and cardiovascular systems of children over time (WHO, 2008; WHO, 2010). Acute clinical lead poisoning could manifest through fatigue, constipation, anemia or neurological disorders. It may also lower the neurological development of children even after the poisoning ceases. Sub- clinical effect of lead poisoning with blood levels below the maximum allowable WHO limit (<0.01 mg/l) could result into decreased IQ, hearing and growth (Bellinger & Bellinger 2006; Landrigan, 1989; Byers & Lord, 1943) not easily captured by standard clinical examinations. A high community exposure may lead to a high number of children with a depressed mean IQ, lower mental capacity and retardation which tend to be chronic and irreversible (Needleman *et al*, 1979; Needleman *et al*., 1990; Burns *et al.*, 1999; Dietrich *et al*., 2001; Cecil, 2008; Wright *et al.*, 2008). During formative years, lead exposure can lead to increased instances of drug abuse, truancy and incarceration (National Research Council, 1992; Needleman *et al*., 1990, 1996, 2002; Dietrich *et al.*, 2001; Nigg & Casey, 2005; Braun *et al.*, 2006; Fergusson *et al.*, 2008; Nigg *et al.*, 2008; Wang *et al.*, 2008; Wright, 2008; Ha *et al.*, 2009). In Kenya effects of lead contamination in water sources have been well documented. Oyoo-Okoth *et al.*, (2010) reported lead levels above the maximum allowable limit in Lake Victoria near Kisumu city (upto 114.1 µg/L). Also, Ndeda and Manohar, (2014) in their analysis of heavy metals in the Nairobi Dam water exposed a very high mean concentration of Lead metal in the water during the dry season (16.78±0.21mg/L) and also during the wet season (11.67±0.20mg/L).

2.3.2 Cadmium (Cd)

Cadmium is a heavy metal that possesses a very high level of toxicity at extremely low concentrations capable of causing acute and chronic health effects due to its non- biodegradability

and translocation between environmental mediums (Nordic Council of Ministers, 2003). It is a non-essential element generating great concern for its accumulation due to industrial practices such as electroplating, galvanizing, fertilizer manufacture/ usage and smelting (Stohs & Bagchi, 1995). It is also released naturally into the soil and aquatic systems e.g. through volcanic eruptions (Nriagu, 1989) and weathering of rocks. The main route for cadmium exposure is through tobacco smoking and food intake. However exposure through water is of great concern due to increased usage of cadmium- containing phosphate fertilizers. Cadmium in fertilizers contributes to its translocation into plants (Nordic Council of Ministers, 2003) and into water run-offs. The maximum allowable drinking water concentration of cadmium is 0.003mg/l (WHO, 2008). Cadmium causes renal tubular damage to kidneys because of its accumulation in the renal cortex resulting into dysfunction due to interference of amino acid and glucose metabolism. Cadmium has also been shown to damage skeletons in both humans and animals (Jarup *et al.*, 1998). Cadmium is classified as a class 1 carcinogen by the International Agency for Research on Cancer (IARC). Chronic exposure may lead to development of lung and prostate cancer (Waalkes, 2000; IARC, 1993). Cadmium occurrence in Kenya has also been studied by Oyoo-Okoth *et al.,* (2010). They found out that considerable levels of accumulated Cadmium existed in the Lake Victoria waters around Kisumu city (80.1µg/L). Also, Ndeda and Manohar (2014) found a considerable mean concentration of cadmium in the Nairobi dam waters during the dry season (5.12±0.18mg/L) and in the wet season (3.76±0.15mg/L).

2.4 Water Treatment Methods.

Municipal drinking water treatment works involves removal of large debris like rocks, pre-conditioning of the water to remove hardness using ion-exchange resins, adjustment of the pH, flocculation to clarify water by settling suspended particles in water, filtration and removal of suspended solids and finally disinfection using chlorine (UNEP, 2010). Household or point-of-use (PoU) water treatment methods employed include boiling, bleaching (using chlorinated agents), filtration, straining water through a cloth, solar disinfection among others (Rosa & Clasen, 2010). Other conventional and pollutant-specific water treatment methods include adsorption (Shaheen *et al.*, 2012), electrochemical deposition (Herdan *et al*, 1998) and ion exchange (Bai & Bartkiewicz, 2009) for heavy metal removal; particulate phosphorus filtration (Lowe *et al.*, 1992) and enhanced biological phosphorus removal also known as E.B.P.R (Maurer & Boller, 1999) for nutrient removal; catalytic ozonation (Legube & Vel Leitner, 1999) and adsorption (Rashed, 2013)

for organic contaminant removal; chlorination (Hua & Reckhow, 2007) and UV treatment (Canonica *et al.*, 2008) for water disinfection; and flocculation and coagulation (Spicer *et al*, 1998) for removal of suspended solids. Reverse osmosis (Greenlee *et al*, 2009) and ultra- filtration (Nakao & Smolders, 1984) can also be employed as polishing steps in water treatment. Among the various heavy metal removal methods, adsorption is the most studied due to its efficient metal targeting effectiveness and simple usage (Zhou *et al.*, 2004). Adsorption happens when molecules or ions (like heavy metals e.g. Pb^{2+}) interact with adsorbent surfaces e.g. zeolites through either the physical Van der Waals forces (physisorption) or through chemical hybridization of their orbitals (chemisorption) leading to bonding between them (www.fisica.unige.it; Atkins, 1999). Various adsorbents have so far been employed successfully in water remediation of heavy metal contaminants. These include rice husk ash for Pb (II) and Cd (II) removal (Teixeira *et al.*, 2004), almond shell for removal of Cr (VI) (Agarwal *et al.*, 2006), chitosan, zeolites, clay and fly-ash for Pb (II), Cd (II) and Cr (VI) removal (Babel & Kurniawan, 2003).

2.5 Adsorption

Adsorption happens when dissolved or suspended substances accumulate at the interface between solid, liquid or gaseous phases due to the action of surface forces (IUPAC, 1997). This could result into chemical bonding (chemisorption) or a van der Waals association (physisorption) between the dissolved substance and the solid phase (Atkins, 1999). Adsorption could either be reversible or irreversible. Reversible adsorption involves physisorbed or weakly chemisorbed species while irreversible adsorption involves strongly chemisorbed species (Lee *et al.*, 2006). However, physico-chemical parameters of the liquid phase such as pH, temperature and concentration could be altered to trigger desorption (Fig. 2.2) of strongly chemisorbed species back onto solution (Worch, 2012).

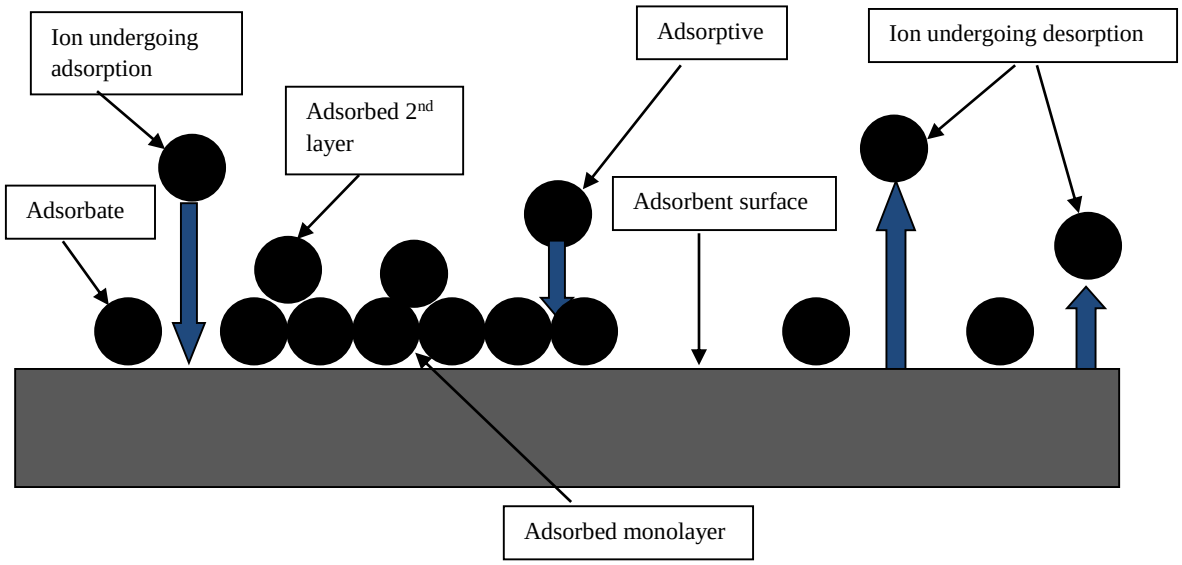

Fig 2.2: A pictorial representation of adsorption (Adopted from https://www.slideshare.net)

Physisorption takes place on all surfaces when the temperature and pressure conditions are right. The involvement of weak van der Waals forces renders physisorption weaker than chemisorption. Its multi layered and indiscriminate adsorption can be driven by enthalpies as low as 20 kJ mol^{-1}. Chemisorption is however highly selective and occurs at specific adsorption sites. Due to the formation of strong covalent bonds, chemisorption has adsorption enthalpies ranging between ~ 40-800 kJ mol^{-1} (Webb, 2003; Atkins, 1999; Boparai *et al*., 2011; Al-Anber, 2011). The Lennard-Jones potential (Equation 2.1) can be used to assess an adsorption process and determine whether it is physisorption or chemisorption in nature (Lennard- Jones, 1924).

$$V_{LJ} = \varepsilon\left(\left(\frac{r_m}{r}\right)^{12} - 2\left(\frac{r_m}{r}\right)^{6}\right) \ldots \text{Equation 2.1}$$

Where:

V_{LJ} is the Lennard- Jones Potential; ε is the potential well depth (minimum potential energy to facilitate bonding); r_m is the distance between particles where there is minimum potential; and r is the inter-particle distance. The term $\left(\frac{r_m}{r}\right)^{12}$ symbolizes the repulsive forces between the adsorbent and the adsorbate whereas the term $2\left(\frac{r_m}{r}\right)^{6}$ symbolizes the attractive forces between the adsorbate and adsorbent (symbolized by the well depth). $2\left(\frac{r_m}{r}\right)^{6}$) is higher for chemisorption than for physisorption. Figure 2.3 shows a Lennard- Jones plot chemisorbed and physisorbed species in the gaseous phase.

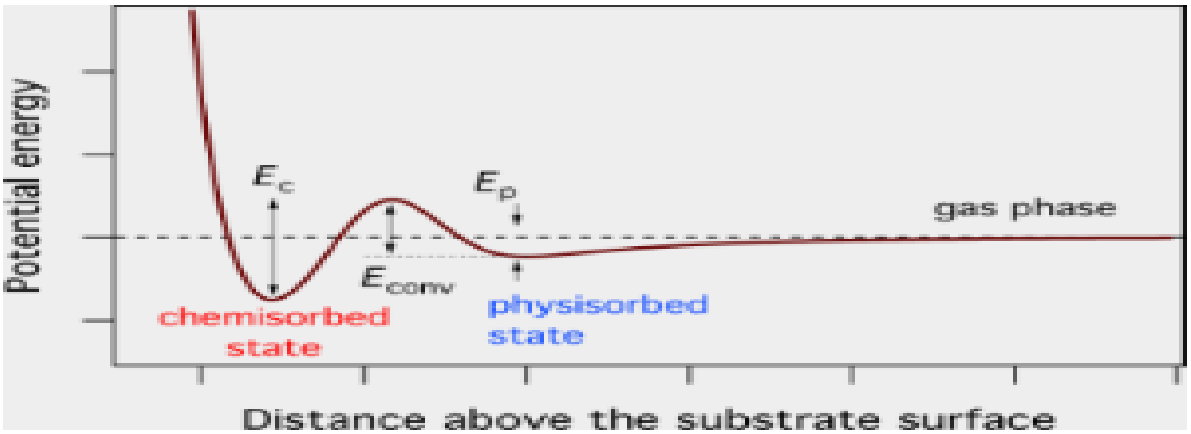

Fig 2.3: Chemisorption and Physisorption depicted by the Lennard- Jones Potential well (http://www.beilstein-journals.org)

Chemisorbed species are usually site specific, one molecule thick and with no lateral movement of sorbed molecules. The adsorption capacity is exhausted when all the empty sites are filled with adsorbed species. However, the first chemisorbed species may be followed by other physisorbed species creating several layers of chemisorbed and physisorbed species (Ho *et al.*, 1991; Lee *et al.*, 2003). Percentage adsorption can be expressed as follows in Equation 2.2.

$$\% \text{ Adsorption} = \frac{C_i - C_f}{C_i} * 100\% \text{...} \quad \text{Equation 2.2}$$

Where:

C_i is the initial metallic concentration in solution; C_f is the final metallic concentration in solution. Commonly used cheap adsorbents for heavy metals include plant materials such as coconut fiber for Pb(II), As(III) and Hg(II) removal (Igwe *et al.*, 2008), rice husk ash for Cu(II), Mn(II) and Pb(II) removal (Mohan & Sreelakshmi, 2008) and waste from tea for Cu(II) and Pb(II) removal (Amarasinghe & Williams. 2007); and silicate materials such as zeolites for Pb(II) and Cd(II) removal (Wingenfelder *et al.*, 2005; Egashira *et al.*, 2012; Terdkiatburana *et al.*, 2008), grafted silica for Pb(II) removal (Chiron *et al*, 2003) , bentonite, montmorillonite for Pb(II), Cd(II) and Cr(VI) removal (Foo & Hameed, 2010), clay and fly-ash for sorption of Pb(II), Cu(II) and Cd(II) (Babel & Kurniawan, 2003). Factors affecting adsorption include pH, temperature, contact time and concentration of pollutants (Hodi *et al.*, 1995; Igwe & Abia, 2003). Others include adsorbent mass (Naidu *et al.*, 2013; Al-Anber, 2011) and chemical conditioning of the adsorbent (Semmens & Martins, 1997).

2.5.1 pH

pH affects the metal ionization and surface charge density of an adsorbent. At very low pH, the concentration of protons is high resulting into a highly positively charged adsorbent surface which repels metal ions from it. At very high pH, the adsorbent surface is negatively charged leading to higher adsorption of metallic ions onto the adsorbent surface (Heidari *et al.*, 2013; Mehdizadeh *et al.*, 2014). Adsorption of lead ions onto a certain biomass (*Tectonia grandis*) was determined at 10.43% at the initial pH of 2.0. However, between pH 3-5, there was a sharp increase in adsorption reaching its maximum at pH of 5.0 where 97.43% of the metal ions were removed (Naidu *et al.*, 2013). Tashauoei *et al* (2010) also observed that optimum cadmium adsorption onto modified nano-zeolite occurred at pH 6 and that no precipitation of cadmium (II)-hydroxide occurred. Optimum cadmium removal from water through adsorption happens at the neutral pH of around 6 (Ayuso *et al.*, 2003; Gupta and Bhattacharyya, 2008; Panuccio *et al.*, 2009). At low pH, it was ascertained that metallic adsorption was very low (Chandra Rao *et al.*, 2006). Highly basic conditions (pH >>7) would ultimately result into precipitation of the metal hydroxides instead of surface adsorption onto the adsorbent (Tashauoei *et al.*, 2010).

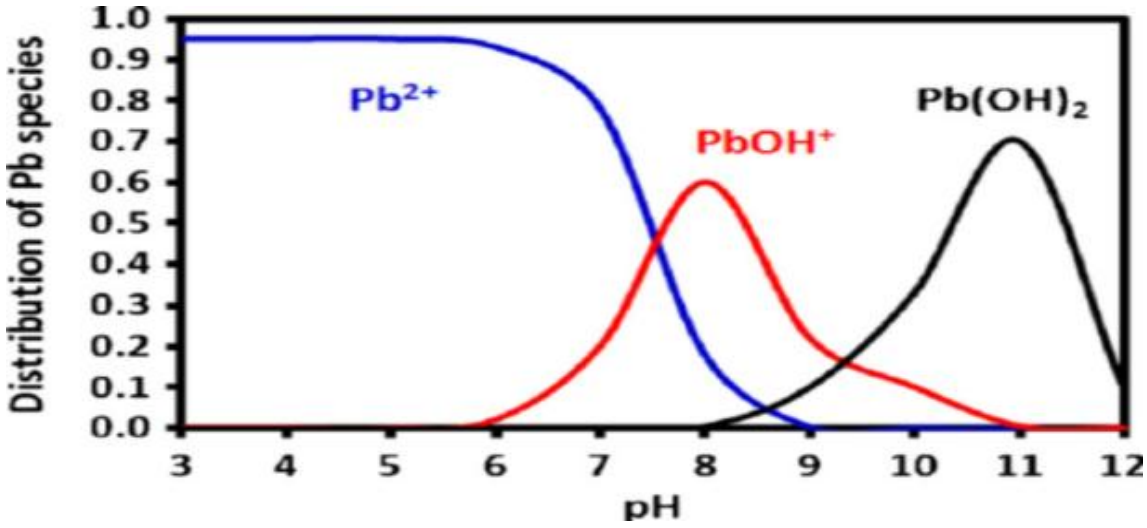

Fig 2.4: Speciation diagram for Lead $_{(aq)}$ complexes (www.researchgate.net; Santasnatchok *et al*, 2015)

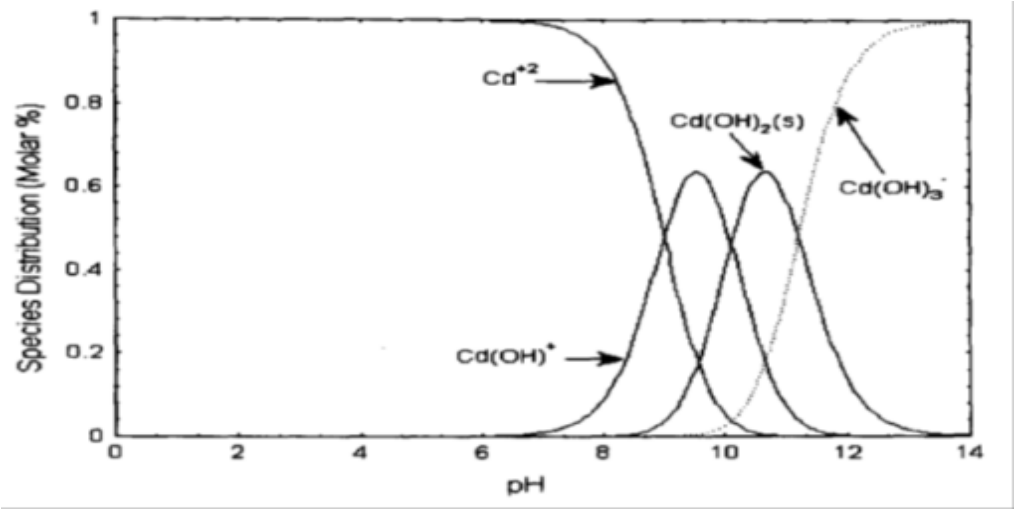

Fig. 2.5: Speciation diagram for Cadmium $_{(aq)}$ complexes (Santasnatchok *et al*, 2015)

At very low pH, metals possess a high solubility in water. However at higher pH, they precipitate as insoluble hydroxides. The table below shows the proportion of precipitation of heavy metals at different pH:

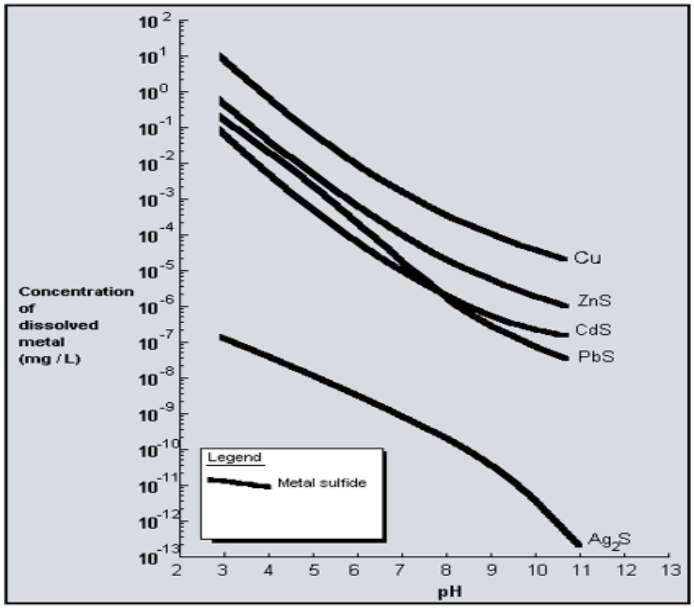

Fig. 2.6: Concentration of different metallic species differing with pH due to precipitation (Hoffland Environmental Inc., 2017).

From the above plot, a concentration of 10^{-5} mg/l of cadmium and lead salts at pH of 7 will reduce to a concentration of $10^{-6.5}$ and 10^{-7} mg/l respectively due to metal hydroxide precipitation at a pH of 11.

2.5.2 Temperature

An adsorption experiment can be defined as either exothermic or endothermic. Exothermic adsorption reactions release heat while endothermic adsorption reaction absorb heat in the process according to the le Chattelier's principle. Spontaneous processes usually occur in order to minimize the Gibbs free energy (ΔG^o) as much as possible at equilibrium (Cramer, 2011) An increase in temperature may result into a decrease in an exothermic reaction but an increase in an endothermic reaction (Duffus, 2002). The difference between an endothermic and exothermic reaction is determined using the Gibbs free energy, ΔG which can be represented in equation 2.3(a):

$\Delta G^o = \Delta H^o - T\Delta S^o$… Equation 2.3 (a)

Where:

ΔG^o is the standard Gibbs free energy; ΔH^o is the standard enthalpy of the system; T is the absolute temperature in K; ΔS^o is the standard entropy change in the adsorbent/ adsorbate system. ΔG^o can also be expressed as the relationship in Equation 2.3 (b):

$\Delta G^o = -RT \ln K_d$… Equation 2.3 (b)

Where:

R is the universal gas constant (8.314 J/ mol. K); T is the absolute temperature in K; K_d is the adsorption equilibrium constant. The adsorption enthalpy (ΔH^o) can be defined as the heat requirement for a system at constant pressure for a reaction to take place.

At a given adsorption enthalpy, the van't Hoff equation relates the change in temperature to the equilibrium constant, K_d. From equation 2.3 (a) and 2.3 (b):

$\Delta H^o - T\Delta S^o = -RT \ln K_d$ …. Equation 2.4

$\ln K_d = \frac{\Delta H^o - T\Delta S^o}{-RT}$ … Equation 2.5

$\ln K_d = \frac{-\Delta H^o}{RT} + \frac{\Delta S^o}{R}$ … Equation 2.6 (van't Hoff Equation)

Where:

K_d is the equilibrium constant of adsorption; ΔH^o is the enthalpy of adsorption; R is the universal gas constant; T is the absolute temperature in K; ΔS^o is the entropy change. The Van't Hoff plot can be made for ln K_d vs 1/T. $-\Delta H^o$/ R defines the slope while the y- intercept is ΔS^o/ R. For

endothermic reactions, the graph slope is always negative while for exothermic reactions, the slope is always positive.

Pandey *et al* (2010) experimentally determined that the percentage adsorption of Cr (VI) onto zeolite reduced from nearly 50% to below 30% when the temperature was raised to 303K from 293K symbolizing an exothermic reaction. Zeolite sorption of heavy metals is a kind of chemical adsorption and it is expected that its activity may be increased with temperature (Lee & Moon, 2001). It was also found out that Cu^{2+} uptake increased with temperature for natural unmodified zeolite (Panayatova, 2001).

2.5.3 Contact time

Adsorption kinetic studies involves determination of the utilization of the adsorption capacity in relation to the contact time between the liquid and solid phases (Tsibranka & Hristova, 2011). Kinetic models allow for adsorption rate estimation and could help develop expression rates which describe reaction mechanisms in the form of pseudo first order or pseudo second order kinetics (Robati, 2013).

The pseudo first order kinetic equation can be expressed as equation 2.7:

$$\ln (q_e - q_t) = \ln q_e - kt \quad \ldots \text{Equation 2.7}$$

Where:

q_t is the metal ions sorbed after time t in mg/g; q_e is the adsorption capacity at equilibrium in mg/g; k_1 is the pseudo first order rate constant; t is the contact time in minutes.

The pseudo second order kinetic model is expressed as Equation 2.8:

$$\frac{t}{q} = \frac{1}{k_2 q_e^2} + \frac{t}{q_e} \quad \ldots \text{Equation 2.8}$$

Where:

t is time taken in minutes; q_e is the adsorption capacity at equilibrium in mg/g; k_2 is the pseudo second order rate constant; q is the amount of ions adsorbed on the adsorbent at any time.

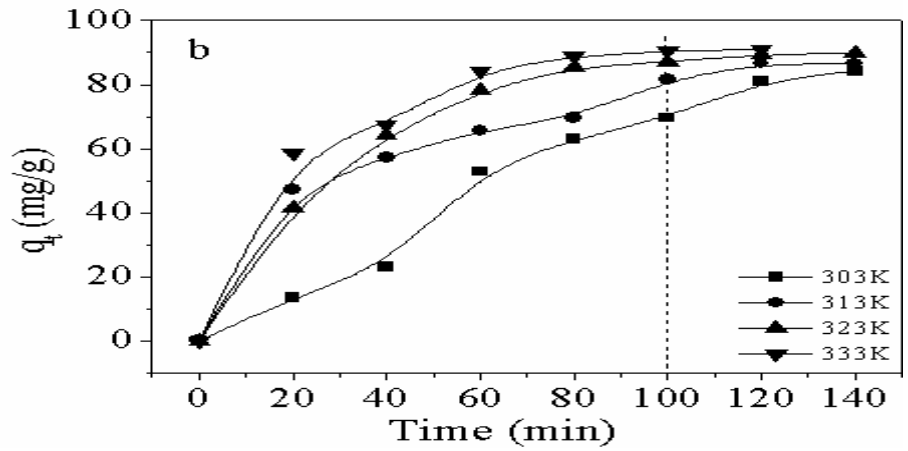

Fig 2.7: A plot showing the adsorption of Cadmium onto zeolites against time and at various temperatures (Fahmy *et al.*, 2016).

Figure 2.6 shows an increase in percentage adsorption of cadmium ions against time at different temperatures. The adsorption of cadmium onto both zeolites and sepiolites fit the pseudo second order model at 293.15K with an R^2 of 0.999 for both materials under the pseudo second order model. (Sharifipour *et al.*, 2015).

2.5.4 Metallic ion concentration

Increase in metal concentration leads to an increase in its adsorption per gram of the adsorbent also known as the adsorption capacity (Ali *et al.*, 2012). At higher metallic concentrations, there is a high probability of active site- adsorbate collisions because of the higher availability of metallic ions in solution (Baral *et al.*, 2009). Isa *et al* (2008) found out that the adsorption capacity of oil palm fibre increased with the concentration of Cr (VI) in solution. Hannah *et al* (2006) also reported an increase in adsorption capacity for Manganese-coated zeolite for Cu (II) and Pb (II) from 0.123 and 0.330 mmol g^{-1} to 0.132 and 0.343 mmol g^{-1} for the two ions respectively. However, the percentage adsorption of the metal ions decreases as the concentration increases due to a reduction in adsorption sites on the adsorbent surface. Erdem *et al.*, (2004) observed this when conducting experiments involving Cu^{2+}, Co^{2+}, Zn^{2+}, and Mn^{2+} adsorption by zeolites.

2.5.5 Adsorbent mass

The initial adsorbate concentration in solution determines the adsorption capacity of any amount of adsorbent (Chen & Wang, 2007; Hamidpour *et al*., 2010; Hojati & Khademi, 2013). More of the adsorbent mass results into an increase in surface area leading to increased adsorption of metal

ions resulting into low density occupancy of the cations (adsorbates) on the adsorption sites (Kaya & Ören, 2005; Sari *et al*., 2007). Chiron *et al* (2003) reported the decrease in adsorption of Pb^{2+} and Cd^{2+} ions per unit mass of grafted silica as the mass of the adsorbent increased. The latter case may happen due to overcrowding and overlapping of adsorbent particles as the mass is increased which leads to overlapping of active sites present at the surface of adsorbents.

2.5.6 Regeneration of adsorbent

Although adsorption is a well-established technology for water purification, its success is largely dependent on the ability of the adsorbent to desorb the target contaminant for efficient reusability (Mthombo *et al.*, 2011). Adsorbents like zeolites have a significantly larger surface area compared to bulk material making it possible for pretreatment using selected conditioning agents such as acids, bases, surfactants to aid in desorption of already adsorbed ions and increase the affinity towards solutes of interest. This step aims to replace surface cations with more exchange-friendly cations such as Na^+, K^+ and NH_4^+ adsorption processes (Semmens & Martins, 1997; Kesraoui-Ouki *et al.*, 1993). Some of the conditioning reagents include NaCl, $Ca(OH)_2$, KCl, HCl, Mg $(OH)_2$, etc. (Zamzow *et al*., 1990; Milan *et al.*, 1997).

2.6 Adsorption Isotherms

Adsorption isotherms describe the maintenance, discharge and mobility of substances from aqueous media onto solid surfaces under constant pH and temperature (Limousin *et al.*, 2007; Allen *et al.*, 2004). An adsorption equilibrium happens when an ion containing solution is contacted with an adsorbent for sufficient tome until a dynamic balance between the concentration of ions in solution and on the surface of the adsorbent is achieved (Kumar & Sivanesan, 2006; Ghiacci *et al.*, 2004). Adsorption isotherm constant (K_d) is the dynamic association between the adsorbate on the adsorbent (q_e) in mg/g and the equilibrium amount of adsorbate in solution (C_e) in mg/L.

$$K_d = \frac{q_e}{C_e} \ldots \text{Equation 2.9}$$

Where:

K_d is the adsorption equilibrium constant or coefficient (L/g); q_e is the amount of adsorbate on the adsorbent in mg/g; C_e is the equilibrium amount of adsorbate in solution in mg/L. Some examples of adsorption isotherms include Langmuir, Freundlich, Brunnauer–Emmett–Teller, Redlich–

Peterson, Dubinin–Radushkevich, Tempkin, Toth, Koble–Corrigan, Sips, Khan, Hill, Flory–Huggins and Radke–Prausnitz isotherms (Foo & Hameed, 2010).

2.6.1 Langmuir Adsorption Isotherm

The Langmuir isotherm assumes that adsorption results into the formation of a monolayer on the surface of the adsorbent. The adsorption energies onto each adsorption site is equal with no movement of the adsorbate along the adsorbent once adsorbed (Vermeulan *et al.*, 1966; Vinod *et al.*, 1997). It can be expressed in the following linear form (Equation 2.10):

$$\frac{C_e}{q_e} = \frac{1}{K_L V_m} + \frac{C_e}{V_m} \quad \ldots \text{Equation 2.10}$$

Where:

C_e: Equilibrium Concentration (mg/L); q_e: Amount of adsorbate adsorbed (mg/g); K_L: Langmuir Isotherm Constant; V_m: Maximum Monolayer coverage capacity (mg/g).

Graph Plot: C_e/q_e vs C_e

Where $1/V_m$ is the slope & $1/K_L V_m$ is the y- intercept.

2.6.2 Freundlich Adsorption Isotherm

The Freundlich isotherm states that different adsorption sites have differing energies of adsorption. The expression gives an indication of a heterogeneous surface with active site distribution over a wide range of adsorbate concentrations. The isotherm mathematically assumes formation of infinite number of layers because of failure to attain an adsorption saturation limit (Freundlich, 1906; Hasany *et al.*, 2002; Erdem *et al.*, 2004). The Freundlich isotherm can be expressed in a linear manner as follows (Equation 2.11):

$$\log q_e = \log K_f + \frac{1}{n} \log C_e \quad \ldots \text{Equation 2.11}$$

Where: q_e is the capacity of metal adsorption onto adsorbent; C_e is the equilibrium concentration of metal in solution (mg/L); K_F and n are Freundlich constants.

Graph Plot: $\log q_e$ vs $\log C_e$

Where $(1/n)$ is the slope and $\log K_F$ is the y- intercept.

2.6.3 Tempkin Adsorption Isotherm

The Tempkin isotherm states that there is a linear relationship between the molecular heat of adsorption and the surface coverage (Tempkin & Pyzhev, 1940; Aharoni & Ungarish, 1977). The linear representation of the isotherm is as Equation 2.12:

$$q_e = \frac{RT}{b_T} \ln A_T + \frac{RT}{b_T} \ln C_e \quad \ldots \text{Equation 2.12}$$

The expression $\frac{RT}{b_T}$ can also be written as B.

Graph Plot: q_e vs ln C_e

Where: A_T is the equilibrium binding constant for the Tempkin isotherm (L/ mg); b_T is the Tempkin Isotherm constant; B is a Constant related to heat of sorption (kJ mol^{-1}); R is the Universal Gas Constant (8.314 x 10^{-3} kJ mol^{-1} K^{-1}); T is the Temperature at 298K.

2.6.4 Dubinin- Radushkevich (DR) Adsorption Isotherm

The Dubinin- Radushkevich isotherm states that an adsorbent is composed of adsorption sites with a different energies and that these energies are distributed in a Gaussian manner (Gunay *et al.*, 2007; Dabrowski, 2001; Arivoli *et al.*, 2007).

The equation can be represented in a linear manner (Equation 2.13):

$$\ln q_e = \ln q_s - \beta \varepsilon^2 \quad \ldots \text{Equation 2.13}$$

Graph Plot: ln q_e vs ε^2

Where: q_s is the maximum capacity of adsorption (mg/g); q_e is the adsorption capacity at equilibrium (mg/g); β is an activity coefficient constant related to adsorption energy (mol^2 J^{-2}); ε is the Polanyi potential which equals $RT \ln(1 + \frac{1}{C_e})$; E is the mean free energy of adsorption (kJ mol^{-1}) which equals $\frac{1}{\sqrt{2\beta}}$ (Erhayem *et al.*, 2015; Horsfall *et al.*, 2004).

2.6.5 Flory-Huggins Adsorption Isotherm

The Flory- Huggins isotherm relates the surface coverage of the adsorption sites with the spontaneity of the adsorption process (Horsefall & Spiff, 2005). The linearized form can be expressed as Equation 2.14:

$$\log \frac{\Theta}{C_o} = \log K_{FH} + n_{FH} \log(1 - \Theta) \ldots \text{Equation 2.14}$$

Graph Plot: log (Θ/C_o) vs log (1- Θ)

Where: Θ is the surface coverage degree; C_o is the adsorbate initial concentration (mg/g); n_{FH} is the Flory- Huggins Isotherm model exponent; K_{FH} is the Flory- Huggins Isotherm equilibrium constant (L/ g).

Θ can be calculated as:

$$\Theta = \frac{1 - C_e}{C_o} \ldots \text{Equation 2.15}$$

Where: C_e is the adsorbate concentration at equilibrium (mg/g); C_o is the initial concentration of adsorbate (mg/g).

2.7 Zeolites

Zeolites are naturally occurring aluminosilicates with a porous, 3-D cage- like structure possessing permanent negative surface charges due to the isomorphic lattice substitution of Si^{4+} ions with Al^{3+} ions in their crystals (Theng, 1974; Rozic *et al.*, 2000) counter-balanced by exchangeable cations (Wang & Peng, 2010) widely used in adsorption, ion-exchange, catalysis and separation (Tosheva & Valtchev, 2005; Yu *et al.*, 2013).

2.7.1 Occurrence and characteristics

Naturally, zeolites are produced by volcanic action in regions such as the Caucasus, the Balkans, the Himalayas, Kenya, Cuba, Switzerland and the United States (Rhodes, 2007). About twenty species of natural zeolites have been reported from sedimentary rocks, but only eight commonly make up the major part of zeolitic rocks. These are analcime, chabazite, clinoptilolite, erionite, heulandite, laumontite, mordenite, and phillipsite (Hay & Sheppard, 2001).

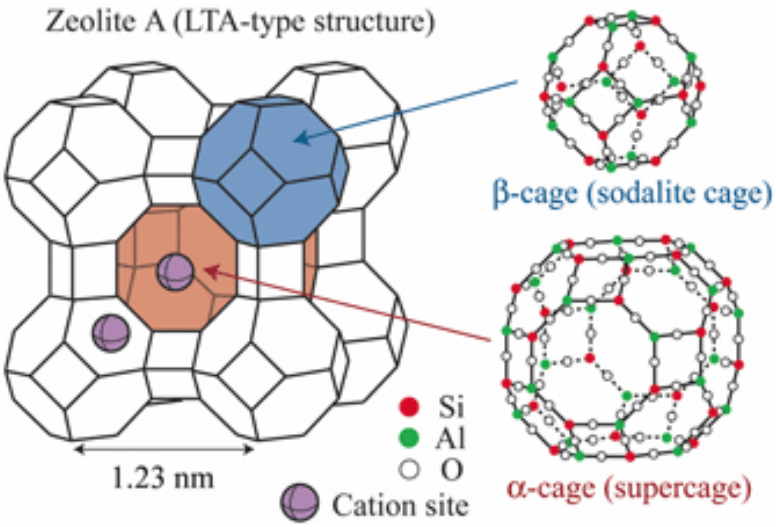

(image from http://www.sssj.org/ejssnt/duan-small.jpg)

Fig 2.8: Faujasite structure depicting the molecular channels (www.sssj.org)

Zeolites can accommodate several cations such as Na^+, K^+, Ba^{2+}, Mg^{2+} and Ca^{2+} due to large empty spaces. Larger molecules and cationic moieties such as water, ammonia, carbonate ions, and nitrate ions can also be accommodated in their lattice. Their general chemical formula is: $M_{nx}/nSi_{1-x}Al_xO_2 \cdot yH_2O$ (Where M = e.g. Na^+, K^+, Li^+, Ag^+, NH_4^+, H^+, Ca^{2+}, Ba^{2+}) (Bhattacharya *et al.*, 2006; Aydin & Kuleyin, 2011; Auerbach *et al.*, 2003). Zeolites exhibit a high adsorption capacity because of their high cation exchange capacity. They also possess catalytic sites with different cage sizes to accommodate molecules of different sizes (Gascon *et al.*, 2012). Zeolites have a high affinity for divalent metallic ions in water and can thus be used for heavy metal adsorption processes (Weller & Dann, 1998; Ouki & Kavannagh, 1999). Panayotova & Velikov (2002) experimentally determined that zeolites had higher uptake ability toward ions with higher ionic radii (Fig. 2.9) and lower enthalpies of hydration. Lead ions demonstrated high uptake ability onto zeolites.

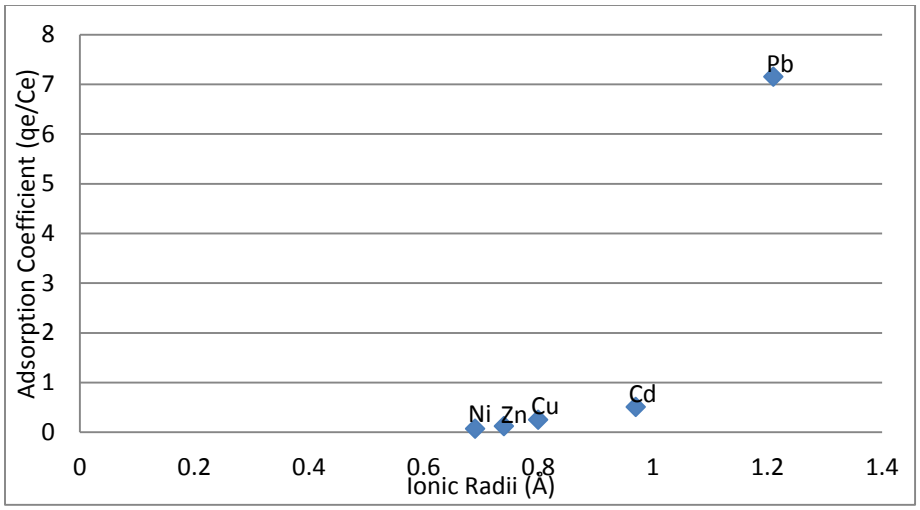

Fig 2.9: Relationship between metal ionic radii and their adsorption coefficient (q_e/C_e) on zeolites (Panayatova &Velikov, 2002).

2.7.2 Removal of pollutants using zeolites.

Surface modification using organic surfactants such as tetramethylammonium (Shaobin & Yuelian, 2011) enables removal of such anionic pollutants from water. Zhang *et al.*, (2007) removed ammonium and phosphates from synthetic wastewater using surface- modified zeolites synthesized from fly ash. Also, Ping *et al.*, (2008) used lanthanum modified zeolite to remove phosphate from waste water. Zeolites also can be used in benzene removal from water (Obiri-Nyarko *et al.*, 2014) and in the reduction of pungent smells from VOCs produced by coffee (Kim & Kim, 2008). Zeolite/ Silver nanocomposites have also been employed in disinfection and microbial detection in water and food (Unalan *et al*, 2014).

2.7.3 Electro-kinetic (Zeta) potential

Effective adsorption by zeolites is governed by their particle sizes. Al- Anber (2010) observed that the smaller zeolite particle size produced higher adsorption percentages for Fe^{3+} ions due to the short transfer path inside the zeolite pore structure. Krishna & Swami (2012) also reported that Chromium removal from synthetic solutions using zeolites increased as the size of the adsorbents reduced in size. However, some ionic conditions in aquatic media in the environment force small zeolite particles to aggregate due to a reduction in their zeta potential (Maurer & Czarnetzki, 2001). The zeta potential is the potential difference between the liquid the particle is dispersed in and the stationery liquid on the dispersed particle (Mc. Naught & Wilkinson, 1997) (Fig. 2.10). The zeta potential depicts the possible dispersion or aggregation of particles when in water. Several factors

affect the zeta potential, including type of particles, pH, dissolved solutes, addition of other substances (heavy metals, surfactants) etc.

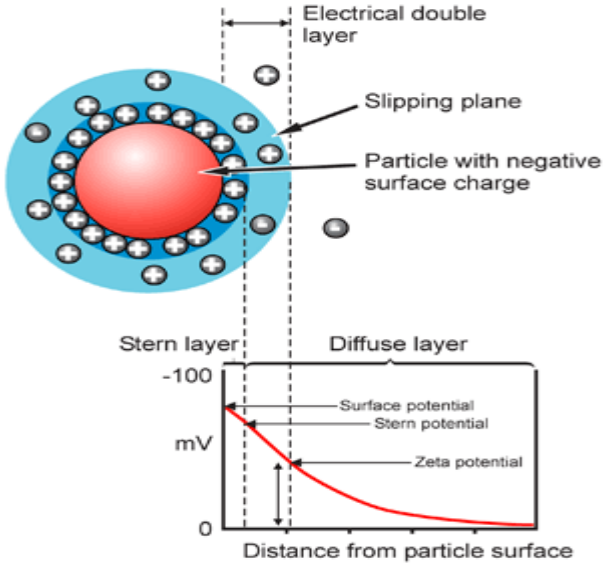

Fig 2.10: Pictorial representation of determination of the zeta potential for negatively charged particles like zeolites (www.nanocomposix.com, 2016).

Particles with a zeta potential of ± 30mV show a tendency to aggregate due to the low potential. This behaviour is demonstrated well at the isoelectric point where the zeta potential of the particles is 0mV (Marsalek, 2012) but can also be influenced by some ionic species in solution (Maurer & Czarnetzki, 2001) (Fig. 2.11).

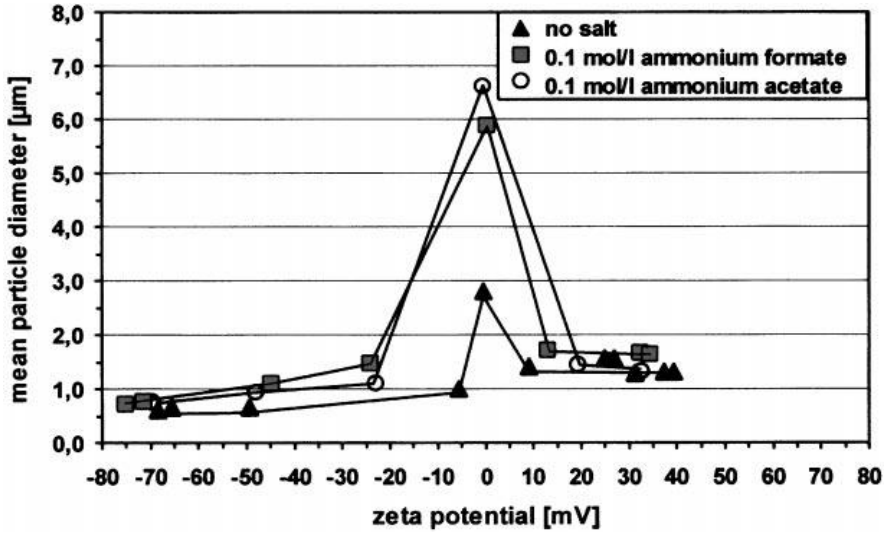

Fig 2.11: Aggregation of zeolite nanoparticles resulting from a reduction of their zeta potential under different electrolytic conditions (Maurer & Czarnetzki, 2001).

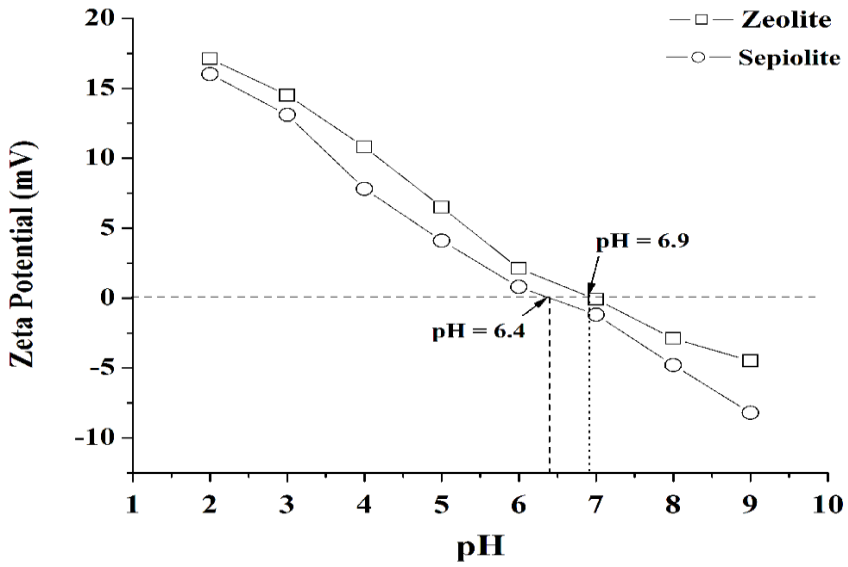

Fig 2.12: point of Zero charge (PZC) determined through pH for zeolites (Sharifipour *et al*, 2015).

Aggregation of particles under different electrolytic conditions affects their flow properties which is not a desired characteristic for adsorption. Incorporation of materials such as polymers to counteract this behaviour which is important for the stability of the adsorbents under various electrolytic conditions (Ulosoy & Simsek, 2004; Crane & Scott, 2012; Nurmi *et al.*, 2004).

2.7.4 Surface Area Determination

The BET (Brunnauer-Emmett-Teller) surface area and porosity analysis method can be used in surface area determination for porous materials such as zeolites. BET porosity analysis method uses physisorption and desorption of nitrogen (typically liquid N_2, 77K) onto a porous solid for surface area determination in order to estimate material porosity. A desorption isotherm of a gas is obtained by measuring the gas desorbed from the porous material as the partial pressure is reduced (Leddy, 2012). The BET adsorption isotherm for gas adsorption can be used to determine the amount of gas (Equation 2.16) adsorbed onto the surface of the porous material:

$$\frac{1}{\mathrm{W}(\frac{\mathrm{P_o}}{P}-1)} = \frac{1}{\mathrm{W_m C}} + \frac{\mathrm{C}-1}{\mathrm{W}_m\,\mathrm{C}}\frac{\mathrm{P}}{\mathrm{P}_o} \quad \ldots \text{ Equation 2.16}$$

Where:

W is the adsorbed gas weight; $\frac{P}{Po}$ is the relative pressure of the N_2 gas; W_m is the weight of monolayer of adsorbate; C is the BET constant. A linear plot of $\frac{1}{W(\left(\frac{Po}{P}\right)-1)}$ vs $\frac{P}{P_o}$, the slope is $\frac{C-1}{W_m C}$ and the y- intercept is $\frac{1}{W_m C}$. The total surface area (S_t) can be derived through Equation 2.17 below:

$$S_t = \frac{W_m N A_{cs}}{N} \ldots \text{Equation 2.17}$$

Where:

S_t is the total sample surface area (m^2); W_m is the adsorbed monolayer weight, N is the Avogadro's number ($6.023* 10^{23}$); A_{cs} is the adsorbate cross-sectional area (16.2 $Å^2$ for Nitrogen gas). Determination of the specific surface area of the sample can be done using equation 2.18:

$$S = \frac{S_t}{W} \ldots \text{Equation 2.18}$$

Where:

S is the specific surface area ($m^2\ g^{-1}$); S_t is the total surface area of sample (m^2); w is the weight of the sample (g).

2.8 Nanocomposites

Nanocomposites are mixtures of two or more physico-chemically different materials with a distinguishable interface at nanoscale. One of the material may form a continuous phase also known as the matrix while the other is the dispersed phase or filler material (Mishra, 2015). In this research, cellulose acetate (CA) will be combined with zeolites to form nanocomposites. Cellulose is the most abundant and natural polysaccharide found on earth especially as plant building material (Klemm *et al.*, 2005). It has been receiving increasing attention due to its biocompatibility, mechanical strength, chemical stability and biodegradation (Gindl & Keckes, 2004; Iguchi *et al.*, 2000; Shoda & Sugano, 2005).

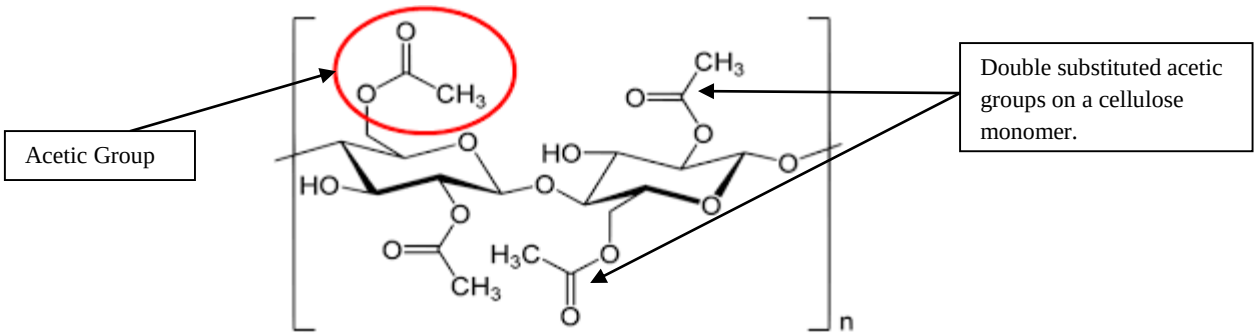

Fig 2.13: The structure of Cellulose diacetate (commons.wikimedia.org).

Cellulose acetates (CA) (Figure 2.13) are essential esters of cellulose synthesized by reacting cellulose and acetic anhydride in an acetic acid environment. Cellulose acetate usually has approximately 2-2.5 acetate substituted groups out of 3 hydroxyl groups. The solubility is dependent on the degree of substitution with acetone and dioxane dissolving low substituted acetates and dichloromethane dissolving higher substituted acetates (Fischer *et al.*, 2008). Cellulose- based nanocomposites have recently attracted increases interest in the scientific community (Daoud *et al.*, 2005; Hong *et al*., 2006; Jiang *et al*., 2008; Liu *et al.*, 2008; Marques *et al*., 2006; Tsioptsias & Panayiotou, 2000; Zhang *et al*., 2007). Several researchers have also exploited cellulose acetate based nanocomposites for various applications including water treatment and gas separations; Ramadhan *et al* (2015) prepared CNT and graphene/ Cellulose acetate membranes for applications in water desalinization; and Kim *et al* (2013) prepared Nano-porous layered silicate AMH-3/cellulose acetate nanocomposite membranes to be used for gas separations.

2.8.1 Polymer Layered Silicate Nanocomposites (PLSNs)

Polymer- layered silicate nanocomposites are part of the organic/ inorganic nanocomposite family. They are composed of two or multi phased materials with the silica acting as the filler material at nanoscale (Zou *et al*., 2008; Nguyen & Baird, 2007). Due to the small sizes of the dispersed materials, polymer/ silica nanocomposites possess a larger surface area compared to traditional composites (Balasz *et al.*, 2006; Winey *et al.*, 2007; Krishnamoorti & Vaia, 2007; Caseri, 2004, 2006, 2007; Schadler, 2003; Schadler *et al.*, 2007a; Schadler *et al.*, 2007b; Schaefer & Justice, 2007).

2.8.2 Polymer Layered Silicate Nanocomposite Synthesis methods

Solution mixing, melt blending and in- situ polymerization are some of the methods used in PLSN synthesis. Others include sol-gel process, electrospinning and self-assembly.

2.8.2.1 Solution Mixing

Solution blending which is used in material processing to attain a good level of mixing happens dissolution or dispersal of both the polymer and the silicate in a suitable solvent for nanocomposite formation (Schadler, 2003; Zhang *et al.*, 2003). The dissolution of polymers in an organic solvent is a slow process leading to the swelling of the outer layer followed by physical disentanglement of the polymer chains as they dissolve (Fig. 2.12) (Olsson & Westman, 2013).

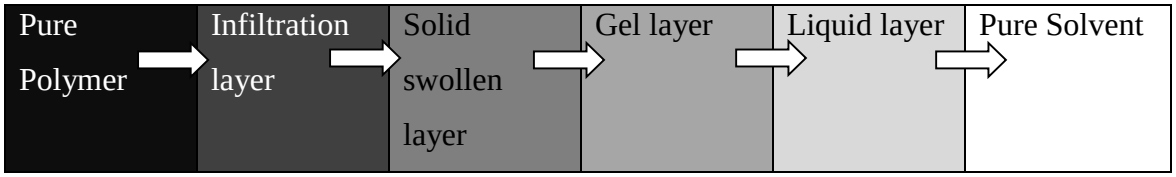

Fig. 2.14 Multi step process for polymer dissolution in an organic solvent. The arrows show the direction continuum from the pure polymer to the pure solvent with complete dissolution of the polymer happening at the liquid layer. (Adapted from Miller-Chou & Koenig, 2003)

Polymer dissolution depends on the negative Gibb's free energy of mixing of the two components as shown in equation 2.19:

$$\Delta G_{mix} = -RT \ln K_{dissolution} < 0 \ldots \text{Equation 2.19}$$

The dissolution constant ($K_{dissolution}$) could be elaborated further through the Flory- Huggins thermodynamic model of polymer dissolution (Bovey & Winslow, 1979):

$$\Delta G_{mix} = -RT (n_1 \ln \Phi_1 + n_2 \ln \Phi_2 + n_1 \Phi_2 X_{1,2}) \ldots \text{Equation 2.20}$$

Where: ΔG_{mix} is the Gibb's energy of mixing; T is the absolute temperature in K; R is the ideal gas constant; n_1 is the number of moles of the solvent; n_2 is the number of moles of the polymer;

Φ_1 is the volume fraction of the solvent; Φ_2 is the volume fraction of the polymer; $X_{1,2}$ is the cumulative energy of the inter-dispersing solvent and polymer molecules.

Kinetics of dissolution can also be positively influenced by mechanical energy such as stirring the polymer-solvent mixture which increases the possibility of the polymer dissolving into the bulk solvent (Olsson & Westman, 2013). This can be explained by the Fick's first law of diffusion as shown in Equation 2.21:

$$J = D\frac{\Delta c}{\Delta x} \ldots \text{Equation 2.21}$$

Where: J is the flux in mol. s^{-1}; D is the diffusion coefficient (m^2 s^{-1}); Δc is the concentration gradient from the particle surface to the solution; Δx is the distance from the particle surface to the bulk solution. D is expressed further in the following equation 2.22:

$$D = D_o\, e^{-\frac{Q_d}{RT}} \ldots \text{Equation 2.22}$$

Where: D_o is a pre-exponential that is independent of temperature (m^2/s); Q_d is the activation energy for diffusion (J/mol.); R is the gas constant (8.314 J/mol.K); T is the absolute temperature in K. However, in real life situations, the concentration gradient is changing with time. In this case Fick's second law of diffusion shown in equation 2.23 can be used.

$$\frac{dC}{dT} = D\frac{d^2C}{dx^2} \ldots \text{Equation 2.23}$$

Where: dC is the change of concentration of the atoms or particles; dT is the change in time; dx is the distance between the surface of the particle and the solution bulk.

2.8.2.2 Melt Blending

Melt blending is preferred in materials processing because of its simplicity, efficiency and environmental friendliness (Oriakhi, 1998; Suprakas & Okamoto, 2002; Zhang *et al.*, 2003). It allows for the mixing of both the polymer and the layered silicate under heat and shear allowing for the formation of exfoliated or intercalated nanostructures depending on the polymer silicate ratio. It is a useful method especially when employing polymers which are difficult to dissolve (Giannelis, 1996; Giannelis, 1999; Vaia & Giannelis, 1997). Intercalation is driven by enthalpic

factors since the entropic reduction due to polymer chain confinement in the crystal lattice is compensated by entropic increase due to increase in the lattice d- spacing resulting into a Lewis base/ Lewis acid interaction between the polymer and the silicate phases (Equation 2.24) (Vaia & Giannelis, 1997; DuBois & Alexandre, 2000).

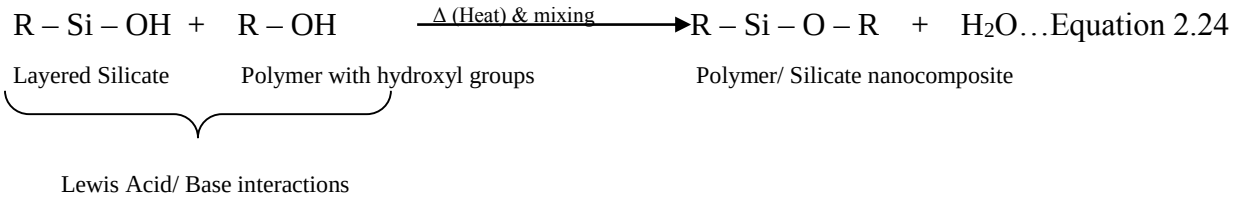

Intercalation will therefore only take place upon overcoming the high polymer-silicate interaction enthalpies by raising the temperature as depicted by the Table 2.1 below:

Table 2.1: Choice of Polymer- Silicate interaction enthalpies by raising the temperature (Vaia & Giannelis, 1997).

ΔG	**ΔH**	**TΔS**	**Feasibility of intercalation**
$\Delta G = \Delta H - T\Delta S > 0$	High	Low	Not favourable
$\Delta G = \Delta H - T\Delta S = 0$	$= T\Delta S$	$= \Delta H$	Not favourable
$\Delta G = \Delta H - T\Delta S < 0$	Low	High	Favourable

Several polymer- silicate nanocomposites have been prepared this way without the need for surface modification; Vaia (1995) prepared Poly (ethylene- oxide)/ Montmorillonite nanocomposites through melt intercalation at a temperature of 80^oC; Mthombo *et al.* (2009) prepared zeolite/ polyvinyl alcohol and zeolite/ ethylene vinyl acetate nanocomposites using melt intercalation at 130^o C.

2.8.2.3 In-Situ Polymerization

In situ polymerization is the dispersal of silicates into a monomer solution followed by bulk polymerization of the monomer to form a nanocomposite (Zou *et al.*, 2008). In-situ polymerization has been demonstrated using several experiments; Reculusa *et al.* (2004) synthesized polystyrene / silica nanocomposites using emulsion polymerization; and Tiarks *et al.* (2001) first reported the preparation of polymer/silica nanocomposites using mini-emulsion polymerization.

2.8.2.4 Sol- Gel process

Nanocomposite formation using sol- gel process involves hydrolysis of a metal alkoxide or silicate followed by a poly- condensation step (Zou *et al.*, 2008). It produces inorganic/ organic composite hybrids possessing very unique properties (Huang, 1985; Chen & Iroh, 1999).

Hydrolysis step:

$>Si\text{-}OR + H_2O \xrightarrow{H+ \text{ or } OH-} >SI\text{-}OH + ROH$ where R= Alkyl group, > = polymer group

Poly-condensation step:

$>Si\text{-}OH + OH\text{-}Si< \xrightarrow{H+ \text{ or } OH-} >Si\text{-}O\text{-}Si< + H_2O$ (Adopted from Zou *et al.*, 2008)

2.8.2.5 Electrospinning

Electrospinning uses an electric field to form a solidified polymer fibre from an electrically charged polymer liquid (Hohman *et al.*, 2001a, 2001b; Reneker *et al.*, 2000; Feng, 2002, Yarin *et al.*, 2001; Yu *et al.*, 2004). It has drawn attention because of the possibility of incorporating nanosized particles in the polymer liquid matrix to produce nanocomposite fibres. The filler material could be manipulated geometrically in order to produce different forms of nanocomposites when dispersed in the polymer matrix (Fong *et al.*, 2002; Wang *et al.*, 2004; Wang *et al.*, 2004a).

2.8.2.6 Self- Assembly

Self assemblied organic- inorganic nanocomposites are formed when the two separate phases are organized spontaneously at nanoscale based on non- covalent interactions. These organized nanocomposites express unique properties because of their dispersion at nano-scale, synergistic properties and high interfacial area (Mc. Caughey *et al.*, 2004). Self-assembled materials utilize hydrophobic interactions, electrostatic interactions, co-ordinate bonding, hydrogen bonding and biomolecular interactions during nanocomposite formation (Zou *et al.*, 2008). A well-known self-assembly method for nanocomposite synthesis is layer by layer electro-deposition of gold nanoparticles onto a polymer- coated glassy carbon electrode using cyclic voltametry for bio-sensing applications.

2.8.3 Polymer Layered Silicate Nanocomposite characterization methods

The structure of polymer layered silicate nanocomposites could either be intercalated or exfoliated. Intercalated structures are formed when polymer chains penetrate the ordered silicate layers (Fig. 2.15 (b)) resulting into an ordered and repetitive structure composed of alternate polymer/ silicate layers at nanometer level (Suprakas & Okamoto, 2003; Krishnamoorti *et al.*, 1996; Giannelis, 1996). In exfoliated structures (Figure 2.15(c)) the silicate phase is completely separated into individual silicate layers which disperse in the polymer matrix losing the crystalline periodicity. It usually happens when the silicate ratio is low (Suprakas & Okamoto, 2003).

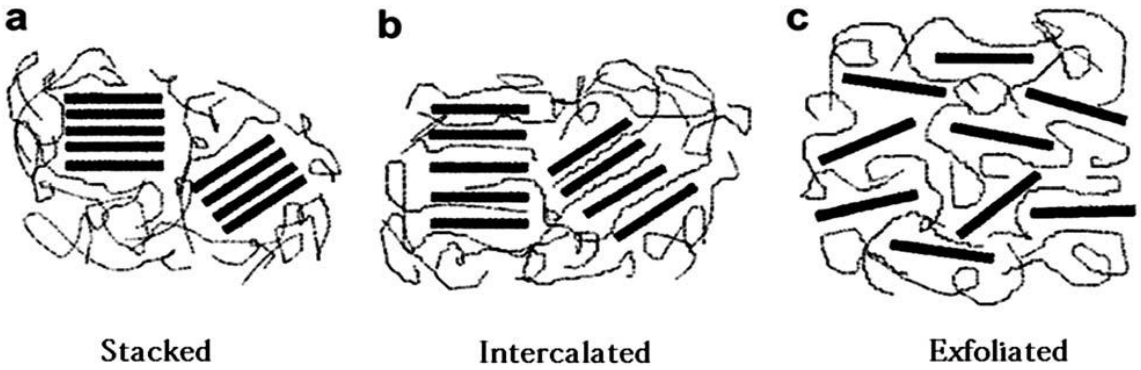

Fig 2.15: Depiction of intercalated and exfoliated polymer- layered silicate nanocomposites (Dichiara *et al.*, 2013).

Powder X-Ray Diffraction Crystallography is a characterization method used to determine intercalation of polymers into crystal lattices. d-spacing increase in the silicate layers could be determined by the shift of the diffraction peaks to lower 2- theta angles for intercalated structures which is not possible for exfoliated structures because of the very large interlayer spacing (>8nm). (DuBois & Alexandre, 2000). FTIR technique can be used to supply evidence of hydrogen bonding for polymer/ silicate nanocomposite structures due to both exfoliation and intercalation by elucidation of the residual silanol- polymer bonding (Hajji *et al.*, 1999; Huang *et al.*, 2005; Bandyopadhyay *et al.*, 2005). Scanning electron microscopy (SEM) uses accelerated electrons to elucidate the surface morphology of materials. The 3-D images produced by SEM analysis are very vital in understanding the surface of materials (Kickelbick, 2007).

2.8.4 Polymer Layered Silicate Nanocomposite properties

Nanocomposites have a much improved Young's Modulus (stiffness) than constituent materials. They also possess better thermo- mechanical properties than the parent materials irrespective of the synthesis route used (Alexandre & DuBois, 2000; Zou *et al.*, 2008). Zheng *et al.*, (2003) after

dispersing silica nanoparticles into epoxy resins discovered that their properties were greatly improved if the nanoparticle dispersion was done uniformly.

Thermo-gravimetric analysis (TGA) & differential scanning colorimetry (DSC) illustrates that the inclusion of the silicate fillers into the polymer matrix suppresses rapid decomposition of the polymer under heat. It also acts as an insulator boosting the material heat capacity (Suprakas & Okamoto, 2003; Zou *et al.*, 2008).

Silicate fillers in the nanocomposite affect gas solubility, diffusivity and permeability because of the increase in voids in the material. This creates room for the material to interact with various gases such as CO_2, N_2 and CH_4 in gas separation systems through hydrogen bonding (Cong *et al.*, 2007; Merkel *et al.*, 2003a; 2003b).

2.8.5 Polymer Layered Silicate Nanocomposite applications

Polymer/ Silicate nanocomposites can be used as size- dependent filters in water purification. Inorganic particles incorporated into polymers as membrane filters enhances the porosity of water due to an increase in the pore size (50-200nm) (Xu & Bhattacharya, 2008). Bulk nanocomposites can also be immobilized onto glass beads which can be employed in columns (akin to ion exchange columns) and utilized in water treatment (Tesh & Scott, 2014). Nanocomposites can also be fabricated into 3-D structures using polymers (Calcagnile *et al*, 2012; Savina *et al.*, 2011), graphene (Cong *et al.*, 2012), carbon (Mc. Farlane *et al.*, 2014) and chitosan (Sankar *et al.*, 2013) and employed in water treatment. Other applications of PLSN materials include coatings (Soloukhin *et al.*, 2002), chemosensors (Su, 2006), gas separations (Cong *et al.*, 2007) and encapsulation of organic light emitting devices (Wang & Hsieh, 2007).

2.9 Instrumental Analysis

Materials, when subjected to electromagnetic radiation can exhibit differing secondary effects such as vibration, electronic transitions, rotation, scattering and diffraction. Lattice and molecular vibrations of the nanocomposites were analysed using Fourier Transform Infra-red (FTIR) spectroscopy. Crystallographic analysis was carried out using Powder X- Ray Crystallography (XRD). Analysis of the metallic ions in water was carried out using Atomic Absorption Spectroscopy (AAS). The morphology of the nanocomposites was elucidated using Scanning Electron Microscopy (SEM) while the elemental composition was assessed using Energy Dispersive X-Ray Spectroscopy (EDX).

2.9.1 Atomic Absorption Spectroscopy (AAS)

Atomic absorption spectroscopy is a technique of measuring quantities for chemical elements such as lead, cadmium, mercury, copper, zinc and other metals present in various environmental samples (Figure 2.14) (Garcia & Baez, 2012).

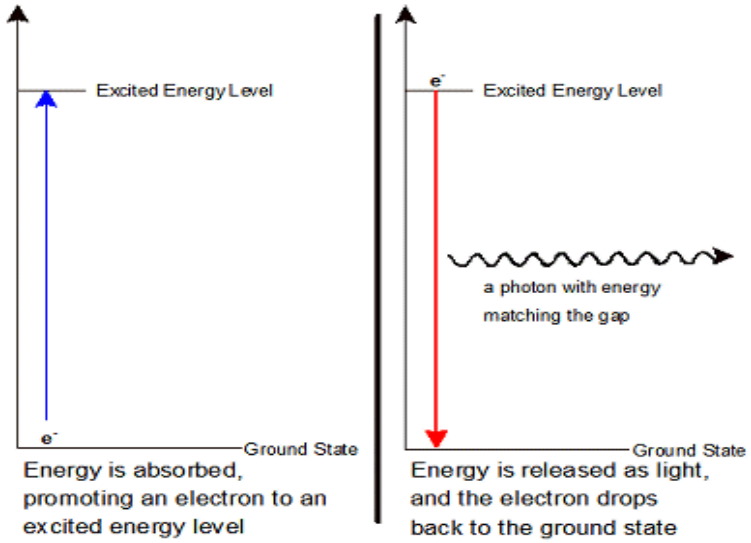

Fig 2.16: A depiction of excitation of energy by an atom's electron leading to AAS analysis (http://kcmcgann.tripod.com, 2017)

When an element in its ground state absorbs energy in the form of radiation, its electrons are excited. As more of these atoms absorb this energy, the amount of light absorbs increases. A correlation between the amount of radiation absorbed and the amount of analyte of interest in the environmental media can be assessed by measurement of absorbed light and correlating it to the Beer- Lamberts Law (Equation 2.25) (Perkin-Elmer Corp., 1996).

$A = \varepsilon bc$…..Equation 2.25

Where:

A is the absorbance; Ɛ is the molar absorptivity (L mol^{-1} cm^{-1}); b is the path-length of the sample cuvette (cm); c is the concentration of the compound (mg/L). Absorbance and transmittance could be expressed as:

$$A = \log\frac{P_o}{P} \quad \ldots \text{Equation 2.26}$$

$$\%T = \frac{P}{P_o} * 100\% \quad \ldots \text{Equation 2.27}$$

Where:

A is the absorbance; %T is the percentage transmittance; P_o is the incident radiation power; P is the radiation leaving the sample. In AAS analysis, the sample is introduced into the system using suction through a fine capillary tube. It is then subjected to acetylene or a graphite flame which evaporates the solvent the sample is contained in, a process called desolvation. Upon further heating, the solid sample is vaporized into a gas then later broken up into free atoms, also called volatilization. Light which has been filtered by a monochromator is then directed to the volatilized samples which absorb part of the light energy at a specific wavelength to excite their electrons. The resultant absorbed radiation can be measured by the detector to determine the concentration of the ions of interest in the medium (Garcia & Baez, 2012).

2.9.2 Fourier Transform Infra-Red (FTIR) Spectroscopy

IR spectroscopy can be used to elucidate the structure, bonding and chemical properties of organic and inorganic minerals and materials (Farmer & Russell, 1964; Farmer, 1974; Decarreau *et al.*, 1992; Russell & Fraser, 1994; Bishop *et al.*, 1994; Petit *et al.*, 1995; Gates *et al.*, 2000; Heller-Kallai, 2001). In an infrared spectrometer, radiation of the wavelength range 400-4000 cm^{-1} is passed through a sample resulting in its partial absorption and transmittance of the rest. Analytes of interest in the sample can be determined by the absorbance of the IR radiation at a specific wavelength or wave number (cm^{-1}) (www.thermonicolet.com). In order for a molecule to be able to absorb infrared radiation, when it vibrates there must be an alteration of the dipole moment of the molecules (Fig. 2.17). Fourier Transform Infra-Red Spectrometry measures the absorbance of IR radiations at different frequencies simultaneously. It could be used to check for vibrations, bending, ring movements etc. in different kinds of bonds as they absorb IR radiation. This can be used in characterization of materials.

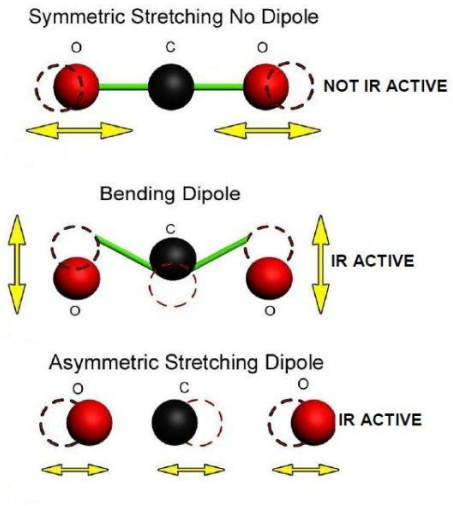

Fig 2.17: Depiction of IR activity using a carbon dioxide molecule. (Source: http://www.azosensors.com)

Infrared radiation originates from a source which is modified using an aperture which adjusts the amount of radiation energy. The adjusted radiation is then directed towards the sample. The beam is then encoded spectrally in the interferometer before being directed to the sample. The amount of radiation absorbed or transmitted through the sample will determine the amount of analyte of interest in the sample. The resultant beam from the sample is then directed to the detector for decoding, digitization and Fourier transformation before the spectrum is availed to the end user for interpretation and further manipulation (www.thermonicolet.com).

2.9.3 Powder X-Ray Diffraction (XRD) Crystallography

X-Ray diffraction crystallography utilizes the scattering effect of X- Rays by crystalline structures such as silicates to elucidate their nature (Zou *et al.*, 2008).

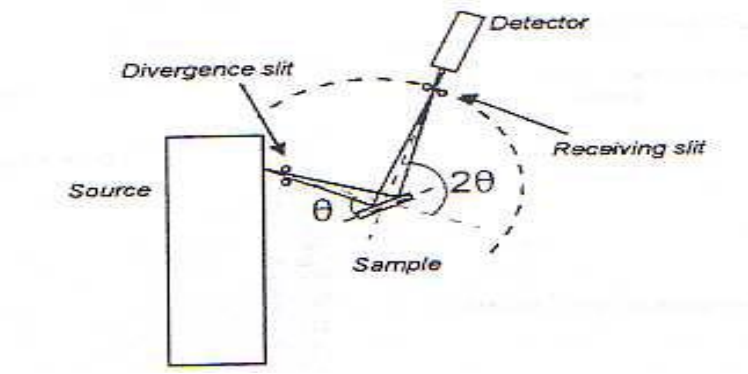

Fig 2.18: Depiction of the working principle of an X-Ray Diffraction Spectrometer (www.xray.tamu.edu).

In XRD, a monochromatic X-ray generated from a cathode tube is directed towards a sample which diffracts them against a scattering angle characteristic of its crystalline atomic structure (Figure 2.18). Qualitative analyses are carried out by comparing the diffraction data (of the unknown sample) against a database of known patterns (www.thermo.com). The diffracted X-ray beam from the sample can be detected when there is an alignment of the X-ray source, sample and the detector to produce the Bragg's diffraction angle. The powder sample contains many mini-crystals which can adopt many possible orientations giving different Miller index peaks on the X-RD spectrum (www.xray.tamu.edu).

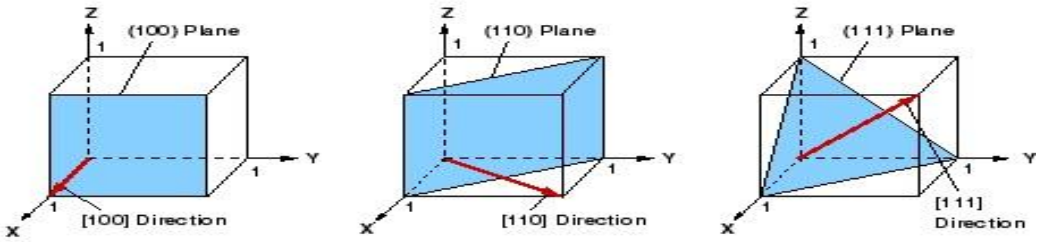

Fig 2.19: Miller indices showing different crystal lattice orientations useful for XRD crystallography (http://blog.nus.edu.sg, 2013)

The Bragg's equation given by equation 2.28 (a) can be used to calculate the interlayer spacing and can be written as:

$n\lambda = 2d \sin\theta$….Equation 2.28 (a)

The crystalline interlayer spacing (d) can be calculated as:

$d = \frac{n\lambda}{2 \sin\theta}$ … Equation 2.28 (b)

Where: n is an integer (1, 2, 3…); λ is the wavelength; d is the interlayer distance in the crystal; Θ is the Bragg's angle. The Braggs angle can be represented as:

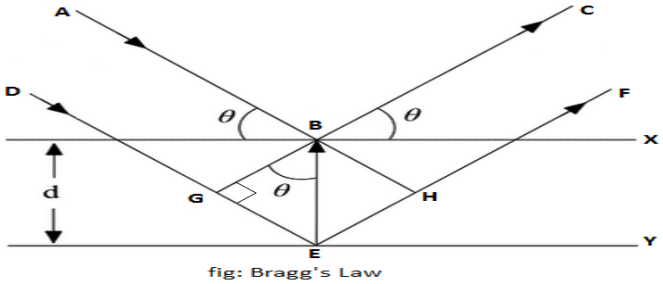

fig: Bragg's Law

Fig 2.20: Bragg's Law depicted with incident ray A approaching at angle Θ and reflected ray C leaving at angle Θ from the horizontal plane X (www.sciencetopia.net).

The Scherrer equation is important in estimation of the crystal thickness. It can be represented as Equation 2.29 below:

$$t = \frac{0.9\lambda}{B\cos\Theta} \quad \ldots \text{ Equation 2.29}$$

Where: t is the thickness of the crystallite, λ is the wavelength of the x- rays (same units with t), Θ is the Bragg's angle and B is the Full- Width at Half-Maximum (FWHM) of the peak (radians) to check instrumental broadening.

2.9.4 Scanning Electron Microscopy & Energy Dispersive X-Ray (SEM/ EDX) Analysis

Scanning electron microscopes use high energy electron beams to constantly interact with the sample under study (Figure 2.21), giving signals which allow the scanning to occur (Newbury, 1990). It creates images using emitted or reflected electrons from the surface of the sample as a result of being struck by incident electrons from a source which get deflected by the atoms of the sample (Kickelbick, 2007).

In this analysis, a highly focused electron jet is directed towards the surface of the sample. This leads to excitation of the surface electrons. As a result, several types of scattered particles can be used to map out the surface morphology of the sample and obtain critical information. These scattered particles include secondary electrons, backscattered electrons and x- rays. The magnification of the SEM images relies on the electron- matter interaction and detector signal processing speed among other factors.

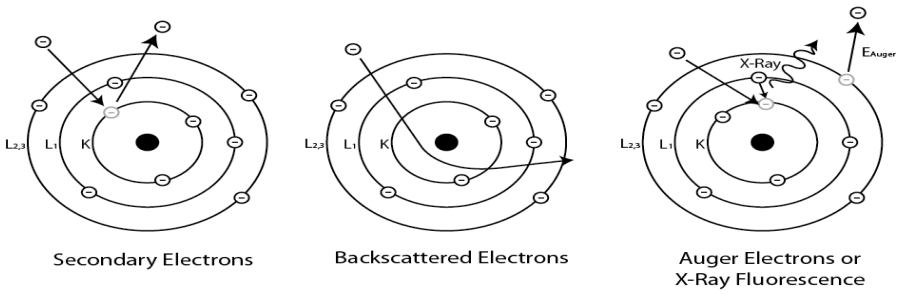

Fig 2.21: Image showing Secondary electrons, backscattered electrons and X- Ray fluorescence/ Auger electrons (https://sites.ualberta.ca, 2012)

Backscattered electrons are elastically scattered from the nuclei of the atoms of the material of interest. In this case, they bear the same energy as the primary electrons thus are very useful in providing clear SEM images. Inelastically scattered or secondary electrons are produced due to primary or incident electrons knocking off surface or inner- shell electrons leading to ionization. These secondary electrons have less energy than that of primary electrons and can be used in contrasting SEM images. Due to their reduced energy threshold, they are usually produced near the sample surface (between 1- 50 nm depth) and are very useful in determining the morphology and topography of the sample. The resolution produced by secondary electrons is dependent on the size of the beam spot and the incident angle of the primary beam. Slight tilting of the sample therefore results into production of more secondary electrons which enhances the image contrast. A pit or cavity on the sample surface can be useful in contrasting the image since the primary electron beam generates secondary electrons which end up trapped in the cavity.

The ionization of inner shell (K- shell) specimen electrons, results into relaxation of outer electrons to occupy the vacancies. This relaxation results into a loss of energy by the outer electrons which is released in the form of x- rays, also called Energy Dispersive X- Ray (EDX) spectroscopy. These x- rays have distinctive wavelengths unique to specific elements of and therefore could be used to characterize materials of interest.

CHAPTER 3

MATERIALS & METHODS

3.1 List of Apparatus, Instruments & Reagents

3.1.1 Equipment and apparatus

The following instruments were used: Atomic Absorption Spectrophotometer (Varian SpectrAA-10 model), Fourier Transform Infra-Red Spectrometer (IRAffinity-IS Shimadzu model), Powder X-Ray Crystallography Diffractometer (PANalytical XRD hich model), Scanning Electron Microscope/ Energy Dispersive X-Ray Spectroscopy (Vegas Tescan SEM/ EDX & ZEISS SEM) and Materials Pulverizer (Siebtechnik model).

The following is a list of apparatus used: Hotplate/Magnetic stirrer (Snijders 34532 model), Electrical weighing Scale (Fisher Scientific A-160 model), Mini-Orbital Shaker (Stuart Scientific SO6 model), oven (Memmert U-400 model) and scientific pH meter (model IQ 150) were used. Other laboratory apparatus used were 500ml, 250ml beakers, volumetric flasks, pipette, measuring cylinder, micro-pipette, pestle and mortar, filter papers, 38µm Sieve, aluminum foil, spatula and petri-dishes.

3.1.2 Chemicals and reagents

Zeolite (Sigma-Aldrich, Modderfontein, South Africa), cellulose acetate (Sigma-Aldrich, Modderfontein, South Africa), sodium hydroxide (Sigma-Aldrich, Modderfontein, South Africa), lead nitrate (Sigma-Aldrich, Modderfontein, South Africa) and cadmium nitrate tetra-hydrate (Sigma-Aldrich, Modderfontein, South Africa); Hydrochloric acid (Fisher Scientific chemicals, South Africa); Dichloro-methane (Pancreac Quimica chemicals, South Africa); and distilled water (University of Nairobi, Analytical Chemistry Laboratory).

3.2 Synthesis of Cellulose Acetate/ Zeolite Nanocomposites.

The ‘as received’ zeolite powder was washed in distilled water before being dried in an oven at 100^{o}C. It was then subjected to sieving using a 38µm sieve to separate the larger particles from the smaller ones. A relevant portion of zeolite mass (<38µm) was dispersed in dichloromethane (mass to volume ratio of 1:10) and stirred in a beaker for 5 minutes. Cellulose Acetate powder was then added to the zeolite/ dichloromethane mixture at different ratios as indicated by the equation 3.1 below and mixed thoroughly using a stirring rod until the solvent evaporated. The ratios of zeolites

used were adjusted to 10%, 20%, 30%, 40% & 50% in mass. The following equation was used to calculate the zeolite loading:

M_c (g) = M_z (g) + M_{ca} (g) ….Equation 3.1

$$\% \text{ Zeolite Loading} = \frac{M_Z(g)}{M_C(g)} * 100\% \ \ldots \text{ Equation 3.2}$$

Where:

M_c is the composite mass in grams; M_z is zeolite mass in grams; M_{ca} is the cellulose acetate mass in grams. The resultant paste (zeolite/ cellulose acetate mixture) (Figure 3.1) was then subjected to oven heating for 4 hours at 160^{o}C. The resultant mixture was then cooled at room temperature for 24 hours after which it was subjected to pulverization using a Siebtechnik Pulverizing instrument (Figure 3.2). The resultant pulverized nanocomposite (<150µm in mesh-size), was washed thrice by soaking it in distilled water impurities removal before being dried for 2 hours at 100^{o}C. The nanocomposite powder (Figure 3.3) was then subjected to physical characterization through FTIR, XRD and SEM analytical methods.

3.3 Physical Characterization of Nanocomposites

Characterization was carried out using an FTIR spectrophotometer, XRD spectrophotometer, Scanning Electron Microscope (SEM) and EDX spectrometry.

3.3.1 FTIR Analysis

A background scan of the air was done by the IRAffinity-1S FTIR spectrometer (University of Nairobi) in order to subtract it from the spectrum obtained from the sample. A sample of the nanocomposite powder was inserted into a sample well and compacted using a metallic presser. The cabinet containing the sample holder was opened and the sample contained in the well was placed in it. The cabinet was closed and then the FTIR analysis run was made in order to obtain a Transmittance spectrum of the samples. The machine automatically made four runs per sample and then averaged them in order to obtain the reading. The sample was then removed from the sample holder and un-mounted from the well. The parts that came into contact with the sample were then cleaned using a piece of cloth soaked in ethanol then the analysis was repeated for another sample. The results were printed for interpretation. The scanning was done from a

wavenumber range of between 500 cm^{-1} to 4500 cm^{-1} using the transmission mode using a 0.5 g sample per analysis.

3.3.2 Powder X-Ray diffraction crystallography

The x-ray diffraction spectra were collected from $10 – 90^0$ 2θ at the rate of 0.5^0/ minute at room temperature on a PANalytical XRD hich diffractometer (BITRI, Gaborone, Botswana) equipped with a Ge (Li) solid detector a radiation source which used a Copper Kα source. The wavelength of the X-Rays was 1.5418 Å. The samples for analysis were 1mm thick to prevent X-Ray penetration. The identification of the material was done through correlating the results with those of the standard diffraction data from the Joint Committee on Powder Diffraction Standards (JCPDS).

3.3.3 Scanning Electron Microscopic Analysis

A 20 kV Vegas Tescan Scanning Electron Microscope equipped with Energy Dispersive Spectroscopy (University of the Free State, Bloemfontein, South Africa) was used for sample morphological analysis. A jet of electrons were produced from a Lanthanum Hexaboride (LaB_6) filament source because of its high resolution even at low accelerating voltages. Specimen charging, beam damage and beam penetration curtailed leading to greater surface detail. For non-conducting samples such as polymers, sputtering with Au/Pd conductive thin layer would prevent charging of the sample's surface. Prior to SEM analysis, the sample was mounted onto an aluminum stub using a double- sided carbon tape then coated with a thin layer (~10-30nm) of 60/40 Au/Pd alloy by means of vacuum sputtering coating using a Denton Desk 1 Sputter- Coater under a 70 motor vacuum.

3.4 Atomic Absorption Spectroscopy Measurements

A Varian SpectrAA-10 AAS Spectrophotometer (Ministry of Mines, G.o.K. Nairobi) was used. The sample to be measured was introduced to the AAS analytical instrument (Figure 3.1) using a fine capillary tube which sucked the sample from the beaker/ flask at a rate of 1ml per minute. It was carried to the nebulizer using a carrier gas (acetylene) which doubled up as the fuel to atomize the sample. This resulted into the evaporation of the solvent and breaking up of the dissolved ions into atoms. The atoms were then bombarded with light with a wavelength of 217nm and 228.8nm for Pb^{2+} and Cd^{2+} respectively (Table 3.1) in order to excite their electrons which in turn released photons of light upon relaxation at specific wavelengths per metal. The detector was able to sense an increase in the amount of photons transmitted and converted it into a function of absorbance.

Table 3.1: Atomic Absorption Spectrophotometer (Varian SpectrAA-10) analytical variance used

Metal ion	Lamp current (mA)	Wavelength (nm)	Slit width (mm)	Fuel	Oxidant	Detection Limit (µg/ml)
Pb^{2+}	6	217	1	Acetylene	Air	0.11
Cd^{2+}	3	228.8	0.5	Acetylene	Air	0.011

Figure 3.1: A Varian SpectrAA-10 AAS Spectrophotometer used for aqueous heavy metal analysis at the Geochemistry Labs, Ministry of Mines (G.o.K), Nairobi.

3.5 Batch adsorption experiments

0.3996g of the Lead Nitrate and 0.5252g of Cadmium Nitrate Tetra-hydrate salts were each dissolved in 250 ml of distilled water to obtain stock solutions of 1000mg/l of Pb^{2+} and Cd^{2+} ions in 250 ml beakers. The concentrations of these metallic ions were confirmed through AAS measurements (Varian SpectrAA-10). These stock solutions were used to make dilutions to facilitate the batch experiments carried out. All experiments results were reported in triplicate, the standard deviation calculated and the mean values used (see Appendix). All the samples were subjected to AAS measurements within 24hours.

Fig 3.2: Batch adsorption experimental set-up using an Orbital Shaker at the Pesticides and POPs Lab, Chemistry Dept. CBPS, UoN.

3.5.1 Varying zeolite loading

For every metal, five 100 ml solutions of 15mg/l were prepared using distilled water from the stock solution of 1000 mg/l in 250 ml volumetric flasks. To each portion, 0.04g of 10%, 20%, 30%, 40% and 50% adsorbent samples were added to every portion. After being covered using an aluminum foil, the flasks were subjected to agitation using a Stuart Mini-Orbital shaker at 100 rpm for 75 minutes then filtered using a 0.5mm Whattman filter paper. Atomic absorption spectrophotometry was used to determine the residual metallic amounts in the solutions.

3.5.2 Varying contact time

For every metal, five 100 ml solutions of 15 mg/l were prepared in 250 ml volumetric flasks. 0.04 g of the 20% zeolite loaded sample was added to each solution containing Pb^{2+} ions while 0.04 g of the 40% zeolite loaded sample was added to each solution containing Cd^{2+} ions. The solutions were then agitated for 5, 10, 20, 40 and 75 minutes on an orbital shaker at 100 rpm. The resultant solutions were filtered using a 0.5mm Whattman filter paper then subjected to AAS measurements for metal determination.

3.5.3 Varying adsorbent mass

Distilled water was used to dilute the stock solution to 27 mg/l solutions. 0.02g, 0.03g, 0,04g, 0.05g & 0.06g of 20% zeolite and 40% zeolite samples were added to the solutions containing Pb^{2+} and Cd^{2+} ions respectively. Solutions for each metallic ion were agitated at 100rpm for 75 min

using a Stuart Mini- Orbital Shaker. The resultant solutions were filtered using a 0.5 mm Whattman filter paper then subjected to AAS measurements to determine the metallic ions concentrations.

3.5.4 Varying metallic ions concentration

The metallic stock solutions were serially diluted to 100 ml portions of 15mg/L, 30mg/L, 45mg/L, 60mg/L and 75mg/L in 250 ml volumetric flasks. 0.06g of 20% zeolite and 40% zeolite samples were added to each of the solutions containing Pb^{2+} and Cd^{2+} ions respectively. Solutions for each metallic ion were agitated at 100rpm for 75 min using a Stuart Mini- Orbital Shaker. The resultant solutions were filtered using a 0.5 mm Whattman filter paper followed by metal detection using AAS analysis.

3.5.5 pH adjustment measurements

Different portions of distilled water had their pH adjusted to 3.02, 4.00, 6.06, 9.08 and 10.08 using Sodium Hydroxide (NaOH), HCl using a pH meter (model IQ 150). These pH adjusted portions of distilled water were used to make 100 ml of 18mg/L metallic ion solutions. 0.06g of 20% zeolite and 40% zeolite samples were added to each of the solutions containing Pb^{2+} and Cd^{2+} ions respectively. Solutions for each metallic ion were agitated at 100rpm for 75 min using a Stuart Mini- Orbital Shaker. The resultant solutions were filtered using a 0.5 mm Whattman filter paper followed by metal detection using AAS analysis.

3.5.6 Varying temperature

The metallic stock solutions were diluted to 100 ml portions of 15mg/L in 250 ml volumetric flasks using distilled water. The diluted metallic solutions were then maintained at room temperature (25^{o}C) while others were heated to 50^{o}C and 70^{o}C using an electric hot plate. 0.06g of 20% zeolite and 40% zeolite samples were added to each of the solutions containing Pb^{2+} and Cd^{2+} ion solutions under different temperatures respectively. Solutions for each metallic ion were then stirred at 100rpm for 5 minutes using a metallic stirrer. The resultant solutions were filtered using 0.5mm Whattman filter paper followed by metallic analysis using AAS technique.

3.5.7 Regeneration by acid conditioning

Adsorbents from previous adsorption experiments (20% zeolite for Pb^{2+}; 40% zeolite for Cd^{2+}) were dried for 2 hours at 100^{o}C. They were then soaked in a solution of 1M HCl for 48 hours before being agitated in the presence of the acid at 125rpm for 1 hour with the mass to volume

ratio being maintained at 1:10. They were then dried for 2 hours at 100°C. For batch adsorption experiments, 30 mg/l solutions were prepared from the metallic solutions. 0.06g of the regenerated 20% and 40% zeolite samples were added to the solutions containing Pb^{2+} and Cd^{2+} ions respectively. Solutions for each metallic ion were agitated at 100rpm for 75 min using a Stuart Mini- Orbital Shaker. The resultant solution was filtered using a Whattman filter paper (0.5mm) followed by metallic determination using AAS analysis.

3.6 Statistical data analysis

Data analysis for the results was done by Microsoft Excel 2007 (2006, Microsoft Corp). Results obtained were represented by use of text, graphs and statistical table to show the interpretation of various variables. ANOVA was also carried out to check statistical integrity of the data.

CHAPTER 4

RESULTS AND DISCUSSION

4.1 Synthesis of Nanocomposites

After solution blending the resultant composite was a thick white paste. Annealing the composite mixture for all zeolite/ cellulose acetate ratios resulted into a composite lump (Fig. 4.1) which after pulverization was reduced to 150µm mesh powder (Fig. 4.2).

Fig.4.1: Composite lump after solution blending before annealing

Fig. 4.2: 150µm mesh- size composite powder after annealing and pulverization

4.2 Fourier- Transform Infra-Red (FTIR) Spectroscopy

Infrared spectroscopy uses bond movement as a result of interaction with infrared radiation to determine the structure of materials. As different chemical functional groups in the material interact with IR radiation at specific signature wavelengths, they reveal the structure of the material and ratios of mixtures of substances within the materials.

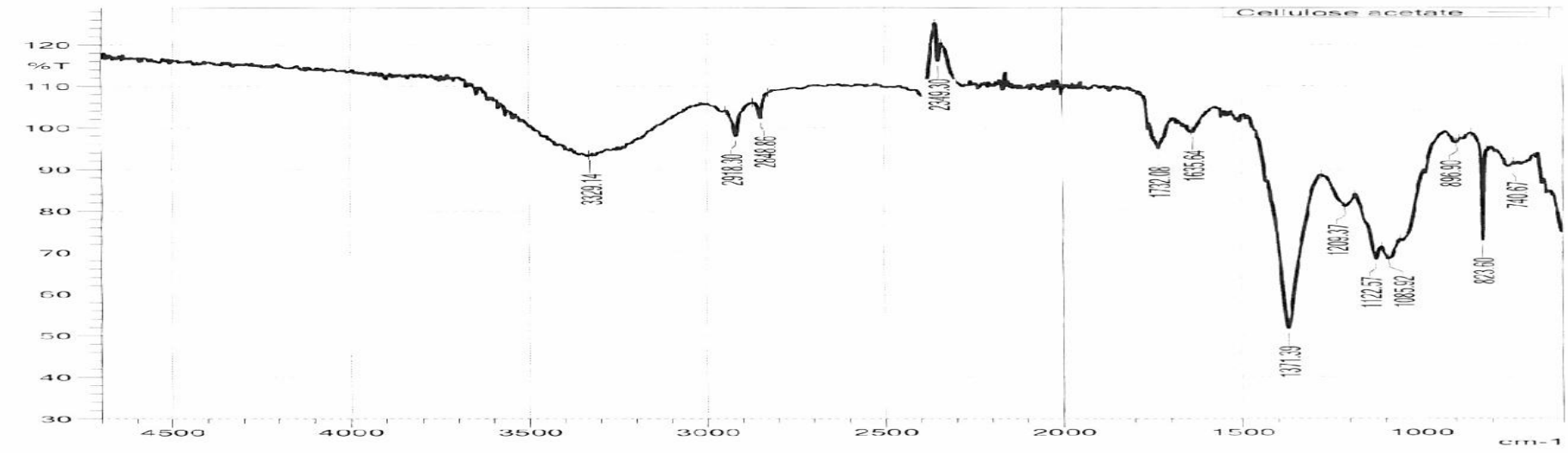

Fig 4.3a: FTIR Spectra for Cellulose Acetate

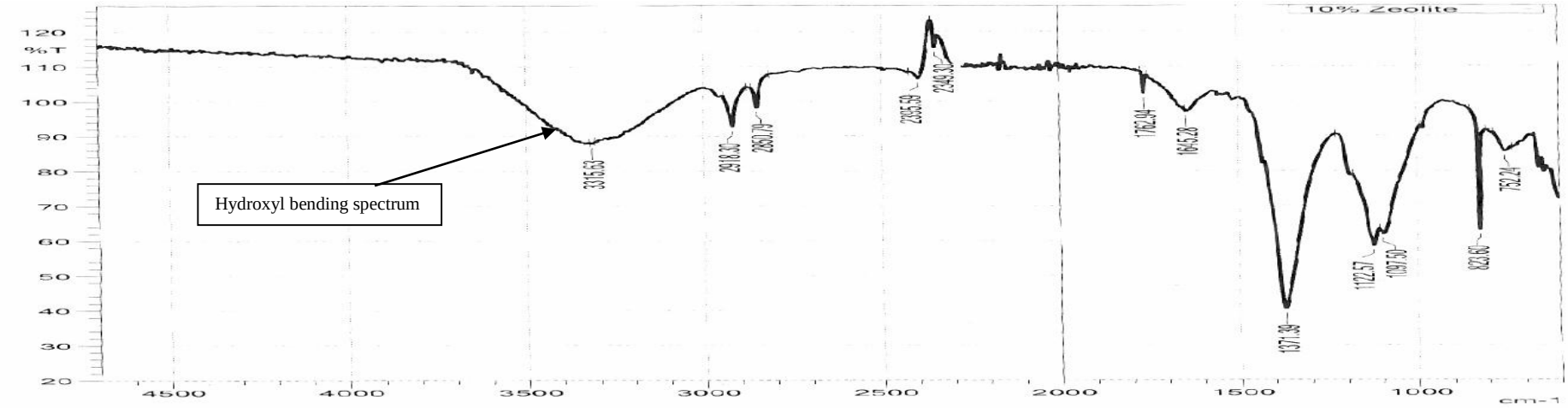

Fig 4.3b: FTIR spectrum for 10% zeolite loaded nanocomposites

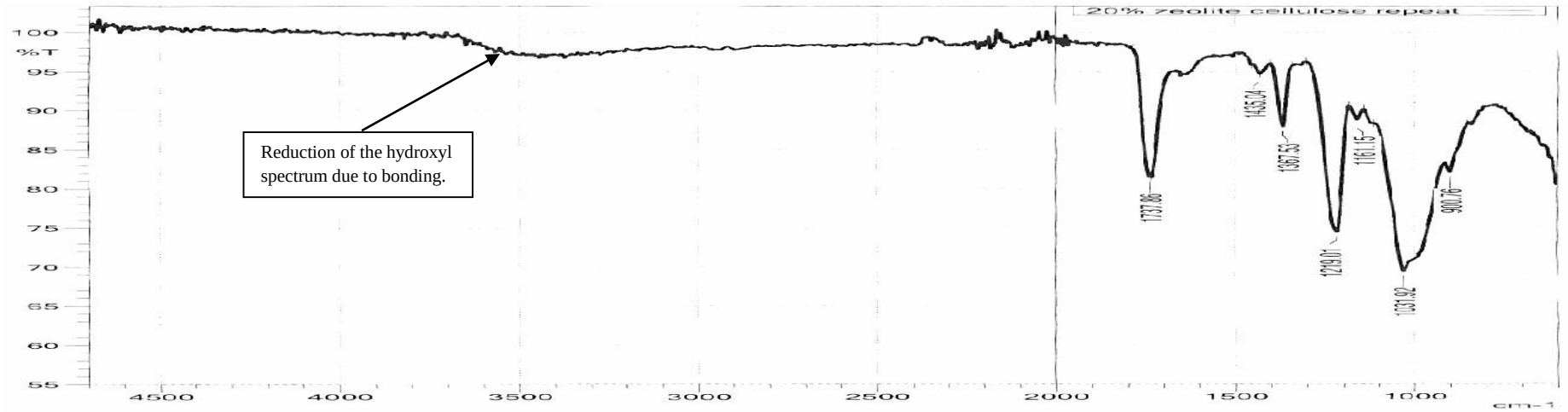

Fig 4.3c: FTIR spectrum for 20% zeolite loaded nanocomposites

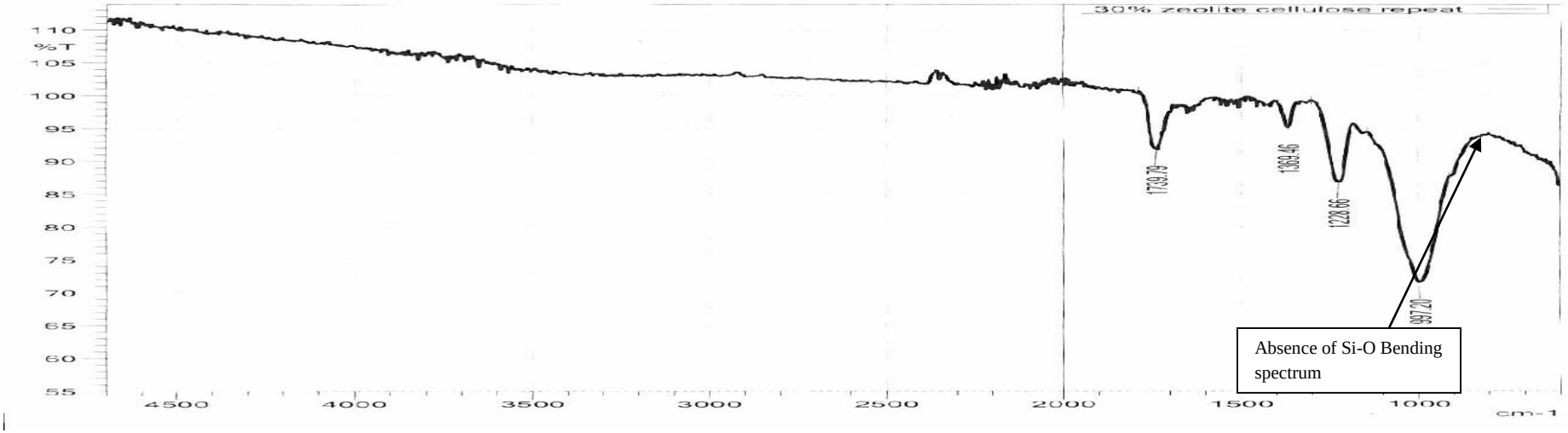

Fig 4.3d: FTIR spectrum for 30% zeolite loaded nanocomposites

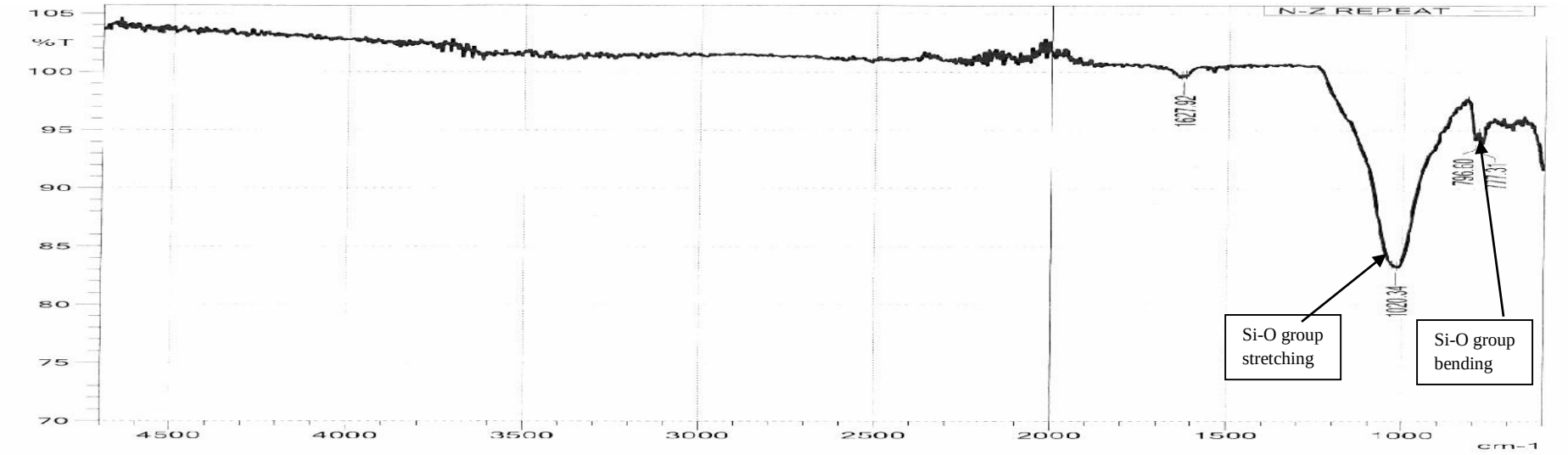

Fig 4.3e: FTIR Spectrum for zeolite

The FTIR analysis shows that the S-O bond bending movement at 796.6 cm^{-1} and the hydroxyl bending spectrum at 3315.33 cm^{-1} was suppressed during the formation of the nanocomposite. This could symbolize bond formation between the two functional groups (Soheilmoghaddam *et al*, 2013a; Soheilmoghaddam *et al*., 2013b). This is shown in the figures 4.3a, 4.3b, 4.3c, 4.3d and 4.3e. Due to intercalation, there is a spectral overlap between the O-Si-O bond spectrum and the C-O spectrum. At 1085.92 cm^{-1}, there is an elongation of the peak with the increase in zeolite loading in the nanocomposites as indicated by Li *et al.*, 2010. Interactions between the zeolite's silanol groups and the cellulose alcoholic groups also leads to the elongation and narrowing of the peak at 1122.57 cm^{-1} as it progresses towards lower wave numbers (Christidis *et al.*, 2003; Banwell, 1983; Sanaeepur *et al.*, 2014; Ibrahim *et al.*, 2005; Madejova, 2003; Farmer, 1974; Mozgawa *et al.*, 2005; Han *et al*., 2011; Mahmoudian *et al.*, 2012; Mahmoudian *et al.*, 2012; Reynolds Research Group, 2012).

Table 4.1:.FTIR Spectra of zeolites (Christidis *et al.*, 2003; Banwell, 1983; Sanaeepur *et al.*, 2014; Ibrahim *et al.*, 2005)

Wave number (cm^{-1})	**Functional Group**	**Transformation**
1020.34	Si (Al)- O- Si (Al) (siloxane/ aluminoxane)	stretching vibrations
796.60/ 777.31	- Si – O group	bond bending
1627.92	H-O- H (water)	Bending
3300-3700	-OH (hydroxyl group)	Stretching

Table 4.2: FTIR Spectra of cellulose acetate (Christidis *et al.*, 2003; Banwell, 1983; Sanaeepur *et al.*, 2014; Ibrahim *et al.*, 2005)

Wave number (cm^{-1})	**Functional Group**	**Transformation**
3329.14	OH (hydroxyl group- high concentration)	bending in plane
2918.30/ 2848.86	CH=CH (methylene group)	asymmetric stretching
1732.8	C= O (aldehyde/ ketone on 6-membered ring)	scissoring/ bending in plane
1635.64	C (O) O^- (carboxylate group on acetic acid)	asymmetric stretching
1371.39	CH_3 (methyl groups on cellulose)	bending vibrations
1085.92/ 1122.57	C–OH (cellulose alcoholic bond)	bending vibrations
896.9	β- Link (cellulose)	Stretching

4.3 Powder X-Ray Diffraction Crystallography (XRD)

Powder XRD crystallography reveals the signature crystal patterns of materials in powder form which could be used to characterize material. According to the Joint Committee on Powder Diffraction Standards (JCPDS), the characterized zeolite showed a signature pattern for the material with the following formula: $Na_2Al_2Si_{1.85}O_{7.7}$:$5.1H_2O$/$Na_2O.Al_2O_3$:$1.85SiO_2 5.1H_2O$ which will simply be referred to as Sodium Aluminum Silicate Hydrate. The X- Ray crystallographic spectrum for zeolite shows high crystallinity with distinctive 2 theta peaks at 7.44°, 10.44°, 12.72° and 16.38° among others. An increase in the 2 theta angle leads to a decrease in the inter-atomic d- spacing in the crystal lattice (Gramlich & Meier, 1971; Treacy & Higgins, 2001; Alexandre & DuBois, 2000). This can be correlated to the Braggs equation:

$\lambda = 2d \sin \Theta$… Equation 4.1

Where: λ = incident x- ray wavelength (1.5418Å); d is the inter-atomic lattice spacing; and Θ is the angle the incident x-rays form against the horizontal sample surface. XRD data of pristine zeolites is elaborated in Figure 4.4.

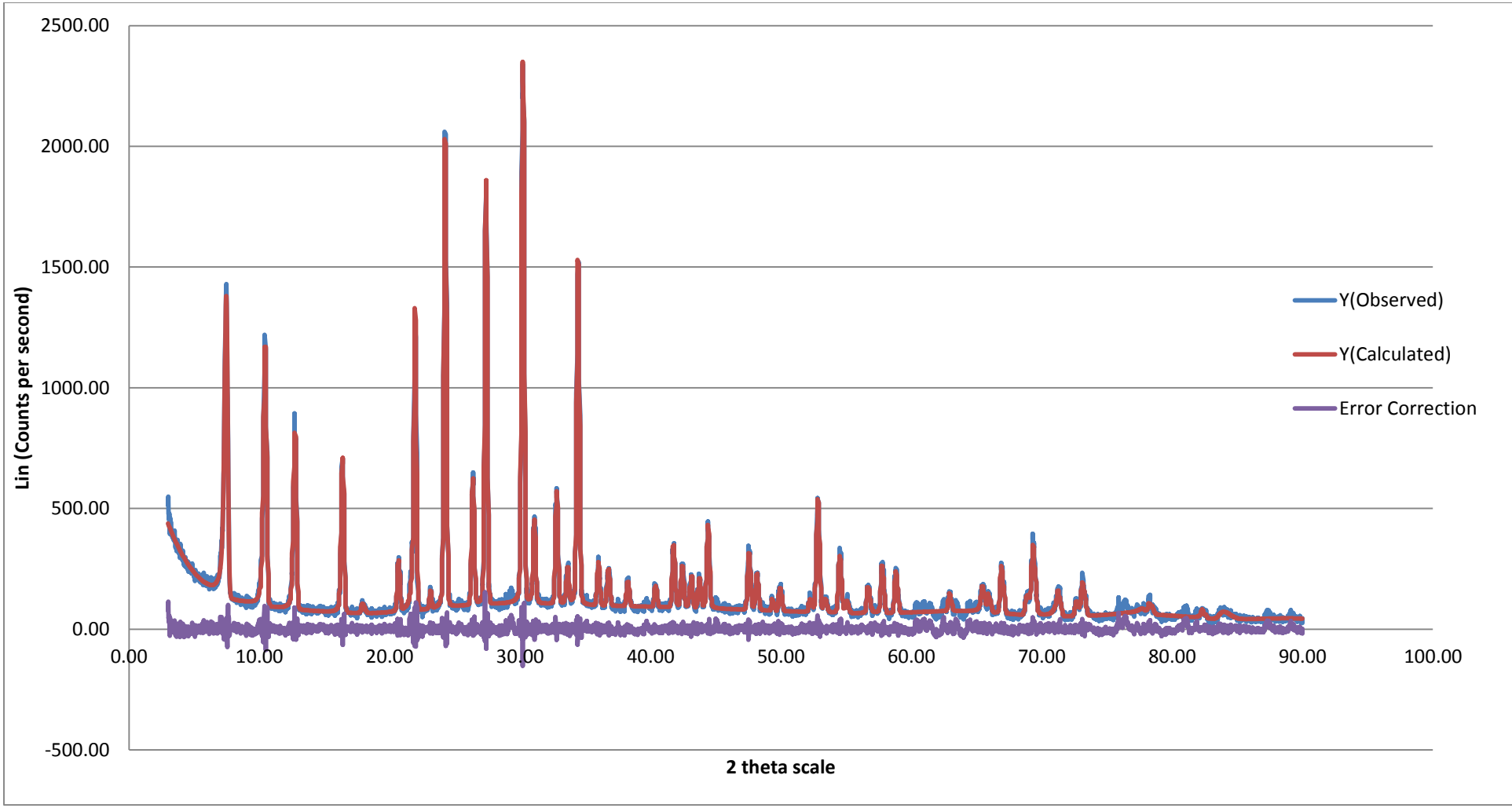

Fig 4.4: XRD Spectrum for pristine zeolite.

Spectra for the nanocomposites at different zeolite loadings (10%, 20% and 30%) were analysed. The characteristic XRD peak for cellulose can be seen which appears as a bulge at 14.9^{o} (small bulge) and 22.5^{o} (large bulge) 2 theta values (Li *et al.*, 2010). As the zeolite loading increases from 10-20%, the peaks become longer and sharper while the cellulosic bulge is suppressed. However, there is little change in the magnitude of the peaks between 20% and 30% zeolite loading. This may mean that there is maximum intercalation at 20% loading. The cellulosic bulge is however suppressed considerably between these two loading percentages as seen in figure 4.5a, 4.5b and 4.5c.

The 2 theta angles for the nanocomposite are significantly lower than for those of the pristine zeolite materials. This is brought about by intercalation which increases the d-spacings of the lattice as reported by Alexandre & DuBois, 2000 (2000) (Figure 4.6).

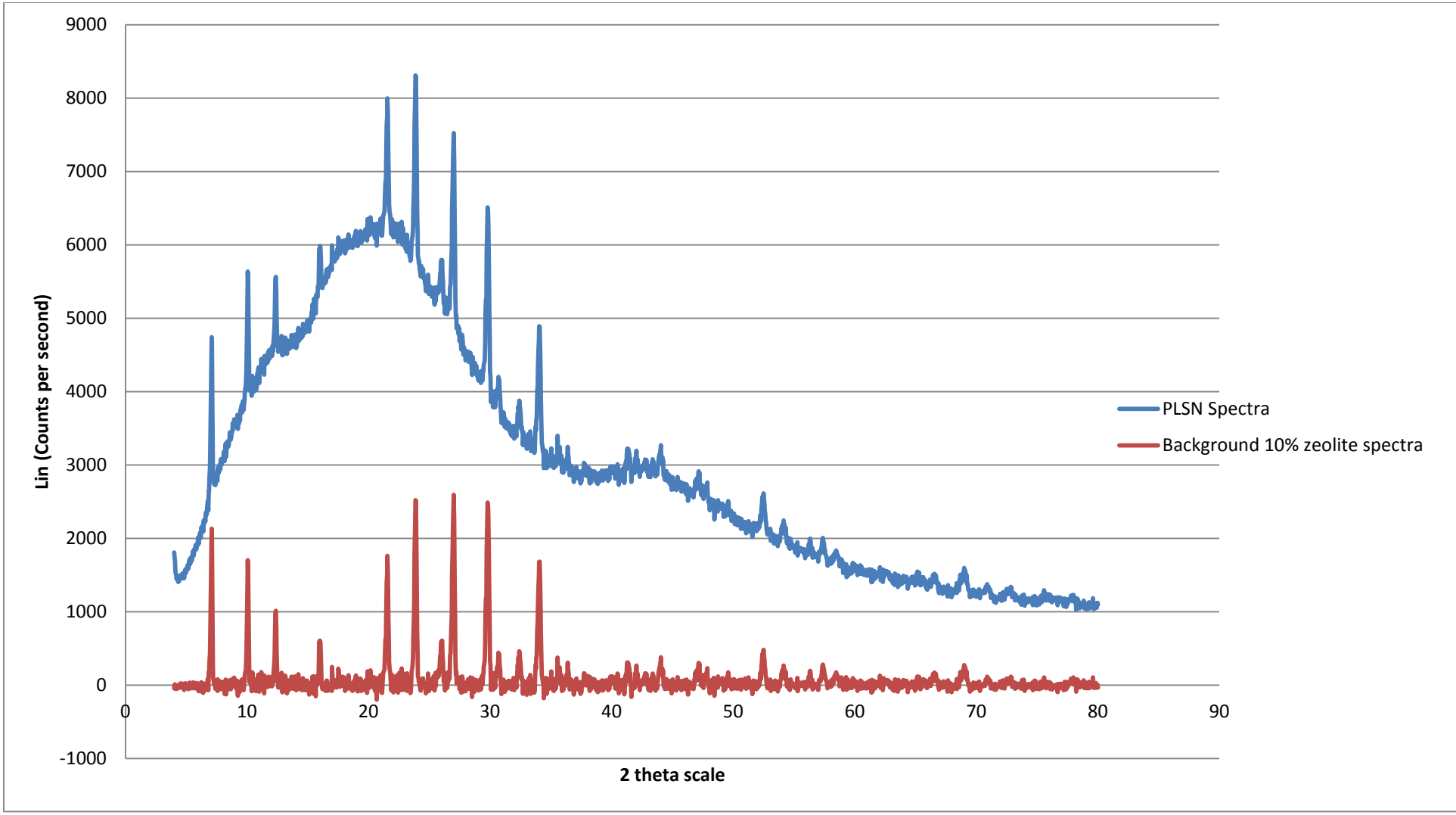

Fig 4.5a: Polymer Layered Silicate Nanocomposite with 10% zeolite loading

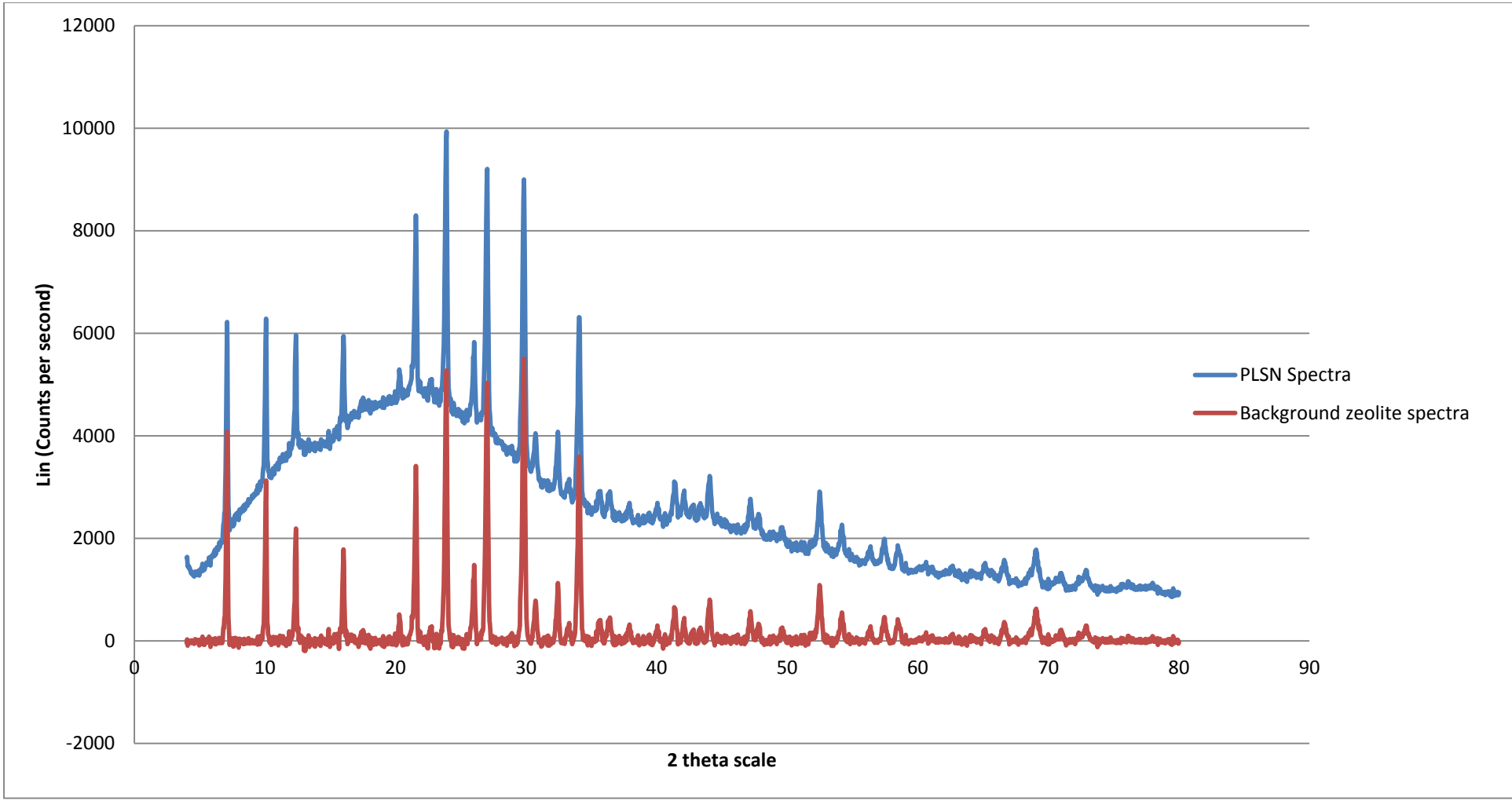

Fig 4.5b: Polymer Layered Silicate Nanocomposite with 20% zeolite loading

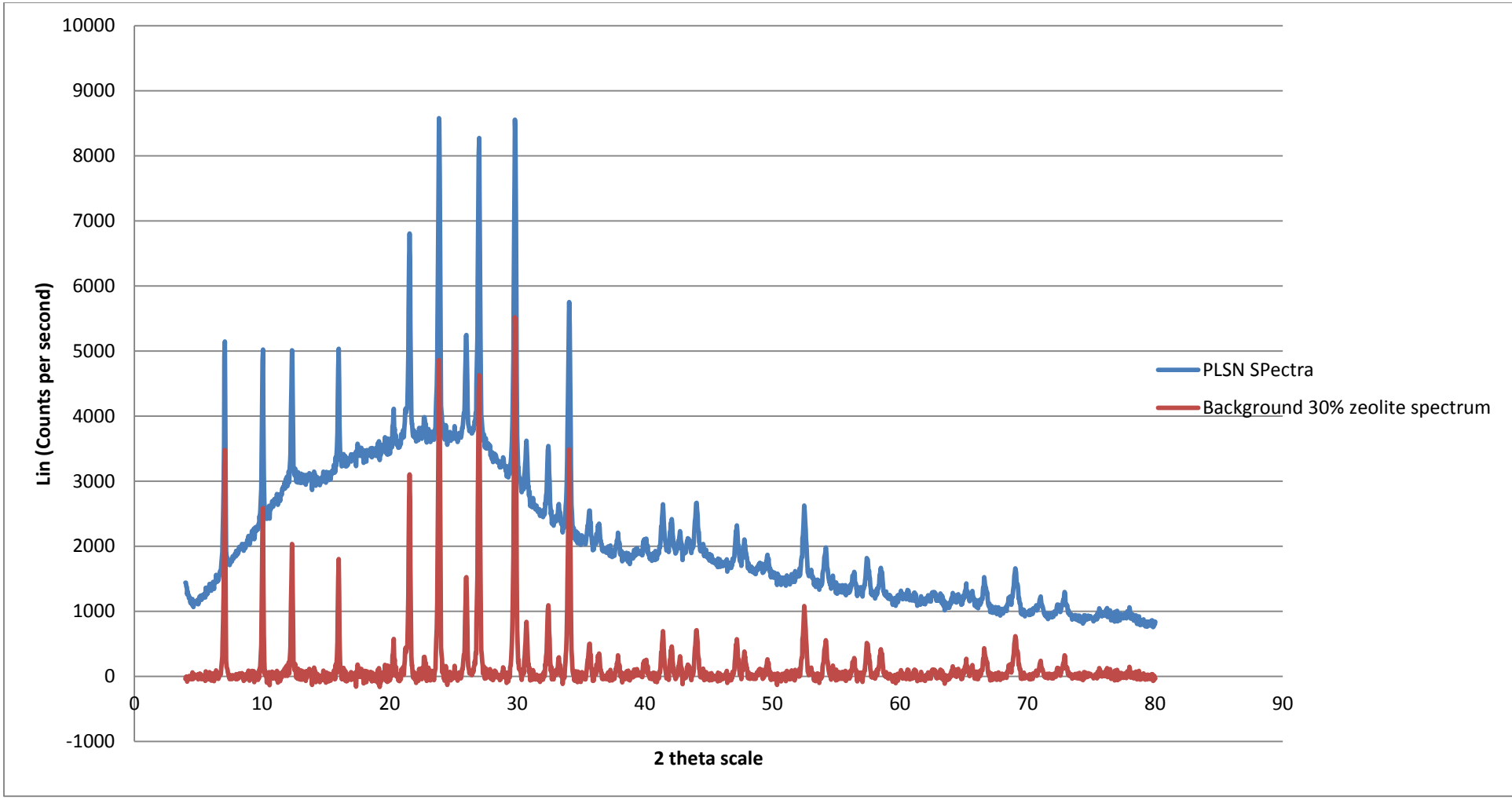

Fig 4.5c: Polymer Layered Silicate Nanocomposite with 30% zeolite loading

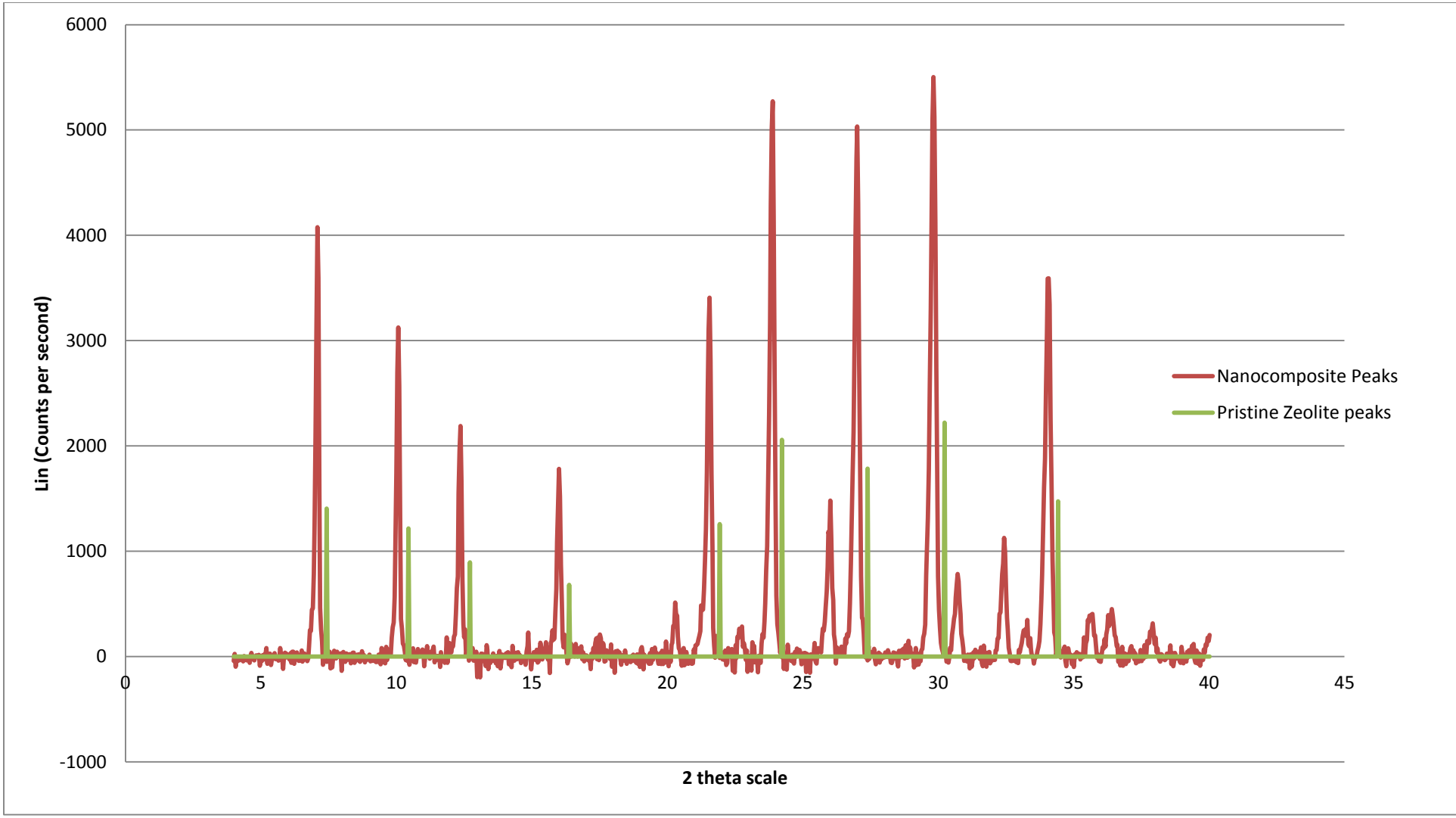

Fig 4.6: XRD Spectra comparing the peaks of pristine zeolite and 20% zeolite- loaded nanocomposites showing diffraction peaks shifting to lower 2 theta angles (Alexandre & DuBois, 2000)

Table 4.3 XRD data

Miller Indices (hkl)	2 theta (Zeolites)	d-spacing (Zeolites) in nm	2 theta (20% Zeolite Composites)	d- spacing (20% Zeolite Composites) in nm
200	7.44	1.188	7.09	1.247
220	10.44	0.847	10.07	0.878
222	12.72	0.696	12.37	0.716
420	16.38	0.541	16.01	0.554
442	21.94	0.405	21.56	0.412
622	24.24	0.367	23.86	0.373
642	27.38	0.326	27.02	0.33
644	30.24	0.296	29.8	0.299
840	34.44	0.26	34.05	0.263

Table 4.3 shows the relationship between the increase in the d-spacing of the crystal lattice and nanocomposite formation. This also results into the reduction of the Bragg's angle (2-theta) value.

4.4 Scanning Electron Microscopy & Energy Dispersive X-Ray Spectroscopy (SEM/ EDX)

SEM/ EDX analyses elucidates both the morphology & the elemental composition of materials. Cellulose acetate- zeolite nanocomposite morphology and elemental composition was visualized using SEM/ EDX analysis. In the analysis, pristine zeolite, 40%, 20% and 10% nanocomposite was analysed. The analysis showed a general increment in porosity of the material with the increase in the ratio of the zeolite. Nanocomposites with lower zeolite loading (Fig. 4.7) showed a smoother surface with large pores under SEM while those with a higher zeolite loading (Fig. 4.8) showed a rougher surface with smaller pores.

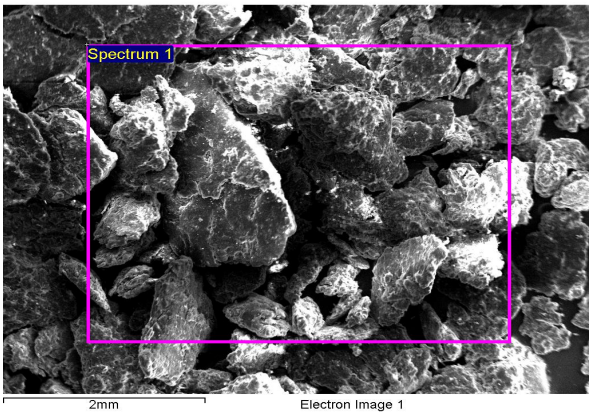

Fig. 4.7. 10% Zeolite loading

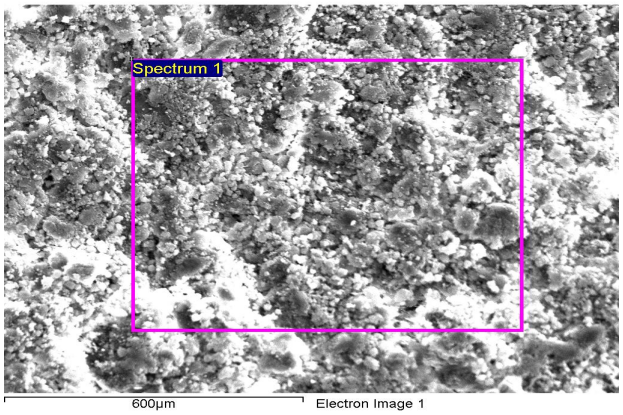

Fig. 4.8: 40% Zeolite loading

Fig. 4.9 shows the SEM micrograph of pristine zeolite showing angular crystal faces which symbolize a highly crystalline structure. Figure 4.10 shows the EDX elemental analysis of the pristine zeolite showing a high silicon, aluminum, oxygen and sodium content.

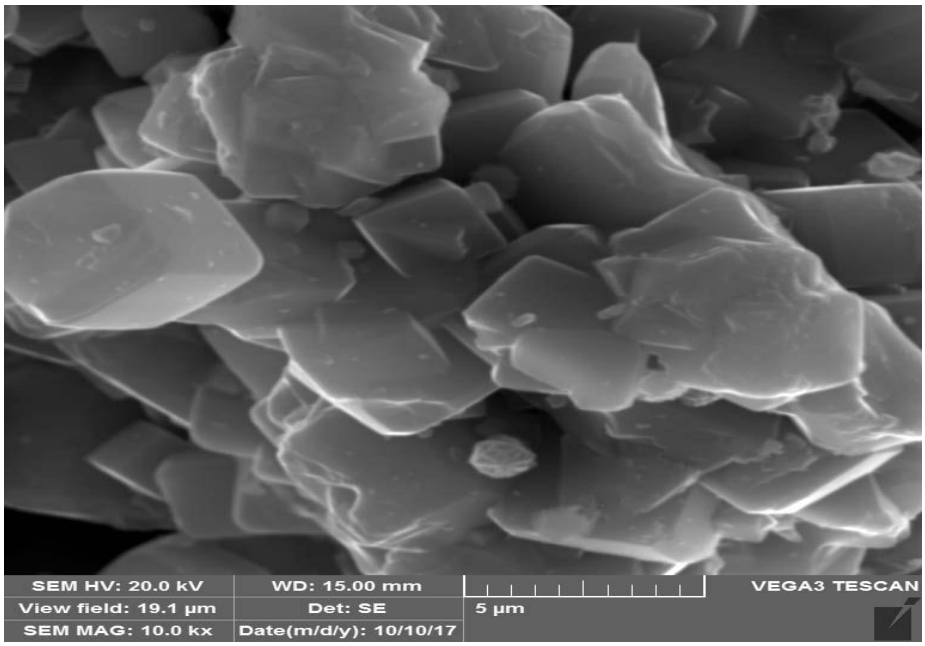

Fig. 4.9: SEM for Pristine Zeolite

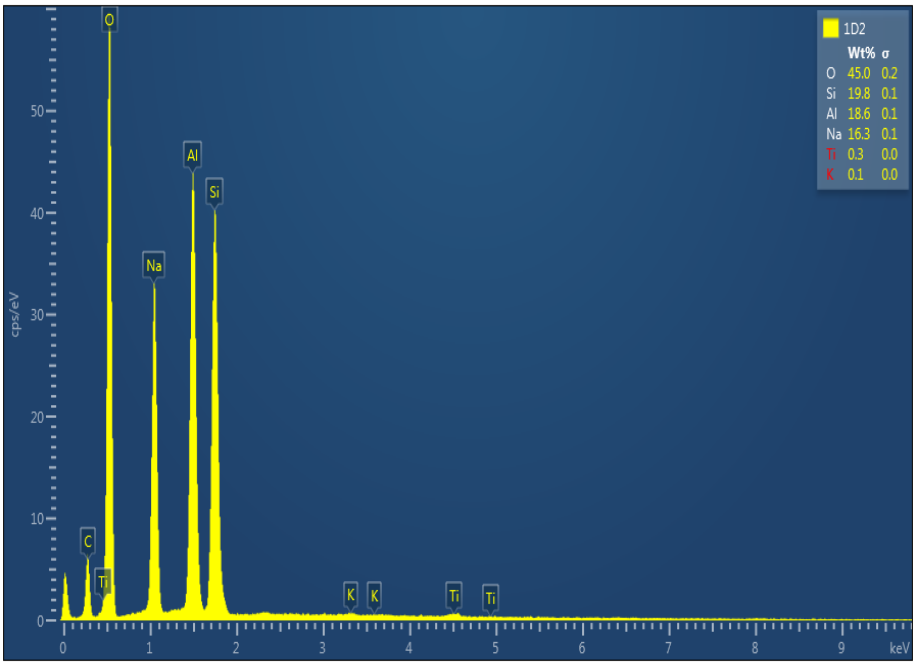

Fig. 4.10: EDX spectrum for Pristine Zeolite

Fig. 4.11 shows the SEM micrograph for nanocomposite with 40% zeolite. The morphology indicates a good dispersion of the zeolite particles within the polymer matrix. The EDX spectrum (Fig. 4.12) shows an increase in the carbon peak symbolizing the incorporation of the cellulose acetate into the nanocomposite material.

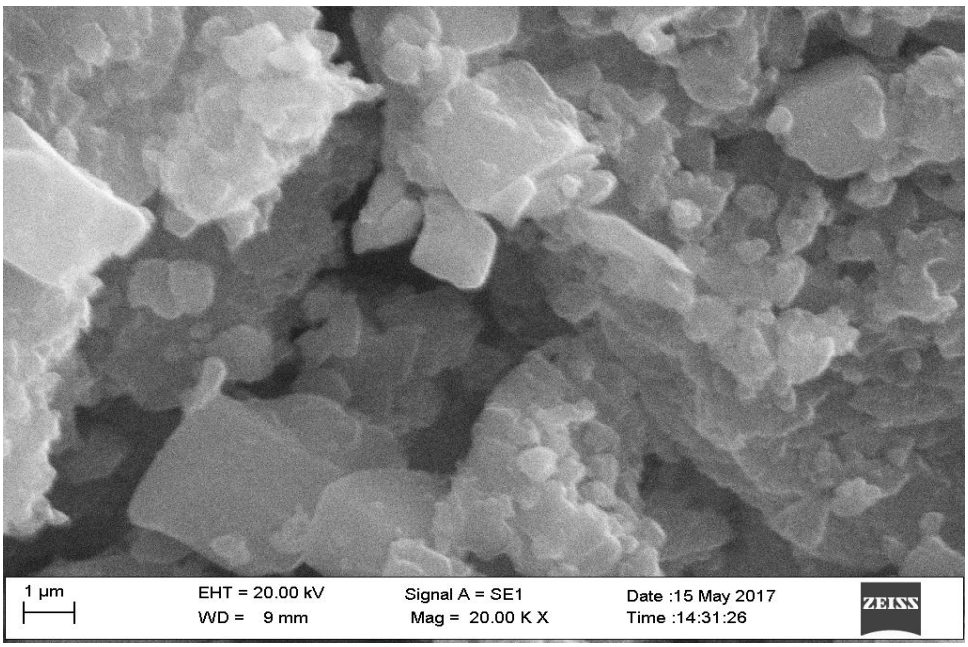

Fig. 4.11: SEM for 40% Zeolite

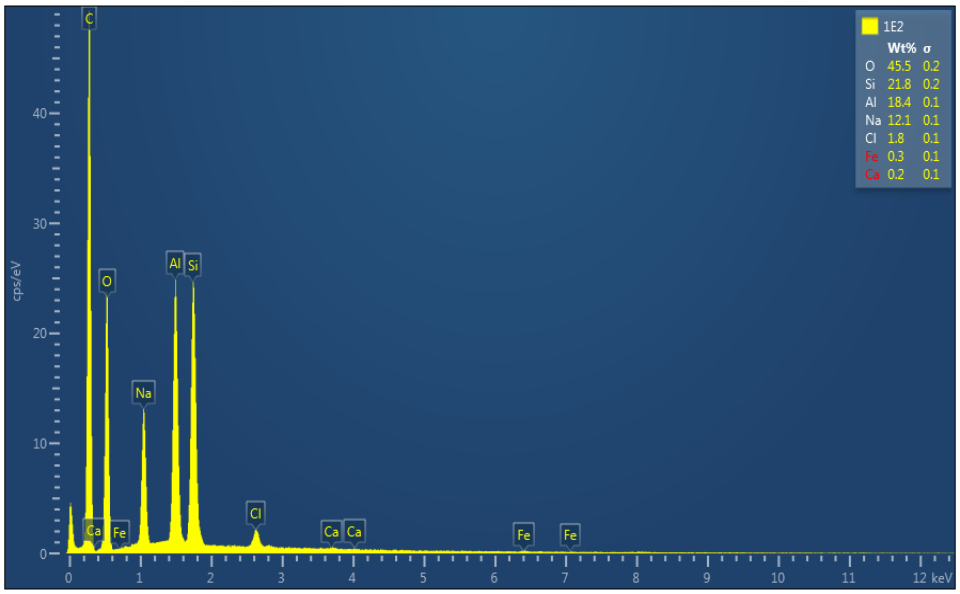

Fig. 4.12: EDX spectrum for 40% Zeolite

Fig. 4.13 shows the SEM micrograph of 20% zeolite- loaded nanocomposite. The zeolite crystals show good distribution however with a reduction in the number of pores. Fig. 4.14 shows an EDX spectrum of the 20% zeolite- loaded nanocomposite. Since the percentage of cellulose is much higher, the carbon peak is very high suppressing other elemental peaks such as those of Sodium, Aluminum and Silicon.

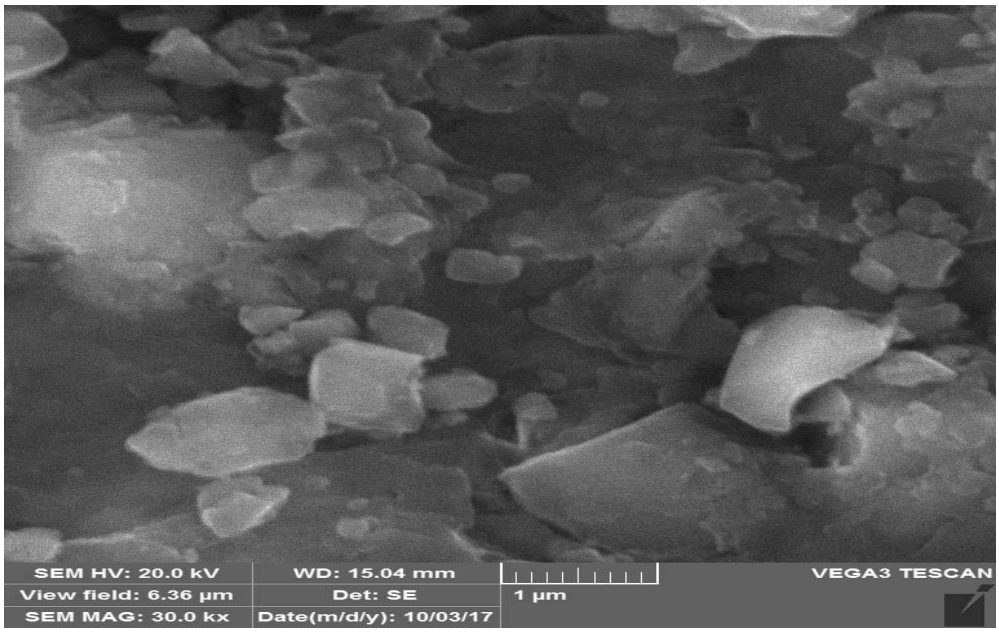

Fig. 4.13: SEM for 20% Zeolite

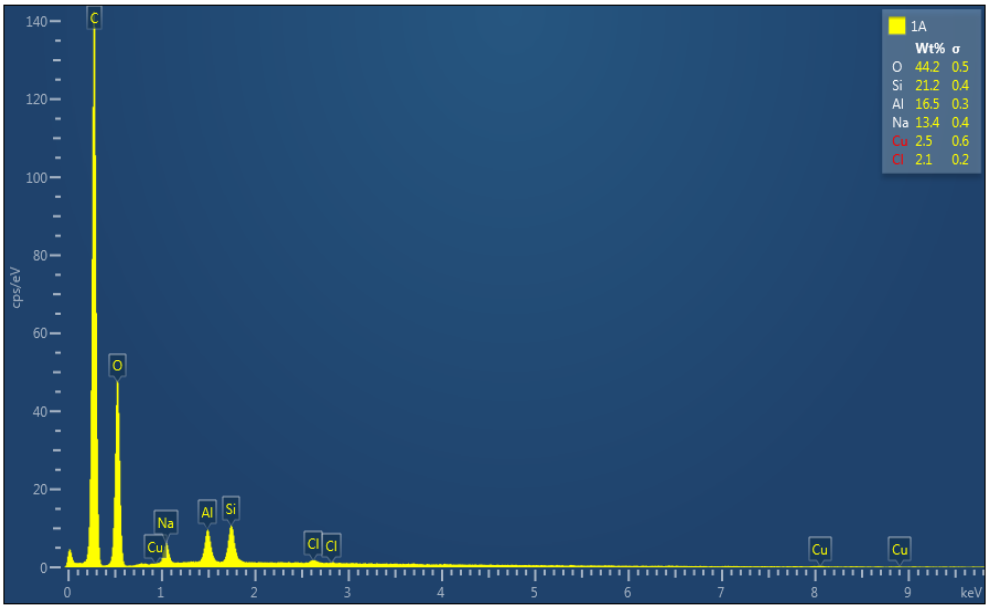

Fig. 4.14: EDX spectrum for 20% Zeolite

Fig. 4.15 shows the SEM micrograph for nanocomposite loaded with 10% zeolite. Due to poor dispersion of the zeolite crystallites, the surface of the nanocomposite is dominated by the polymer matrix. The EDX spectrum (Fig. 4.16) shows an increase in the carbon spectral peak showing the high cellulose acetate content in the material.

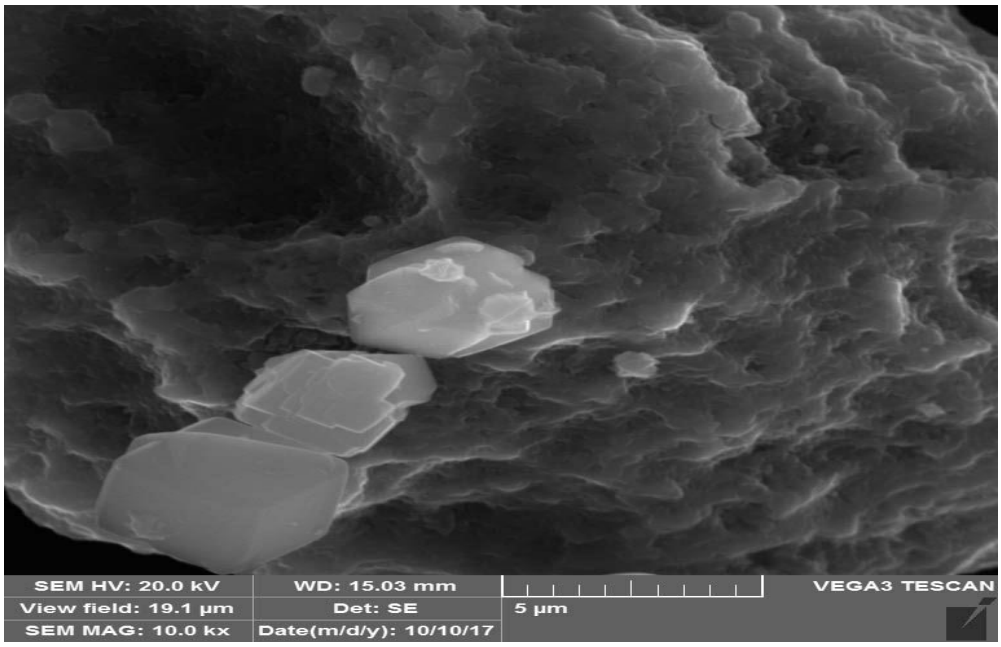

Fig. 4.15: SEM for 10% Zeolite

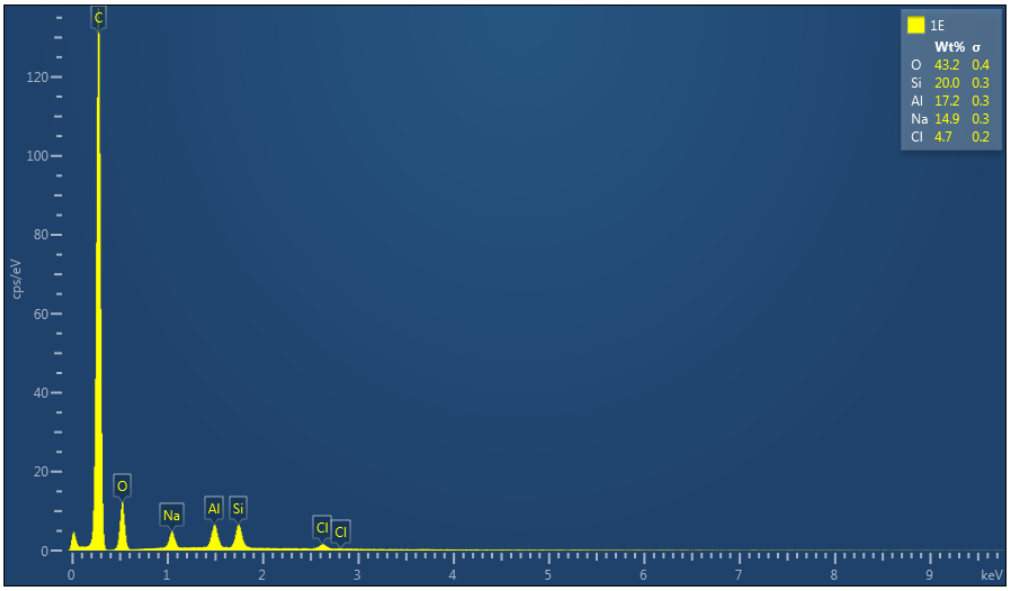

Fig. 4.16: EDX spectrum for 10% Zeolite

4.5 Batch Adsorption Experiments

4.5.1 Effect of zeolite loading on adsorption

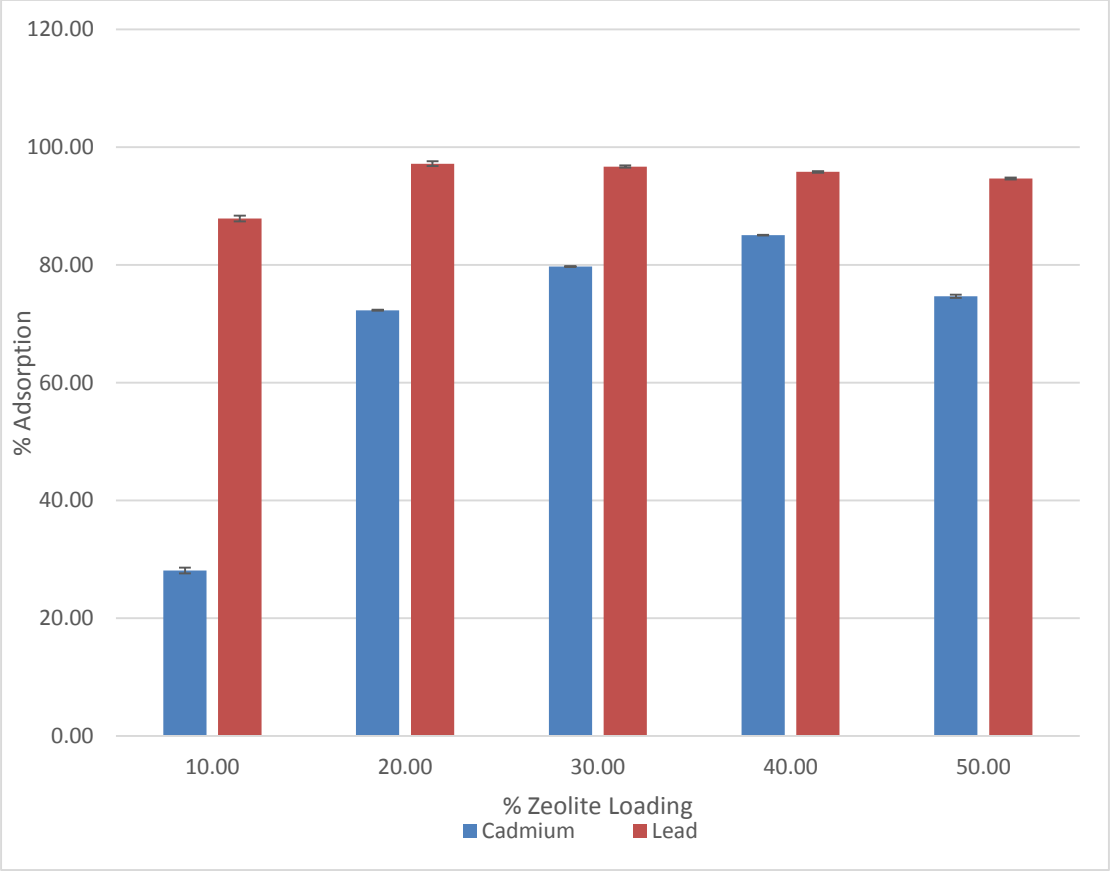

Fig 4.17: Comparative analysis of adsorption of Lead and Cadmium ions onto nanocomposites with different zeolite loadings (see Appendix 1).

According to Fig. 4.17, the optimum zeolite loading for maximum lead and cadmium adsorption was 20% and 40% respectively. 97.20% of the lead ions and 85.06% of the cadmium ions were sorbed. The adsorption behaviour for the varying ratios was Gaussian in nature with composites with 10% and 50% zeolite loading having the lowest adsorption of the metals. The maximum adsorption was at 20% for Lead and 40% for Cadmium. 10 % zeolite loading was below the optimum polymer- silicate mixing ratio for maximum intercalation to occur as displayed by the FTIR and XRD diagrams. Above 40% zeolite loading particle aggregation occurred due to their low electro-kinetic potential (zeta potential) when under neutral pH conditions (Maurer & Czarnetzki, 2001). Lead ions were also more readily adsorbed onto the 20% zeolite loaded nanocomposite. This might be because 20% zeolite loaded nanocomposite had insufficient pores

with adequate sizes to accommodate the larger tetra hydrated Cadmium ion (Kaya and Ören, 2005; Wingenfelder *et al.*, 2005). Thus the maximum adsorption of hydrated Cadmium ions occurred with a zeolite loading of 40%.

4.4.2 Effect of contact time on adsorption

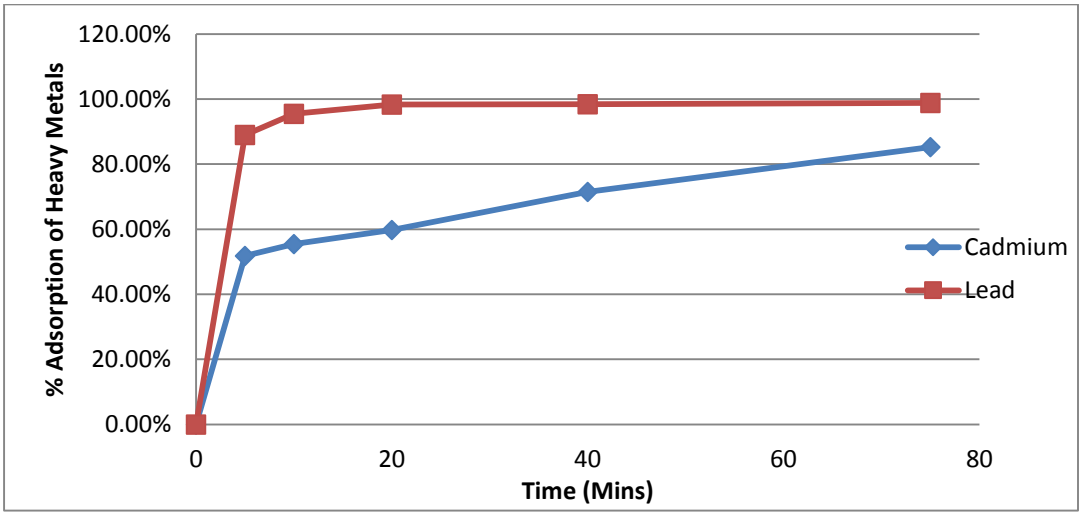

Fig. 4.18: Comparative analysis of lead and cadmium sorption against time (See Appendix 2).

Figure 4.18 shows that the metal adsorption was rapid during the first 20 minutes because of abundant available sites for metallic adsorption. With time the sites became occupied and the adsorption slowed down until saturation was reached (Sharifipour *et al.*, 2015). Zeolites have a higher affinity for lead as compared to cadmium as illustrated by the following series: Pb^{2+} >Cu^{2+} >Cd^{2+} >Zn^{2+} >Cr^{3+} >Co^{2+} >Ni^{2+} (Inglezakis *et al*, 2002). They seem to have a higher affinity for metals with a larger ionic radius as described by Panayatova &Velikov (2002). In the study of adsorption of lead with time, it is observed that initially adsorption increases linearly with time. Very high initial adsorption rates were recorded before the adsorption values reached a plateau (Buasri *et al*, 2008). The initial sorption of metals is very fast followed by a slower rate of sorption where mush smaller amounts of the metal are taken up (Hamidpour *et al*, 2010). This happens due to rapid initial occupation of the available sorbent sites. This process results into a saturation of the sorbent sites leading to attainment of equilibrium (Zhang & Hou, 2008). As also reported by Kaya and Ören, 2005; Wingenfelder *et al.*, 2005, the adsorption large size of the cadmium nitrate tetra hydrate ion onto the zeolite is hindered by small pores.

4.4.2.1 Kinetic models for lead adsorption onto nanocomposites (See Appendix 3)

The adsorption of Lead onto nano-zeolites was plotted on both pseudo first order and pseudo second order kinetic models. The results are indicated in figures 4.19 and 4.20 below.

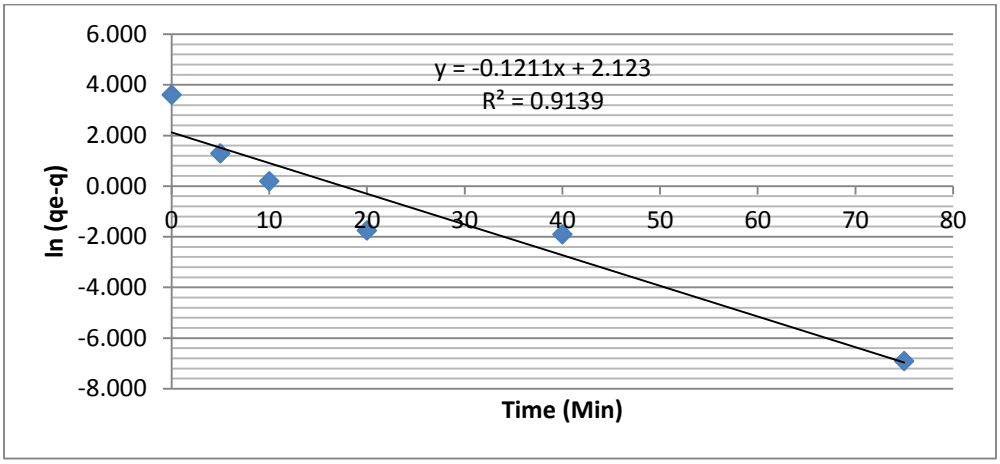

Fig 4.19: Pseudo First Order Kinetic Model for Lead adsorption onto nanocomposites.

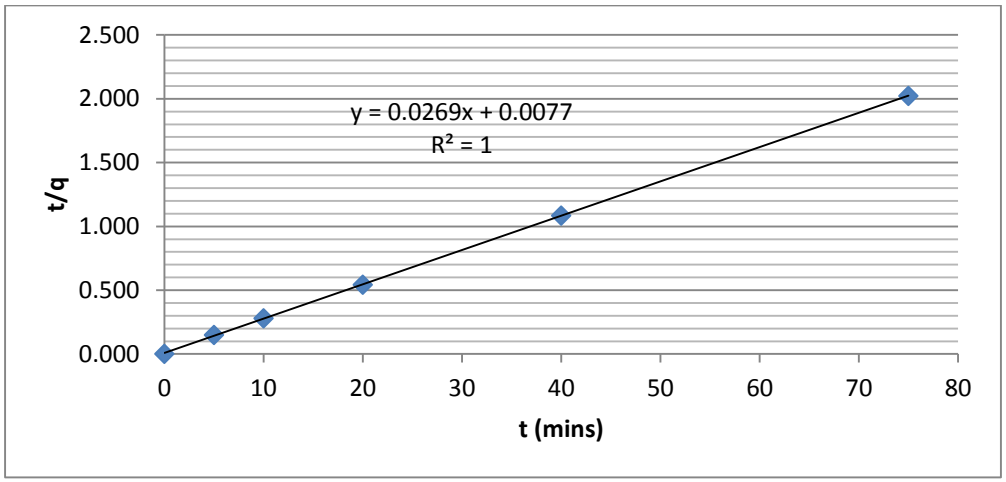

Fig 4.20: Pseudo Second Order Kinetic model of Lead adsorption onto nanocomposites.

The R^2 for the Pseudo first order plot was 0.913 (figure 4.20) while that for pseudo second order was 1. Metal adsorption onto zeolites had a better pseudo second order kinetic model fit as reported by both Sharifipour *et al* (2015) and Robati (2013).

4.4.2.2. Kinetic models for cadmium adsorption onto nanocomposites (See Appendix 3)

The values for Cadmium adsorption from solution by nanocomposites were also fitted into the pseudo first and pseudo second order kinetic models. The results are indicated in figures 4.21 and 4.22 below.

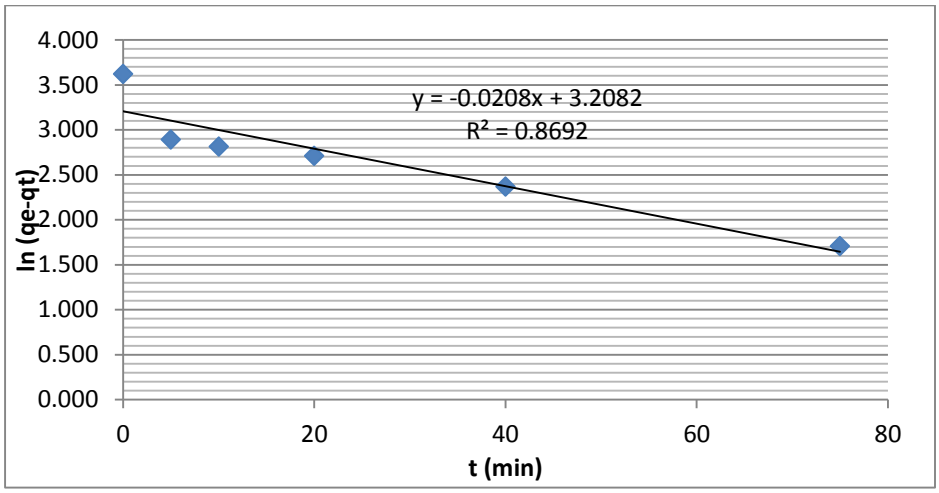

Fig 4.21: Pseudo First Order Kinetic model for Cadmium adsorption onto nanocomposites.

The correlation for the pseudo first order model was 0.852 while that of the pseudo second model was 0.982. The adsorption of cadmium also follows a pseudo second order model in agreement with Chandra Rao *et al*, (2006).

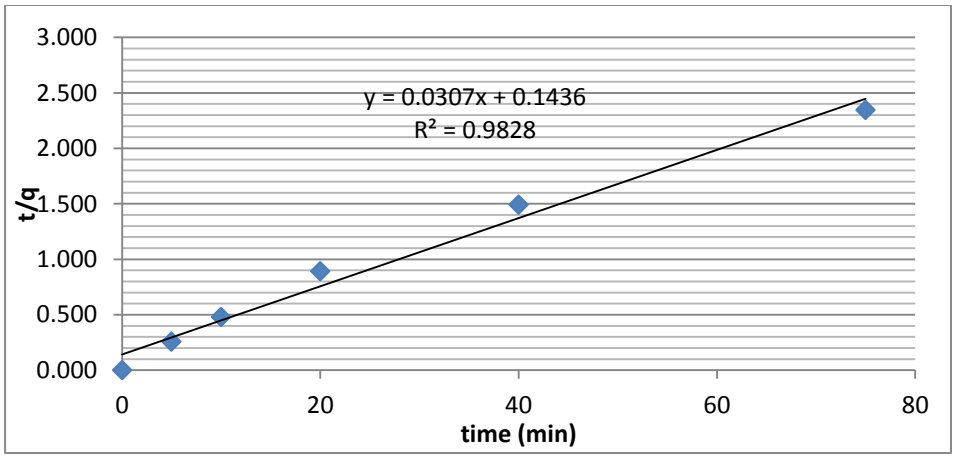

Fig 4.22: Pseudo Second Order Kinetic model for the adsorption of cadmium onto nanocomposites.

Table 4.4: The rate constants values from the pseudo order kinetic model for lead and cadmium ions adsorption

	Pseudo first order parameters		**Pseudo second order parameters**	
Metal ion	k_1 (s^{-1})	R^2	k_2 ($M^{-1}.s^{-1}$)	R^2
Pb^{2+}	0.121	0.913	0.0966	1
Cd^{2+}	0.020	0.869	0.0063	0.982

The k constant for the pseudo order kinetic equations is a number that describes the attainment of equilibrium by reactions over time. The pseudo-first order constant, k_1 describes the equilibrium attainment when there is only one rate-limiting reactant while the pseudo second order constant, k_2 is important when there are two rate-limiting reactants. k_2 is lower than k_1 because it displays a higher sensitivity (Aly *et al.*, 2014; Aly & Luca, 2013). The units for the pseudo first order reaction (k_1) is s^{-1} while that of the pseudo second order reaction (k_2) is $M^{-1}.s^{-1}$.

4.4.3 Effect of the adsorbent mass on adsorption

The percentage adsorption against the mass of the adsorbent for both Lead and Cadmium ions were fitted in a graph as shown in figure 4.23 below. The comparison between adsorption capacity and mass is depicted in figure 4.24.

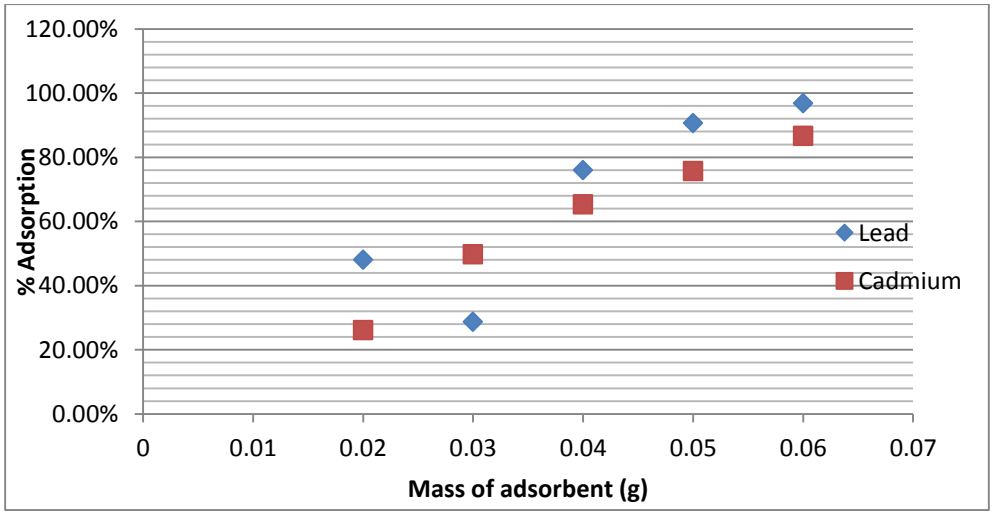

Fig 4.23: Comparative adsorption of Lead and Cadmium ions onto varying masses of zeolite nanocomposites (See appendix 4).

Metal removal from solution increased with the dosage of the adsorbent (Figure 4.23) due to an increase in adsorbent sites allowing for a higher metallic uptake by the adsorbent (Kaya and Ören, 2005; Sari *et al*. 2007; Almeida *et al*, 2009).

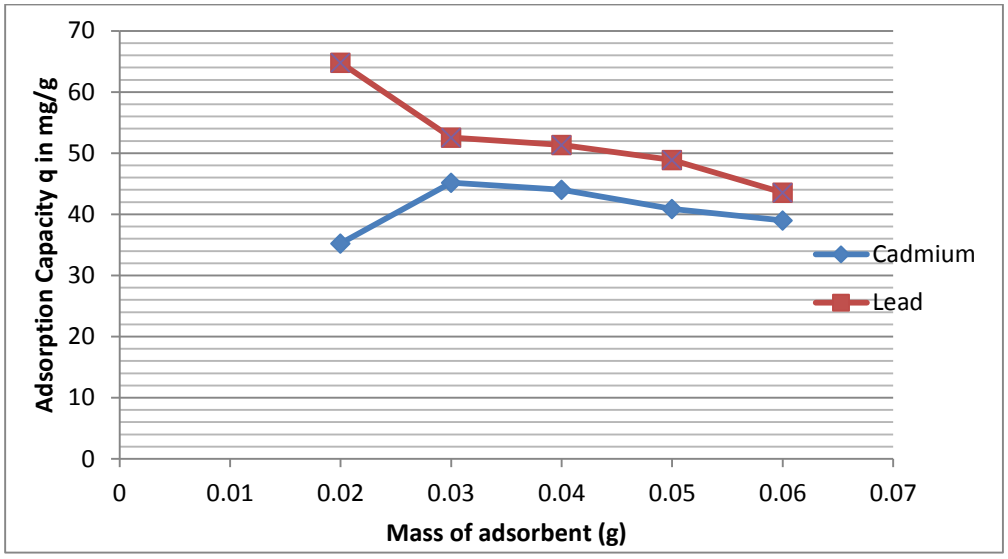

Figure 4.24: Mass of adsorbents vs adsorption capacity for metallic ions onto nanocomposites.

The increase in the mass of sorbent reduced the amount of ions sorbed per unit weight of sorbent (Fig. 4.24). This happened due to overcrowding and overlapping of adsorbent particles as their mass increased which led to overlapping of active sites present at the surfaces of adsorbents (Chiron *et al*, 2003). As the mass of the adsorbent increased, the adsorbate (metal ion) had more adsorption sites at its disposal leading to the distribution of metal ions across the increased adsorbent surface thus lowering their density on the adsorbent. Therefore, according to Chen *et al* (2010), the decrease in adsorption capacity (q_e) at higher dosage is because of unsaturation of adsorbent sites because of increase in adsorbent mass. The adsorption of cadmium ions at a lower adsorbent dosage were impeded probably due to the large cadmium nitrate tetra-hydrate ions having few adsorption sites due to the low adsorbent dosage. At low adsorbent dosage, percentage adsorption of lead was higher than for cadmium. At lower adsorbent masses, the adsorption of cadmium was curtailed because of the ionic size of the salt used (cadmium nitrate tetrahydrate).

4.4.4 Effect of varying metallic ion concentration on adsorption

The values for varying adsorption of both Lead and Cadmium dependent on the metallic ion concentration are depicted in figures 4.25 and 4.26.

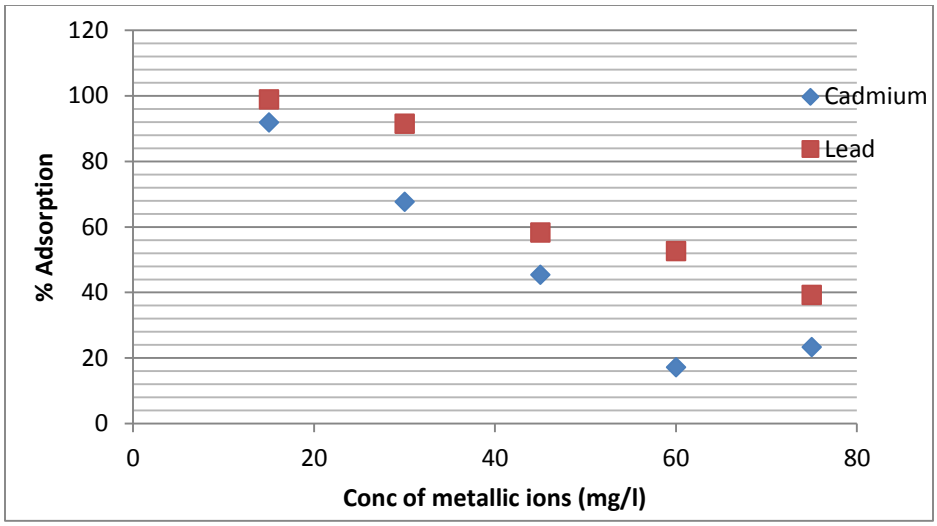

Fig. 4.25: Comparative Adsorption of Lead and Cadmium ions on varying concentrations of metallic ions in solution (See Appendix 5).

Varying metallic concentrations is a good way to determine the nature of an adsorbent. K_d values illustrate the ratio between the ions adsorbed onto the nanocomposite at equilibrium (q_e) and the ions in solution at equilibrium (C_e). The K_d values (q_e/ C_e) increase with the dilution of metal ions in solution (Figure 4.25). Higher K_d values at lower metallic concentrations is because of adsorption sites having higher binding energies and selectivity for ions. However, at higher concentrations, there is a reduction in binding energy because of occupation of sorption sites resulting into lower K_d values (Shaheen *et al.*, 2009; Saha *et al.*, 2002). At higher concentrations, the ratio of occupied adsorption sites to the non-occupied ones was less as compared to the number of adsorbate particles present in solution. Therefore, diffusion of these adsorbates (Pb^{2+} and Cd^{2+}) through the active pore sites of the adsorbent became highly competitive and the saturation of these sites was rapidly attained resulting in low percentage removal of the heavy metals (Nameni *et al.*, 2008; Tiwari *et al.*, 2007). There was a higher cation uptake at lower concentrations because of more adsorption sites being available. At higher concentrations, the metal ions saturated the adsorption sites resulting into a low cation uptake and decreased adsorption rate (Gunay *et al.*, 2007).

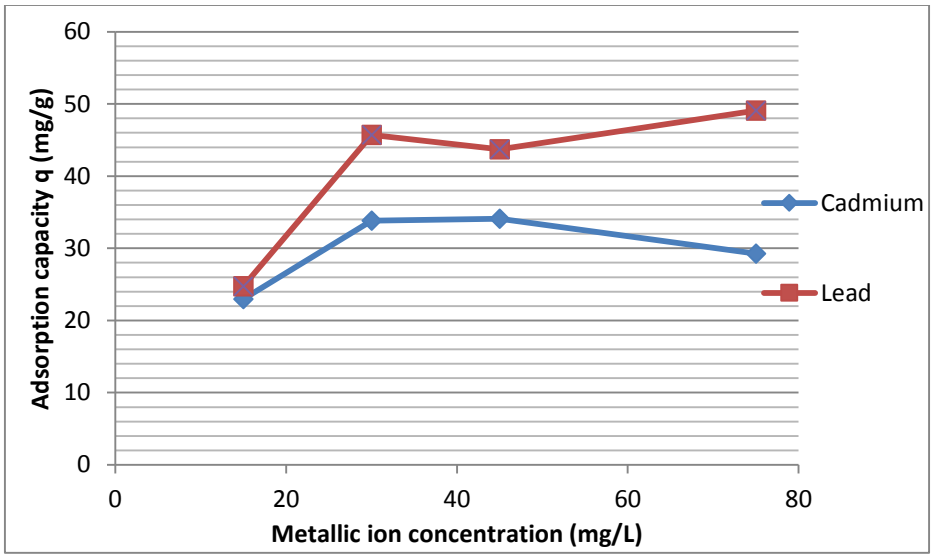

Figure 4.26: Adsorption capacity of nanocomposite vs concentration of metallic ions.

The relation between the adsorption capacity of the adsorbent and metal concentration has been evaluated. Adsorption capacity generally increased as the concentration of ions in solution also increased (Ali *et al.*, 2012; Naidu *et al.*, 2013). This is because at a higher metallic concentration, the probability of adsorbate- adsorbent collision and subsequent adsorption is much higher than when the metal concentration was low (Isa, *et al*., 2008). There was however a lower adsorption capacity demonstrated at higher cadmium ion concentrations probably due to the cadmium nitrate tetra-hydrate ions being inhibited due to their size. It can also be seen from figure 4.26, the percentage adsorption of cadmium onto the zeolite reduces for higher metallic concentrations compared to lead. The adsorbent demonstrates a lower adsorption capacity of cadmium adsorption at higher concentrations due to the large size of the cadmium salt used (cadmium nitrate tetrahydrate).

4.4.5 Effect of pH on adsorption.

The adsorption of both Lead and Cadmium was determined under different pH conditions as indicated in Figure 4.27 below.

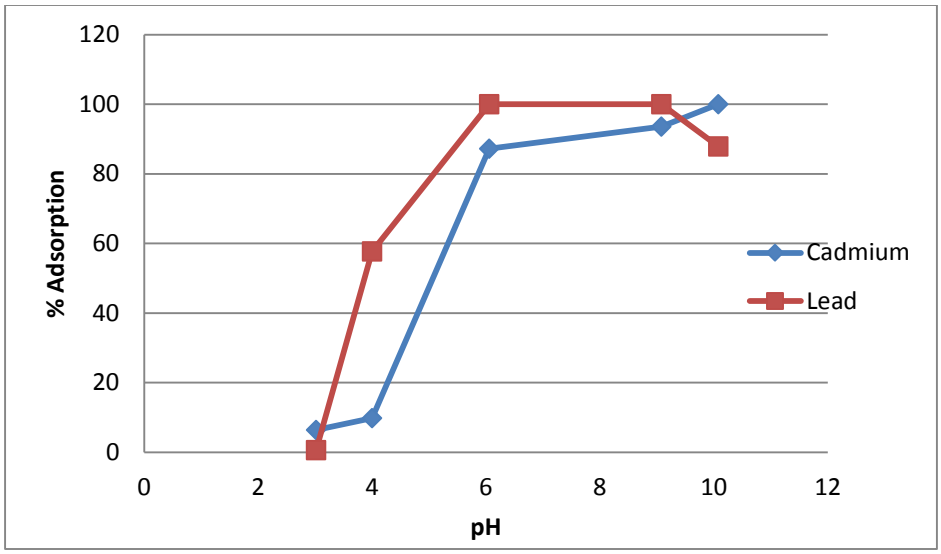

Fig 4.27: Effect of pH on the adsorption of Lead and Cadmium ions onto nanocomposites (See Appendix 6).

Figure 4.27 shows the percentage adsorption as a function of pH value. At very low pH, very little adsorption takes place. The percentage increase in adsorption with an increase in pH until at a pH of 8 where maximum removal of lead takes place. Cadmium removal is maximum at a pH of 10 due precipitation of the hydroxide. At low pH of 3 and below, the zeolite surface is occupied by H^+ ions which make it harder for metallic adsorption to take place (Tobin *et al.*, 1984) because of high binding site competition between the hydrogen ions (H^+) and the metallic species (M^{2+}) (Yakout & Ali, 2011). Adsorption of Cd^{2+} and Pb^{2+} onto the Zeolites generally increases as the pH increases. When the pH > 6, the percentage removal of metals was high due to precipitation of metals complexes (Sparks, 2003). At low pH (<4), the predominant cadmium species is Cd^{2+}. Other species such as $Cd(OH)_2$ and $Cd(OH)^+$ exist in very small amounts. There is competition between H^+ and metallic ions for uptake onto adsorption sites (Kaya and Ören, 2005). Almost no Cd^{2+} removal was found when the operated pH was in more acidic conditions (pH 2) (Yao-Jen *et al.*, 2012). Lead was best removed at pH• 6-9, when the prevailing species were Pb^{2+}. When the pH>10, there is a slight decrease in the uptake of lead because of anionic hydroxo- complexes formation such as $Pb(OH)^{6-}$ which have a low affinity for the cation exchange sites on the zeolites. Cadmium of the other hand does not form these complexes thus ends up being more effectively (Morel and Hering, 1993) removed by precipitation at very high pH values where $Cd(OH)_2$ species prevail (Vaca-Mier *et al.*, 2001). The higher removal of cadmium as compared to lead at high pH can therefore be due to the ease of precipitation of Cadmium ions as compared to the Lead

ions and not adsorption onto the zeolite nanocomposites. The low adsorption capacity of the zeolites at pH of less than 5 can be attributed to the dissolution of the zeolite crystal structure by the acidic medium (Ali & Abidin, 2006).

4.4.6 Effect of temperature on adsorption

The percentage metallic adsorption was plotted against temperature (figure 4.28). The Van't Hoff Thermodynamic plots for the adsorption of both metals were also plotted (figure 4.29 and figure 4.30).

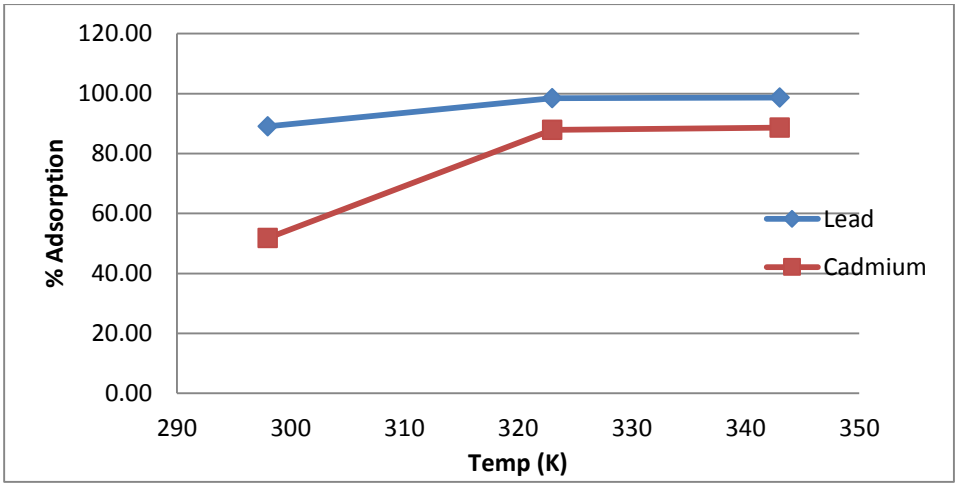

Fig: 4.28. Comparative percentage adsorption of Lead and Cadmium ions onto nanocomposites against temperature (See Appendix 7)

The Van't Hoff thermodynamic plots were used to determine whether a reaction is exothermic or endothermic in nature. They can be derived from the following expression:

$\ln K_d = \frac{-\Delta H^\circ}{RT} + \frac{\Delta S^\circ}{R}$ … Equation 4.2

Where: K_d is the adsorption constant at equilibrium; ΔH^o is the molar enthalpy of adsorption; ΔS^o is the molar entropy of adsorption; R is the ideal gas constant; T is the absolute temperature in K. The van't Hoff plot shows that metallic adsorption onto the nanocomposites is an endothermic reaction.

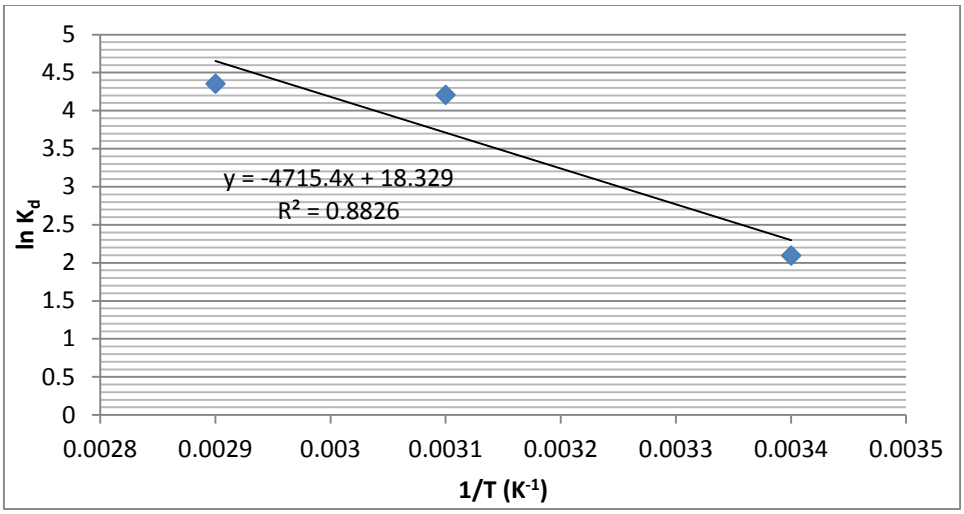

Fig 4.29: Van't Hoff Thermodynamic plot for lead adsorption onto nanocomposites.

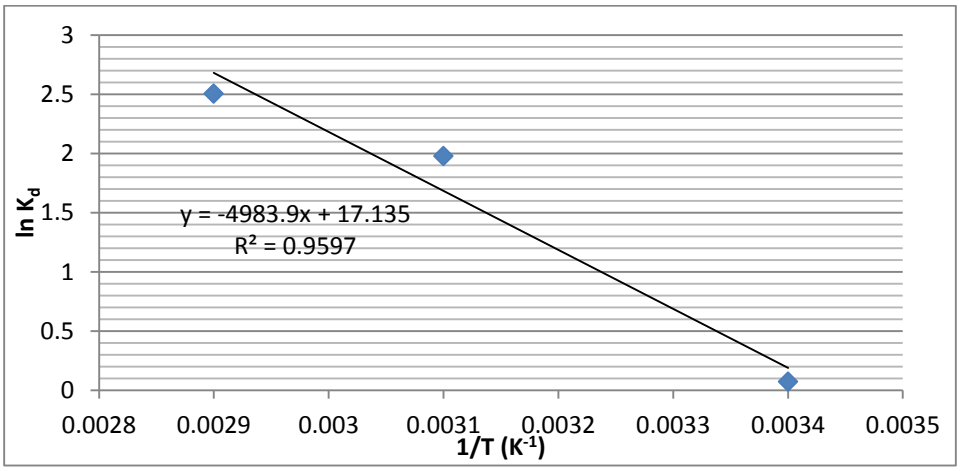

Fig 4.30: Van't Hoff Thermodynamic plot for Cadmium adsorption onto nanocomposites.

The thermodynamic parameters for the adsorption process can be represented below for both metals:

$\Delta G^o = \Delta H^o - T\,\Delta S^o$...Equation 4.3

Table 4.5: The thermodynamic parameters for the adsorption of lead and cadmium onto nanocomposite

Metal ion	**ΔH^o (kJ/mol.)**	**ΔS^o (J/mol.K)**	**$\Delta G^o_{(298K)}$**	**$\Delta G^o_{(323K)}$**	**$\Delta G^o_{(343K)}$**
Pb^{2+}	37.87	150.65	-7.024	-10.790	-13.810
Cd^{2+}	41.43	142.40	-0.887	-4.437	-7.277

The molar enthalpy of adsorption (ΔH^o) for both metals (Table 4.5) is positive signifying that the adsorption reactions are endothermic in nature. It is also above 20kJ/mol. signifying that the adsorption reactions have a greater energy requirement than normal physisorption reactions as stated by Atkins (1999) thus could be termed as weakly chemisorptive in nature. This is supported by the fact that the heavy metal cations get adsorbed onto specific sites on the nanocomposites and not generally on the surface of the adsorbent. Also, it can be noted that the energy requirement for Cd^{2+} is slightly higher than that of Pb^{2+} signifying that the affinity for Pb (II) ions for zeolite is higher than that of Cd (II) ions. The standard molar entropy of adsorption (ΔS^o) is also positive for both metals. It means that the adsorbent/ adsorbate system results in a higher increase in disorder as compared to them existing independently within the same system. However, the adsorption of Pb (II) results into a larger positive entropic change as compared to Cd (II). The higher affinity that the nanocomposites have for the Pb (II) ions is also driven by the higher increase in entropy generated by their adsorption as compared to Cd (II) ions. A lower ΔH^o and a higher ΔS^o increase the ΔG^o of the adsorption system. Pb (II) ions are more spontaneously adsorbed as compared to Cd (II) ions at all the temperatures used. Thus these results agree with the earlier obtained results that lead adsorption is higher for all the assessed parameters.

4.4.7 Effect of regeneration by acid conditioning

Regeneration of the nanocomposite was done using HCl acid. The effect of 3 cycles of regenerative adsorption by nanocomposites after regeneration is depicted in Figure 4.29 below.

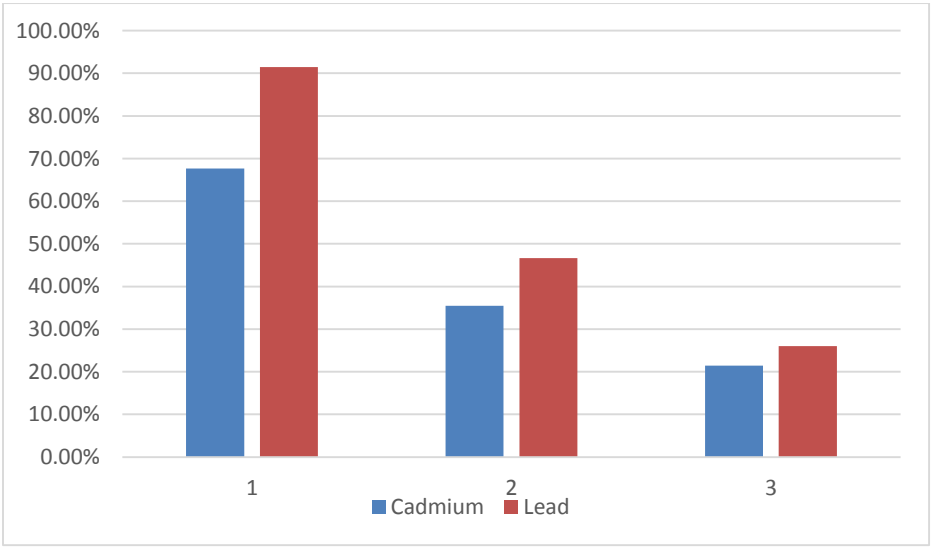

Fig 4.31: Adsorption of lead and cadmium on regenerated nanocomposites for three cycles (Appendix 8).

Acid condition of used zeolites for regeneration improved the adsorbent's cation exchange capacity due to removal of bound cations and amorphous silica fragments which would prevent adsorption (Tsitsishvili *et al.*, 1992; Athanasiadis & Helmreich, 2005). The higher affinity of the H+ ions for the zeolite pores compared to the metallic species at low pH enabled substitution of the metallic spp. with the H+ ions on the zeolite surface. In acidic medium, the hydroxonium ions replaced the bound metallic ions regenerating the nanocomposite for further adsorption experiments (Mthombo *et al.*, 2011). Lead adsorption (30ppm) from solution reduced from 91.47% (first cycle) to 46.67% (second cycle) then to 25.98% (third cycle) after regeneration due to acid conditioning. Cadmium adsorption (30ppm) from solution reduced from 65.67% (first cycle) to 35.5% (second cycle). It further reduced to 21.43% during the third adsorption cycle. This implies that the samples can be reused but with a lower adsorption efficiency. The regeneration of the adsorption sites using KCl or NaCl could be better because the Na^+ and K^+ ions are much more easily exchanged with Pb^{2+} and Cd^{2+} ions than H^+ ions in solution.

4.5 Adsorption Isotherms

Metal adsorption was fitted onto the Langmuir, Freundlich, Tempkin, Dubinin-Radushkevich and Flory-Huggins isotherms and best linear correlations determined to illustrate the adsorption behaviour.

4.5.1 Langmuir Adsorption Isotherm.

The Langmuir equation is written as follows:

$$q_e = \frac{V_m K_l C_e}{1+K_l C_e} \quad \ldots \text{Equation 4.4}$$

It can be linearized into the following expression:

$$\frac{C_e}{q_e} = \frac{1}{K_l V_m} + \frac{C_e}{V_m} \quad \ldots \text{Equation 4.5}$$

Where: C_e is the metallic concentration at equilibrium (mg/l); q_e is the metallic ions adsorbed at equilibrium (mg/g); K_L is the Langmuir isotherm constant; V_m is the maximum capacity for monolayer coverage (mg/g).

Graph Plot: $\frac{C_e}{q_e}$ vs C_e

Where:

$1/V_m$ is the slope & & $\frac{1}{K_l V_m}$ is the y- intercept.

V_m determines the usage of the adsorbent. If it is greater than 1, then it means that the ions would be removed more effectively if they have a higher concentration while if it's less than 1, then the ions would be removed more effectively if their concentration is lowered (Wallace *et al*, 2003; Malakootian *et al*, 2009). The adsorption curves of Lead and Cadmium were fitted onto the Langmuir Isotherm as shown in Figure 4.30 and 4.31.

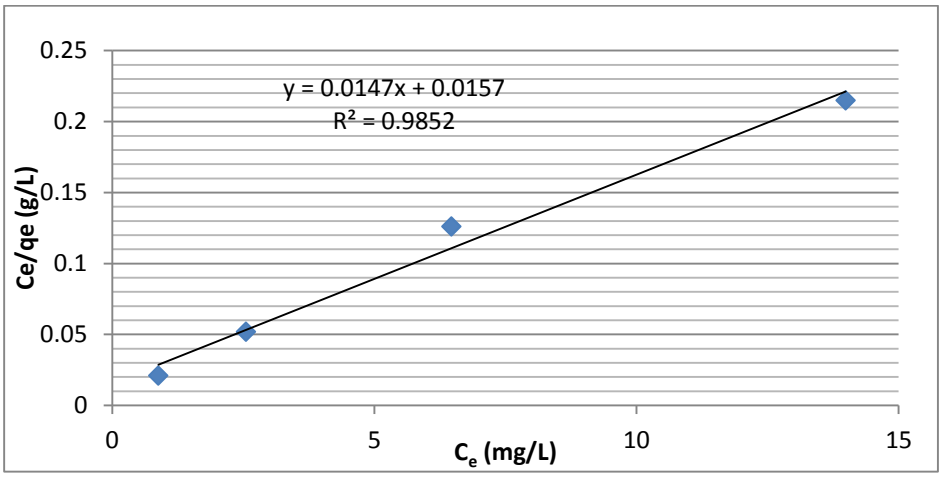

Fig 4.32: Langmuir Isotherm for Lead adsorption onto nanocomposites.

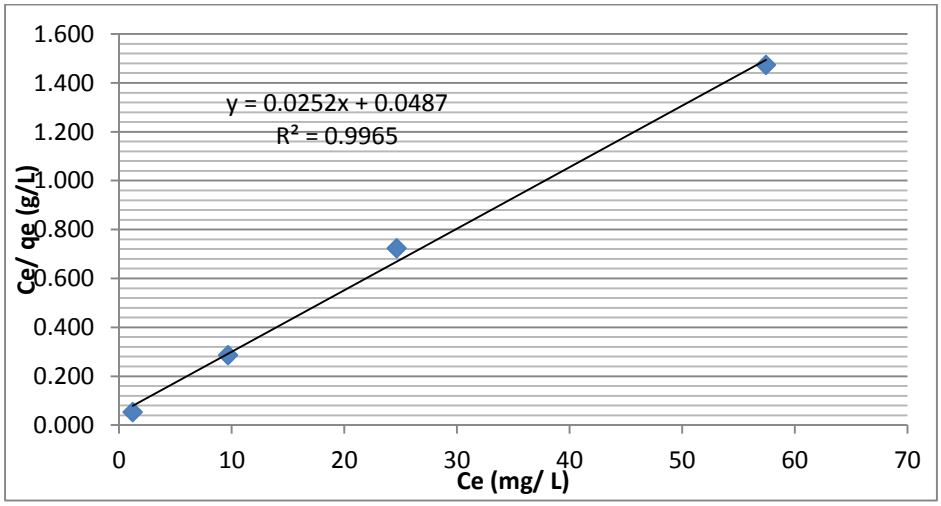

Fig 4.33: Langmuir Isotherm for Cadmium adsorption onto nanocomposites.

In the experiment, the equilibrium concentration (C_e) for the Langmuir Isotherm for Pb^{2+} was determined to be much lower than that of Cd^{2+}. Pb^{2+} had a maximum Ce of 13.99 mg/L while Cd^{2+} had a maximum C_e of 57.45 mg/L. This showed lead adsorption at equilibrium was higher than

that of cadmium. The Langmuir isotherm is the best fit for adsorption of both Pb^{2+} (Figure 4.32) and Cd^{2+} (Figure 4.20). R^2 for Cd^{2+} was 0.996 while the R^2 for Pb^{2+} was 0.985. The good fit in the Langmuir isotherm is an indication of monolayer adsorption which favors occupation of a specific number of adsorption sites (Mthombo *et al.*, 2011, 2009; Mishra *et al.*, 2013).

R_L is an important dimensionless Langmuir equilibrium parameter (Weber & Chakravarti, 1974) which can be mathematically expressed as follows in Equation 4.6:

$$R_L = \frac{1}{(1+\frac{K_l}{C_o})} \quad \text{… Equation 4.6}$$

Where: C_O is initial concentration; K_L is the Langmuir isotherm constant. The adsorption can be termed as irreversible if R_L is equal to zero, favorable if $0<R_L<1$, unfavorable when $R_L>1$ and linear when R_L is equal to 1 (Oke *et al*, 2008; Saswati & Ghosh, 2005). The adsorption nature of $Pb^{2+}$and Cd^{2+} show a favourable behaviour (Table 4.6) based on Langmuir adsorption isotherm.

Table 4.6: Langmuir Isotherm parameters for lead and cadmium adsorption onto nanocomposites

Metal ion	Langmuir isotherm constant (K_l)	Maximum monolayer coverage capacity (V_m)	R^2	Equilibrium parameter(R_L)
Pb^{2+}	0.933	71.43	0.985	0.0141
Cd^{2+}	0.521	40.00	0.996	0.0249

4.5.2 Freundlich Adsorption Isotherm

The Freundlich Isotherm equation can be written as:

$$q_e = K_F\, C_e \frac{1}{n} \quad \text{… Equation 4.7}$$

And can be linearized the following way:

$$\log q_e = \log K_F + \frac{1}{n}\log C_e \quad \text{… Equation 4.8}$$

Where: q_e is the metal adsorption capacity of the nanocomposite at equilibrium (mg of metal ion adsorbed/g of adsorbent); C_e is the metal concentration at equilibrium (mg/L); K_F and n are the Freundlich constants which determine the curvature and steepness of the isotherm.

Graph Plot: $\log q_e$ vs $\log C_e$

Where

$\frac{1}{n}$ is the slope and $\log K_F$ is the y- intercept.

The adsorption curves of Lead and Cadmium were fitted in the Freundlich Isotherm as depicted in Figure 4.34 and Figure 4.35.

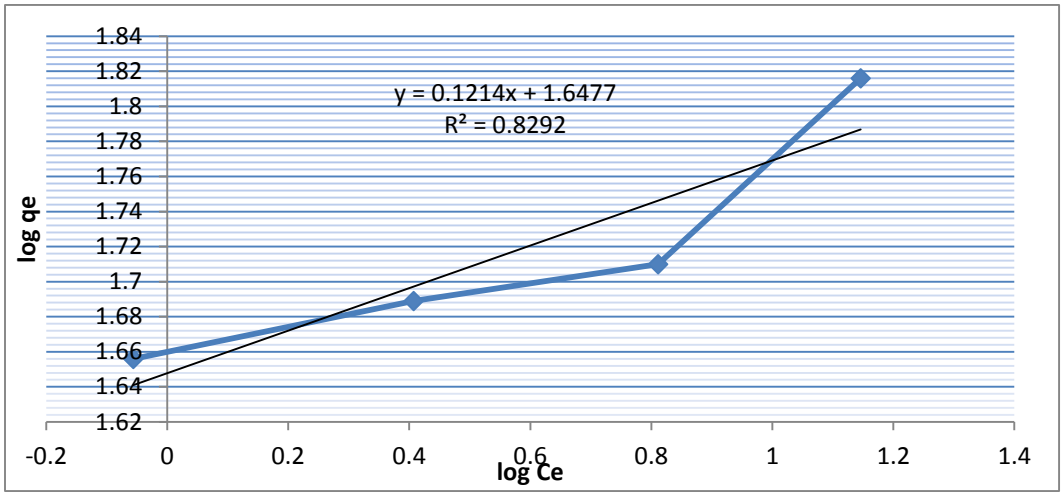

Fig 4.34: Freundlich Isotherm for Lead adsorption onto the nanocomposite.

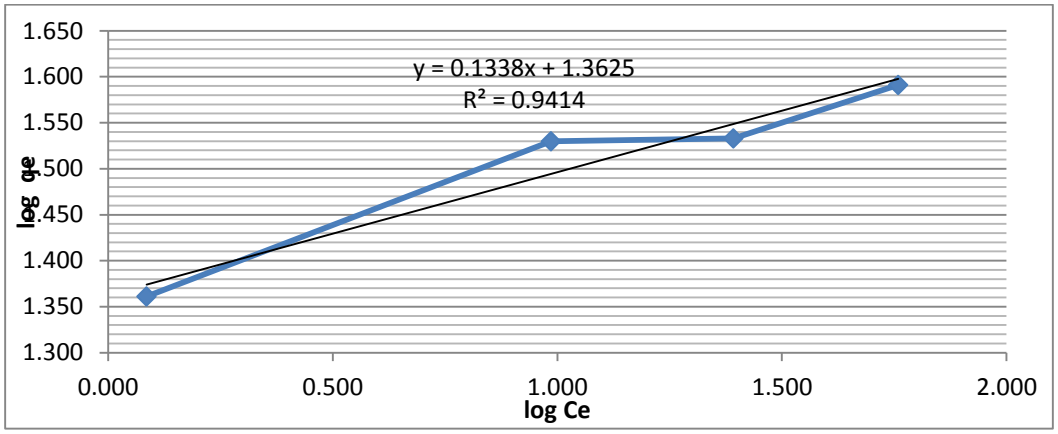

Fig 4.35: Freundlich Isotherm for the adsorption of Cadmium onto the nanocomposites.

The lower log C_e for Pb^{2+} (Figure 4.34) compared to those of Cd^{2+} (Figure 4.35) showed that the remaining metallic conc. after adsorption is lower for Pb^{2+} than for Cd^{2+}. The adsorption of Pb^{2+} is therefore higher than Cd^{2+}. The lower log q_e values for Cd^{2+} compared to those of Pb^{2+} showed a higher affinity for Pb^{2+} ions than for Cd^{2+} ions. The linear regression for Pb^{2+} for the Freundlich isotherm was 0.829 while it was 0.941 for Cd^{2+}.

Table 4.7: Freundlich Isotherm Parameters for lead and cadmium adsorption onto nanocomposites

Metal ions	K_F Freundlich constant (for isotherm curvature)	1/n Freundlich constant (for isotherm steepness)	R^2
Pb^{2+}	44.361	0.121	0.829
Cd^{2+}	23.014	0.133	0.941

The values of $\frac{1}{n}$ obtained for the adsorption of lead and cadmium had a range of $0< \frac{1}{n} <1$ (Table 4.7) indicating that the adsorption process of both metals was spontaneous (Goldberg, 2005). K_F, which approximately indicates sorption capacity shows that Pb^{2+} adsorption was significantly higher than that of Cd^{2+} (Table 4.7).

4.5.3 Tempkin Adsorption Isotherm

The Tempkin Isotherm can be represented as follows:

$$q_e = \frac{RT}{b_T \ln(A_t C_e)} \ldots \text{Equation 4.9}$$

And can be linearized as follows:

$$q_e = \frac{RT}{b_T} \ln A_t + \frac{RT}{b_T} \ln C_e \ldots \text{Equation 4.10}$$

Graph Plot: q_e vs ln C_e

Where: A_T is Tempkin isotherm equilibrium binding constant (L/ g); b_T is the Tempkin Isotherm constant; R is the Universal Gas Constant (8.314 x 10^{-3} kJ mol^{-1} K^{-1}); T is the Temperature at 298K. The adsorption curves for Lead and Cadmium were fitted into the Tempkin Isotherm as depicted in Figure 4.36 and 4.37.

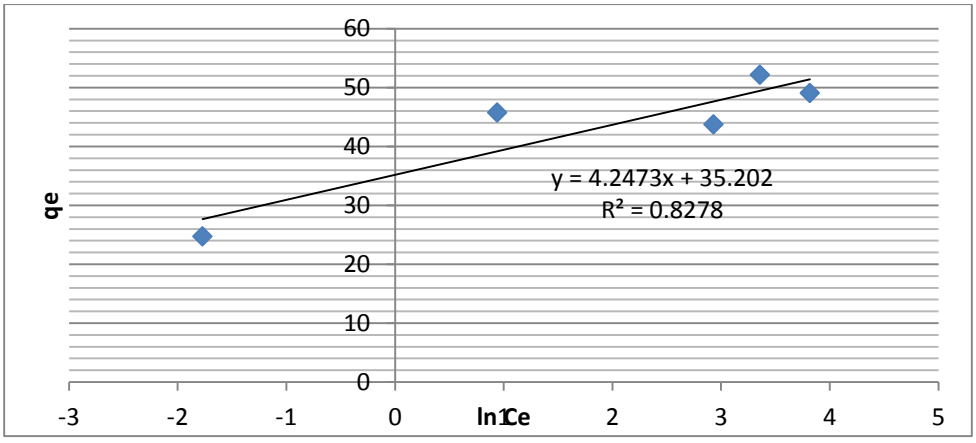

Fig 4.36: Tempkin Isotherm for the adsorption of Lead onto nanocomposites.

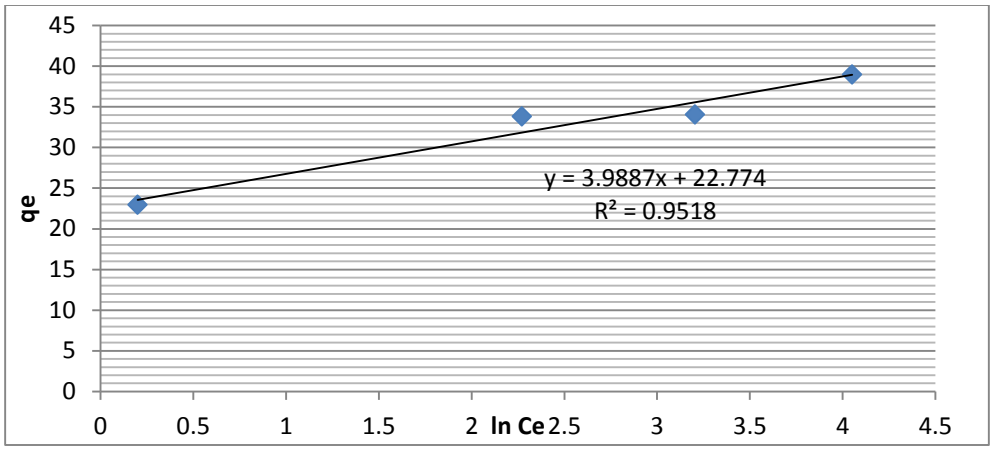

Fig 4.37: Tempkin Isotherm for the adsorption of Cadmium onto nanocomposites.

Table 4.8: Tempkin isotherm parameters for lead and cadmium adsorption onto nanocomposites

Metal ion	Tempkin isotherm equilibrium binding constant (A_T)	Tempkin isotherm constant (b_T)	R^2
Pb^{2+}	3.976	583.369	0.827
Cd^{2+}	0.301	621.257	0.951

The Temkin Isotherm binding constant, A_T, indicated a higher affinity for Pb^{2+} than that of Cd^{2+} ions. Lead ions had an A_T of 3.976 L/g while that of Cadmium was 0.301 L/g (Table 4.8) showing that the nanocomposite had a higher affinity for Lead than for Cadmium. These results are similar to findings from Farouq & Yousef (2015) whereby the A_T for Copper ion adsorption onto mussels was found to be 3.969L/g. Gunay *et al* (2007) also found out that the adsorption of Lead onto raw Clinoptilotite had an A_T of 2.091 L/g.

4.5.4 Dubinin- Radushkevich Adsorption Isotherm

The Dubinin- Radushkevich (DR) adsorption isotherm can be represented by the following expression:

$q_e = q_s \exp(-\beta\varepsilon^2)$ …Equation 4.11

And can be linearized as follows:

$\ln q_e = \ln q_s - \beta\varepsilon^2$ ...Equation 4.12

Graph Plot: ln q_e vs ε^2

Where: q_s is the maximum adsorption capacity (mg/g); q_e represents the adsorption capacity at equilibrium (mg/g); β is an activity coefficient constant related to adsorption energy ($mol^2\ J^{-2}$) which can be related to the following expression- $E = \frac{1}{\sqrt{2\beta}}$; ε is the Polanyi potential which can be represented as $\varepsilon = RT \ln(1 + \frac{1}{C_e})$; E is the Mean free energy of adsorption (kJ mol^{-1}) (Erhayem *et al.*, 2015; Horsfall *et al.*, 2004). The adsorption curves for Lead and Cadmium were plotted on the Dubinin Radushkevich Isotherm as depicted in Figures 4.38 and 4.39 below.

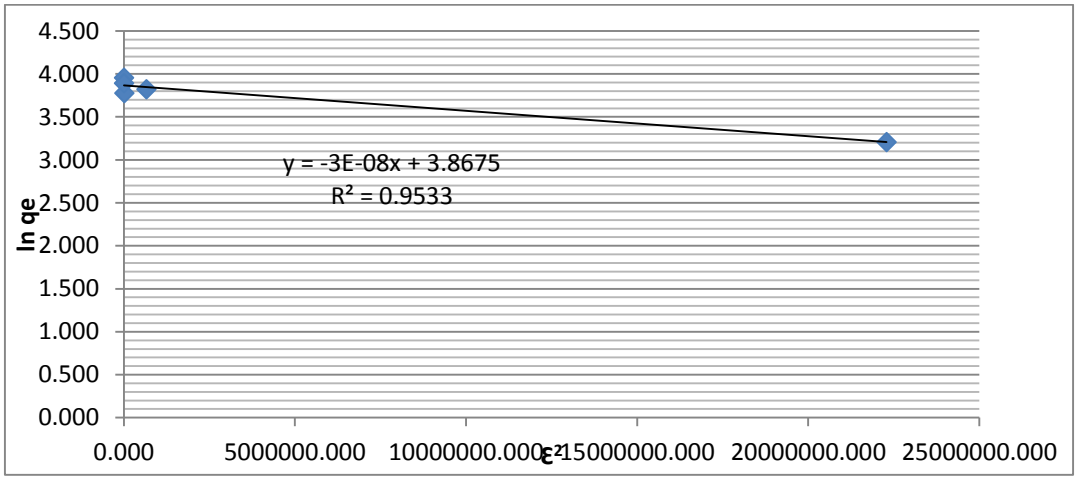

Fig 4.38: Dubinin Radushkevich Isotherm for Lead adsorption onto nanocomposites.

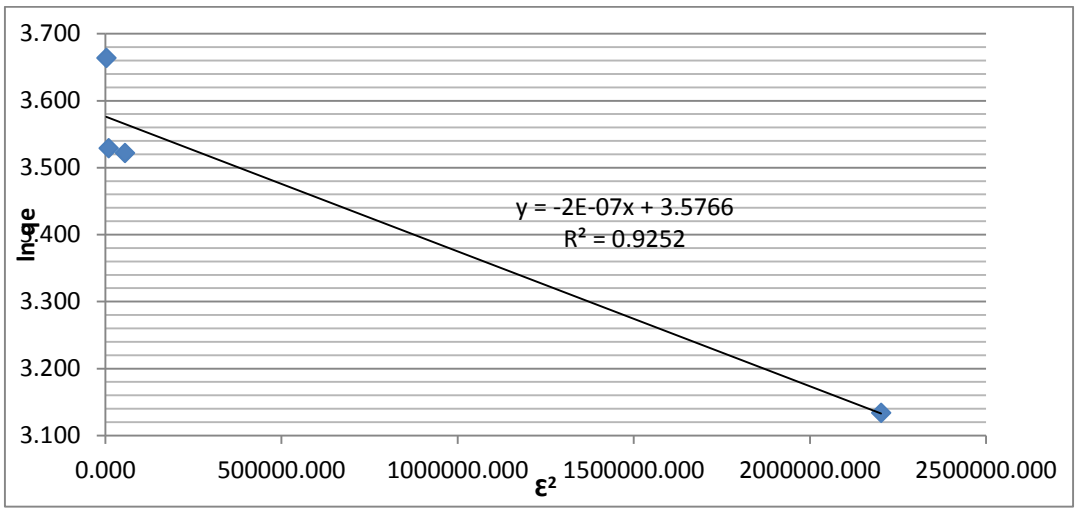

Fig 4.39: Dubinin Radushkevich Isotherm for Cadmium adsorption onto nanocomposites.

Table 4.9: Dubinin- Radushkevich isotherm parameters for lead and cadmium adsorption onto nanocomposites

Metal ion	**R^2**	**Maximum sorption capacity (q_s, (mg/g))**	**Activity coefficient constant (β ($mol^2\ J^{-2}$))**	**Ave. Energy of adsorption (E ($kJ\ mol^{-1}$))**
Pb^{2+}	0.95	47.79	-3×10^{-8}	-4.082
Cd^{2+}	0.93	35.73	-2×10^{-7}	-1.581

The DKR isotherm shows a good linear regression with the adsorption of Pb^{2+} (Figure 4.38) and Cd^{2+} (Figure 4.39) ions. Metal adsorption onto the nanocomposites is energy dependent. The lowest energy sites are occupied first by the metal ions followed by the higher energy sites. The average energy of adsorption for both metal ions (Table 4.9) seem to correlate well with those determined using thermodynamic experiments since the adsorption of lead has a higher spontaneity compared to that of cadmium ions in both cases.

4.5.5 Flory- Huggins Adsorption Isotherm

The Flory- Huggins Isotherm can be represented as follows:

$$\frac{\Theta}{C_o} = K_{FH}\,(1-\Theta)^{n_{FH}} \quad \ldots \text{Equation 4.13}$$

And can be linearized as follows:

$$\log\frac{\Theta}{C_o} = \log K_{FH} + n_{FH}\log(1-\Theta) \quad \ldots \text{Equation 4.14}$$

Plot: $\log\frac{\Theta}{C_o}$ vs log (1- Θ)

Where: Θ is the surface coverage degree; C_o is the Adsorbate initial concentration (mg/g); n_{FH} is the Flory- Huggins Isotherm model exponent; K_{FH} is the Flory- Huggins Isotherm equilibrium constant (L/ g).

Θ can be calculated as:

$$\Theta = \frac{1-C_e}{C_o} \quad \ldots \text{Equation 4.15}$$

Where: C_e is the concentration of the adsorbate at equilibrium (mg/L); C_o is the Adsorbate initial concentration (mg/L). The adsorption curves for both Lead and Cadmium were fitted into the Flory-Huggins isotherm as depicted in Figure 4.40 and 4.41.

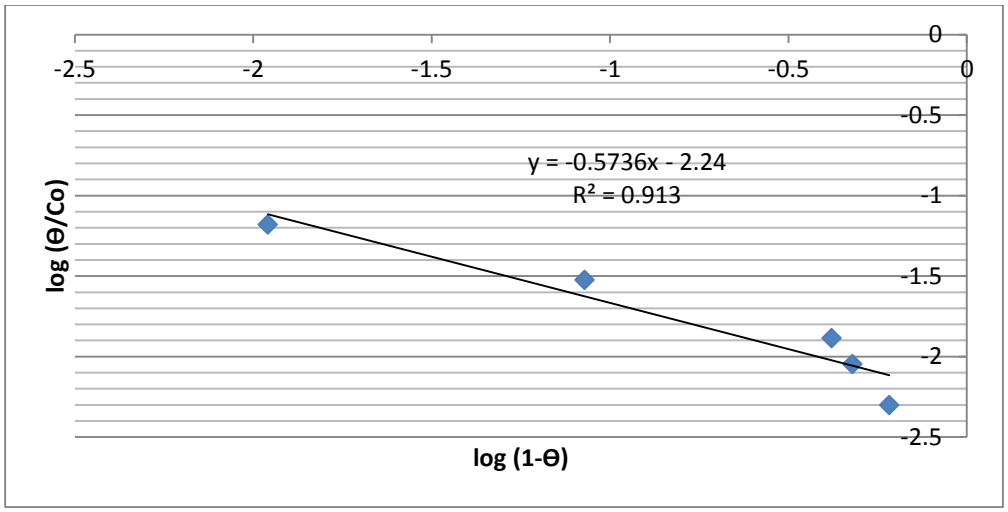

Fig 4.40: Flory- Huggins Isotherm for Lead adsorption onto nanocomposites.

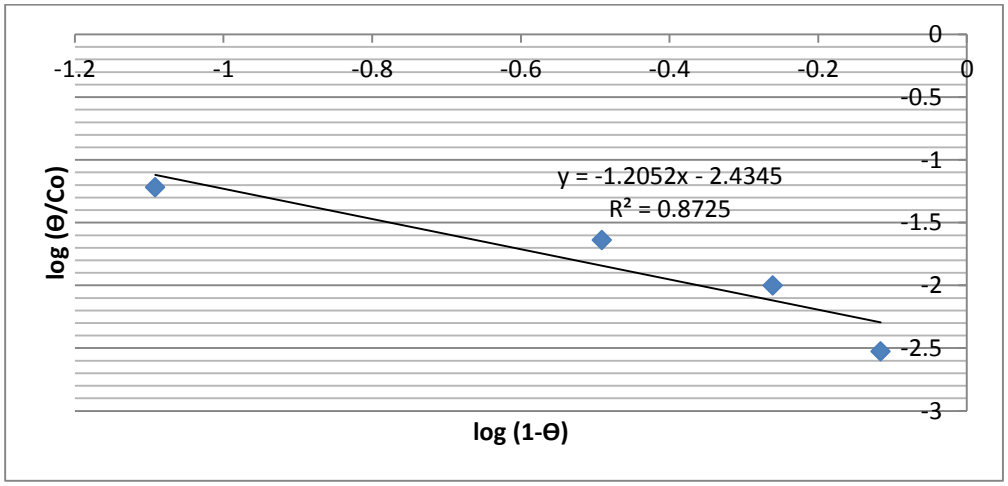

Fig 4.41: Flory- Huggins Isotherm for Cadmium adsorption onto nanocomposites.

Table 4.10: Flory- Huggins Isotherm Parameters for lead and cadmium adsorption onto nanocomposites

Metal ion	**R^2**	**Flory- Huggins isotherm equilibrium constant (K_{FH})**	**Flory- Huggins isotherm model exponent (n_{FH})**
Pb^{2+}	0.913	5.75×10^{-3}	-0.573
Cd^{2+}	0.872	3.68×10^{-3}	-1.205

The linear regression for the adsorption of both Pb^{2+} (Fig. 4.40) and Cd^{2+} (Fig. 4.41) ions was acceptable when plotted on the Flory- Huggins Isotherm. The Flory-Huggins adsorption constant for Lead ($5.75x10^{-3}$) ions was higher than that of Cadmium ions ($3.68x10^{-3}$). Lead ions showed a stronger adsorption onto zeolites compared to Cadmium because of their more negative Gibbs energy. Nechifor *et al* (2015) showed that the Flory Huggins constants for phosphate adsorption onto cellulose were governed by the Gibbs energy of adsorption at that particular temperature. Adsorption of Phosphate ions onto 10µm cellulose membrane showed a ΔG^o of -39.10 kJ/ mol. while for 50 µm showed a ΔG^o of -55.8kJ/mol. The K_{FH} for the 10µm membrane adsorption was $9x10^{-8}$ while that of the 50 µm was 1.12. The isotherm constant (K_{FH}) shows more affinity for Pb^{2+} by the nanocomposites than Cd^{2+}. The x-axis for Pb^{2+} has a plot of higher negative values than for Cd^{2+} (Table 4.10) showing that the surface coverage of the nanocomposites by Pb (II) ions is higher than that of Cd (II) ions because of the higher affinity the nanocomposites have for Pb (II) ions.

CHAPTER 5

CONCLUSIONS AND RECOMMENDATIONS

5.1 Conclusions

Zeolite/ Cellulose acetate nanocomposites were successfully synthesized and were found to be very useful for effective heavy metal removal from aqueous systems. They were successfully characterized using FTIR, SEM, EDX and powder XRD methods to reveal their bond structure, crystallinity and morphology. They removed upto 96.7% of Lead ions and 85.06% of Cadmium ions from solution. The effectiveness of heavy metal removal was assessed under varied conditions including as pH, temperature, contact time, zeolite percentage loading, concentration of the metallic ions and adsorbent dosage. The heavy metal removal was found to be more accurately estimated by the Langmuir Isotherm predicting a high likelihood of monolayer adsorption. At low pH, heavy metal removal was slowed by competition between metal and hydrogen ions. The optimum pH for optimum heavy metal removal from solution was found to be between 6- 9. At this pH range, 100% of the Lead ions and 87.2%- 93.6% of the Cadmium ions were sorbed by the nanocomposites. The adsorption of both metals was found to be endothermic (increases with increase in temperature) with maximum adsorption taking place at a temperature of 343K. The removal of the metals from solution increased with contact time. The maximum amount was adsorbed after 75 minutes. Sorption of both metals fitted better in the pseudo second order kinetic model compared to the pseudo first order model. 20% Zeolite loading was optimum for the lead removal from solution while 40% zeolite loading was optimum for the Cadmium ion removal. As the concentration of the metallic ions increased, their percentage removal from solution reduced significantly. 98.87% of Lead ions were removed from 15ppm solution while only 39.35% was removed from 75ppm solution after 75 minutes contact time while the values for Cadmium were 91.87% for 15ppm solution and 23.40% for 75ppm solution. As the adsorbent dosage increased, more metal ions were removed from solution. The metallic adsorption was plotted on Langmuir, Freundlich, Tempkin, Dubinin- Radushkevich and Flory- Huggins isotherms. The Langmuir isotherm fitted best for both metal ions with lead ions having a correlation (R^2) of 0.985 while that of cadmium being 0.996.

5.2 Recommendations

1. Fabrication of zeolite-polymer composites could be done using other polymers such as polyacrylamide, poly (metha) methacrylate or polyvinyl alcohol and tested for heavy metals adsorption.

2. Employment of the nanocomposites in heavy metal removal from real water samples.

3. An adsorption isothermal study can be carried for both lead and cadmium at different temperatures.

4. Column adsorption experiments could be carried out to estimate the breakthrough curves for the adsorption of both lead and cadmium using the nanocomposites.

5. Comparative regeneration studies could be carried out using different salts such as KCl, NaCl and NH_4Cl.

REFERENCES

Abd El-Rahman. K. M., El-Kamash A. M., El-Sourougy M. R., Abdel-Moniem N. M. (2006). Thermodynamic modeling for the removal of Cs^{2+}, Sr^{2+}, Ca^{2+} and Mg^{2+} ions from aqueous waste solutions using zeolite. *Journ. of Radioanal Nucl. Chem.* **268(2):** 221–230.

Agarwal. G. S., Bhuptawat. H. K., Chaudhari. S. (2006). Biosorption of aqueous chromium(VI) by tamarindus indica seeds. *Bioresource Technol.* **97:** 949–956.

Ahan. Y. S. & Basoglu. F. & Gu¨cer. S.(2007). ICP-MS analysis of a series of metals (Namely: Mg, Cr, Co, Ni, Fe, Cu, Zn, Sn, Cd and Pb) in black and green olive samples from Bursa, Turkey. *Food Chemistry* **105:** 395–399.

Aharoni. C & Ungarish. M.(1977). Kinetics of activated chemisorption. Part 2. Theoretical models. *J. Chem. Soc. Faraday Trans.* **73:** 456–464.

Al-Anber. M. and Al-Anber. Z. (2008). Utilization of natural zeolite as ion-exchange and sorbent material in the removal of iron. *Desalination.* **255:** 70 – 81.

Al-Anber. M. (2007). M. Removal of Iron (III) from Model Solution Using Jordanian Natural Zeolite: Magnetic Study. *Asian J. Chem.* **19(5):** 3493-3501.

Al-Anber. M. (2010). Removal of High-level Fe^{3+} from Aqueous Solution using Jordanian Inorganic Materials: Bentonite and Quartz. *Desalination.* **250:** 885- 891.

Al-Anber. M. (2011). *Thermodynamics Approach in the Adsorption of Heavy Metals, Thermodynamics - Interaction Studies - Solids, Liquids and Gases*. Dr. Juan Carlos Moreno PirajÃ¡n (Ed.). Mu tah University, Jordan. ISBN: 978-953-307-563-1.

Alexandre. M. & Dubois. P. (2000). Polymer-layered silicate nanocomposites: preparation, properties and uses of a new class of materials. *Materials Science and Engineering*. **28:** 1-63

Ali. H. O., and Abidin K. (2006). Factors Affecting Adsorption Characteristics of Zn^{2+} on Two Natural Zeolites, *J. Hazard. Mater.* **131:** 59-65.

Ali. I., Mohammed. A., Tabrez A. K. (2012). Low cost adsorbents for the removal of organic pollutants from wastewater. *Journal of Environmental Management* **113:** 170-183.

Allen. S. J., Mckay. G. & Porter. J. F. (2004). Adsorption isotherm models for basic dye adsorption by peat in single and binary component systems. *J. Colloid Interface Sci.* **280:** 322–333.

Almaraz B. P., Trocellier P. and Rangel D. I. (2003). Adsorption of aqueous Zn (II) species on synthetic zeolites. *Nuclear Instruments and Methods in Physics Research* **210:** 424-428.

Almeida. C. A. P, Debacher. N. A, Downs. A. J., Cottet. J and Mello C. A. D. (2009). Removal of Methylene Blue from Colored Effluents by Adsorption on Montmorillonite Clay. *Journal of Colloid Interface Science*, **332(1):** 46-53.

Aly. Z & Luca. V. (2013). Uranium extraction from aqueous solution using dried and pyrolyzed tea and coffee wastes. *J. Radioanaly. Nucl. Chem.* **295(2):** 889-900.

Aly. Z., Graulet. A., Scales. N., Hanley. T. (2014). Removal of aluminium from aqueous solutions using PAN-based adsorbents: characterisation, kinetics, equilibrium and thermodynamic studies. *Journal of Environmental Science and Pollution Research* **21:** 3972-3986.

Amarasinghe. B.M.W.P.K., Williams. R.A. (2007). Tea waste as a low cost adsorbent for the removal of Cu and Pb from wastewater. *Chem. Eng. J*. **132:** 299–309.

Arivoli S, Kalpana K, Sudha R and Rajachandrasekar T. (2007). Comparative study on the adsorption kinetics and thermodynamics of metal ions onto acid activated low cost carbon. *E J Chem.* **4:** 238-254.

Arivoli S, Venkatraman B R, Rajachandrasekar T and Hema M. (2007). Adsorption of ferrous ion from aqueous solution by low cost activated carbon obtained from natural plant material. *Res J Chem Environ.* **17:** 70-78.

Athanasiadis K. & Helmreich B. (2005). Influence of Chemical Conditioning on the Ion Exchange Capacity and on Kinetic of Zinc Uptake by Clinoptilolite. *Water Research*. **39(1):** 1527-1532.

Atkins P. (1999). *Physical chemistry.* 6th Edn. Oxford University press. London, pp 857- 864.

Auerbach. S. M., Carrado. K. A., Dutta. P. K. (2003). *Handbook of Zeolite Science and Technology*. Marcel Dekker, Inc. New York/ Basel.

Aydin. F. & Kuleyin. A. (2011). The Effect of Modification and Initial Concentration on Ammonia Removal from Leachate by Zeolite. World Academy of Science, Engineering and Technology *International Journal of Environmental, Chemical, Ecological, Geological and Geophysical Engineering*. **5:** 6.

Ayuso, E. A.; Sanchez, A. G.; Querol, X., (2003). Purification of metal electroplating waste waters using zeolites. *Water Res.*, **37 (20**): 4855-4862

Babel., S. & Kurniawana, T. A., (2003). Low cost adsorbents for heavy metal uptake from contaminated water: A review. *Journal of Hazardous Material B*. **97**: 219-243.

Bai. Y. & Bartkiewicz. B. (2009). Removal of Cadmium from wastewater using ion exchange resin Amberjet 1200H Columns. *Polish Journ. Of Environmental Studies.* **18(6):** 1191.

Balazs, A. C.; Emrick, T.; Russell, T. P. (2006). Nanoparticle- polymer Composites: Where two small worlds meet. *Science.* **314:** 1107- 1110.

Bandyopadhyay, A.; De Sarkar, M.; Bhowmick, A. K. (2005). Poly(vinyl alcohol)/ Silica hybrid nanocomposites by sol-gel techniques: Synthesis and Properties. *J. Mater. Sci.* **40:** 5233- 5241

Banwell. C. N (1983). *Fundamentals of Molecular Spectroscopy (3rd Edition).* McGraw-Hill, London.

Bao-hua. Z., De-yi. W., Chong. W., Sheng-bing. H., Zhen-jia. Z., Hai-nan. K. (2007). Simultaneous removal of ammonium and phosphate by zeolite synthesized from coal fly ash as influenced by acid treatment. *Journal of Environmental Sciences* **19:** 540–545.

Baral. S.S., Das N., Chaudhury G.R., Das S.N. (2009). A Preliminary study on the adsorptive removal of Cr(VI) using seaweed *Hydrilla verticillata*. *J. Hazard. Mater.* **171**:358–369.

Bellinger. D. C. & Bellinger. A. M. (2006). Childhood lead poisoning: the torturous path from science to policy. *Journal of Clinical Investigation*, **116(4)**:853–857.

Bhattacharya A.K., Mandal S.N., and Das S.K. (2006). Adsorption of Zn(II) from aqueous solution by using different adsorbents. *Chem. Eng. J.*, **123:** 43-51.

Bishop. J. L., Pieters. C. M., Edwards. J. O. (1994). Infrared spectroscopic analyses on the nature of water in montmorillonite. *Clays Clay Mineral*. **42:** 702.

Biswas M, Sinha Ray S. (2001). Recent progress in synthesis and evaluation of polymer–montmorillonite nanocomposites. *Adv Polym Sci* **155:** 167–221.

Boparai, H. K., Joseph, M. and O'Carroll, D.M. (2011). Kinetics and thermodynamics of Cadmium ion removal by adsorption onto nano zero-valent iron particles. *J. Hazard. Mater.*, **186:**458-465.

Bovey, F.A. and Winslow, F.H. (1979). *Macromolecules. An Introduction to Polymer Science.* Academic Press Inc. NewYork City.

Braida, W. J., Pignatello. J. J., Lu. Y., Ravikovitch. P. I., Neimark. A. V., & Xing. B. (2003). Sorption Hysteresis of Benzene in Charcoal Particles. *Environ. Sci. Technol*., **37:** 409-417

Bralley J.A., Lord R.S. (2001). *Laboratory Evaluations in Molecular Medicine.* The Institute for Advances in Molecular Medicine, Norcross GA.

Brathwaite. R. L. and Rabone. S. D. C. (1985) Heavy metal sulphide deposits and geochemical surveys for heavy metals in New Zealand. Proceeding;- of a Seminar on Heavy Metals in the New Zealand Environment © *Journal of the Royal Society of New Zealand*, **15(1):** 363-370

Braun. J., Kahn. R. S., Froehlich. T., Auinger. P. & Lanphear. B. P. (2006). Exposures to environmental toxicants and attention deficit hyperactivity disorder in U.S. children. *Environmental Health Perspectives*. **114(12):** 1904–1909.

Brunnuer. S., Emmett. P. H. & Teller. E. (1938). Adsorption of gases in multi-molecular layers. *J. Am. Chem. Soc.* **60 :** 309–316.

Buasri. A., Chaiyut. N., Phattarasirichot. N., Yongbut. P. and Nammueng. L. (2008). Use of Natural Clinoptilolite for the Removal of Lead (II) from Wastewater in Batch Experiment. *Chiang Mai J. Sci*. 2008; **35(3)**: 447-456

Burçin. M., Ozgul. P., Ozdemir. D. and Celik. K. (2013). Cadmium Adsorption on Modified Turkish Clinoptilolite. *International Journal of Chemical, Environmental & Biological Sciences (IJCEBS.)* **1(5)**: 2320–4087.

Burns. J. M., Baghurst. P., Sawyer. M. G. and Tong. S. (1999). Lifetime low-level exposure to environmental lead and children's emotional and behavioral development at ages 11–13 years. The Port Pirie Cohort Study. *American Journal of Epidemiology*, **149:**740–749.

Burwell, R. (1976). IUPAC- Physical Chemistry division. Commission on colloid and surface chemistry. Manual of symbols and terminologies for physicochemical quantities and units. *Pure and Applied Chem.* **46:** 71-90.

Byers. R. K. & Lord. E. E. (1943). Late effects of lead poisoning on mental development. *Am J Dis Child* **66(5):** 471–494

Calcagnile. P., Fragouli. D., Bayer. I. S., Anyfantis. G. C., Martiradonna. L., Cozzoli. P. D., Cingolani. R., Athanassiou. A. (2012). Magnetically Driven Floating foams for the removal of oil contaminants from water. *ACS Nano* **6(6):** 5413- 5419 .

Callender, E. (2004). Heavy metals in the environment-historical trends. *Treatise Geochem.* **9:** 67–105.

Canonica. S., Meunier. L & von Gunten. U. (2008). Phototransformation of selected pharmaceuticals during UV treatment of drinking water. *Water. Res.* **42(1-2):** 121-128.

Carr, G. M. and Neary. J. P. (2008). Water Quality for Ecosystem and Human Health, 2nd Edition. United Nations Environment Programme Global Environment Monitoring

System. Retrieved 14 July 2009, from http://www.gemswater.org/publications/pdfs/water_quality_human_health.

Caseri, W. (2004). In *Encyclopedia of Nanoscience and Nanotechnology*; Nalwa, H. S. Ed.; American Scientific Publishers: Stevenson Ranch, CA, **6:** 235-247.

Caseri, W. R. (2006). Nanocomposites of Polymers and Inorganic Particles: Preparation, Structure and Properties. *Mater. Sci. Technol.* **22:** 807- 817.

Caseri, W. (2007). In *Hybrid Materials. Synthesis, Characterization, and Applications*; Kickelbick, G., Ed.; Wiley-VCH:Weinheim, Germany. Chapter 2.

Cecil K. M., Brubacker. C. J., Adler. C. M., Dietrich. K. N., Altaye. M., Egelhoff. J. C., Wessel. S., Elangovan. I., Hornung. R., Jarvis. K. and Lanphear. B. P. (2008). Decreased brain volume in adults with childhood lead exposure. *PLoS Medicine*, **5(5)**:e112

Chandra Rao. P. G.., Satyaveni S., Ramesh A., Seshaiah K., Murthy K.S.N., and Choudary N.V., (2006). Sorption of cadmium and zinc from aqueous solutions by zeolite 4A, zeolite 13X and bentonite. *J. Environ. Manag.*, **81:** 265-272.

Chaudhary, M. and Kumar, M. (2012). Sorgum vulgare and pennisetum typhoedum as useful biosorbents for the removal of heavy metal ions from water solution. *International Journal of BioChemiPhysics.* **20:** 1-6.

Chen, H. and Wang,A. (2007). Kinetic and isothermal studies of lead ion adsorption onto palygorskite clay. *J. Colloid. Interface Sci*., **307:** 309-316.

Chen J.H., Li G.P., Qing Lin Liu Q.L., Ni J.C., Wu W.B., Lin J.M. (2010). Cr(III) ionic imprinted polyvinyl alcohol/sodium alginate (PVA/SA) porous composite membranes for selective adsorption of Cr(III) ions. *Chem. Eng. J.* **165:** 465–473.

Chen, Y.; Iroh, J. O. (1999). Synthesis and characterization of Polyimide/ Silica Hybrid Composites. *Chem. Mater*. **11(5):** 1218.

Chiron. N., Guilet. R. & Deydier. E. (2003) Adsorption of Cu(II) and Pb(II) onto A grafted silica: Isotherms and Kinetic Models. *Water Res.,* **37:** 3079-3086.

Christidis, G. E., Moraetis, D., Keheyan, E., Akhalbedashvili, L., Kekelidze, N., Gevorkyan, R., (2003). Chemical and thermal modification of natural HEUtype zeolitic materials from Armenia, Georgia and Greece. *Applied Clay Science.* **24(1–2):** 79–91.

Cloete. T. E., de Kwaadsteinet. M., Botes. M. & Lopez- Romero. J. M. (2010). *Nanotechnology in Water Treatment Applications.* Caister Academic Press. ISBN 978-1-904455-66-0.

Colborn. T., A. Soto, and F. vom Saal. (1993). Developmental effects of endocrine-disrupting chemicals in wildlife and humans. *Environmental Health Perspectives.* **101(5)**: 378–384.

Colella. C, Misaelides. P., Macasek. F., Pinnavaia. F. (Eds.) (1999). *Environmental applications of natural zeolitic materials based on their ion-exchange properties, in*: Application of Natural Microporous Materials in Environmental Technology, Kluwer, NATO Science Series vol. E362 (Applied Sciences), Dordrecht, 1999, pp. 207–224.

Cong, H. L.; Hu, X. D.; Radosz, M.; Shen, Y. Q. (2007). Brominated Poly(2,6-diphenyl-1,4-phenylene oxide) and its Silica Nanocomposite membranes for Gas separation. *Ind. Eng. Chem. Res.* **46(8):** 2567-2575.

Cong, H. L., Radosz, M., Towler, B. F., Shen, Y. Q. (2007). Polymer-inorganic nanocomposite membranes for gas separation", Separation And Purification Technology *Sep. Purif. Technol.* **55(3):** 281-291.

Cong. H. P., Ren. X. C., Wang. P., Yu. S. H., (2012). Macroscopic Multifunctional Graphene based Hydrogels and Aerogels by a metal ion induced self-assembly process. *American Chemical Society (ACS) Nano.* **6(3)**: 2693-2703.

Cramer. C. (2011). Statistical Molecular Thermodynamics Notes, University of Minnesota, USA.

Crane. R. A. & Scott. T. B. (2012). Nanoscale zero-valent Iron: Future prospects for an emerging water treatment technology. *J. Hazard. Mater.* **211–212:** 112-125.

Čurković, Š, Cerjan-Stefanović, L., T. Filipan, (1997). Metal ion exchange by natural and modified zeolites. *Water Research* **31**: 1379-1382

Daoud, W. A., Xin, J. H., & Zhang, Y. H. (2005). Surface functionalization of cellulose fibers with titanium dioxide nanoparticles and their combined bactericidal activities. *Surface Science*. **599:** 69–75.

Dabrowski. A. (2001). Adsorption—from theory to practice. *Adv. Colloid Interface Sci*. **93:** 135–224.

Decarreau. A., Grauby. O., Petit. S. (1992). The actual distribution of octahedral cations in 2: 1 clay minerals: results from clay synthesis *Appl. Clay Sci.* **7:**147.

Decher, G. & Hong, H.-G. (1991). Build- Up of ultrathin multilayer films by self-assembly process, 1 consecutive adsorption of anioninc and cationic bipolar amphiphiles on charged surfaces. *Makromol. Chem. Macromol. Symp.* **46(1):** 321- 327.

Dichiara. A., Li. W. and Bai. J. (2013). Effective synergistic effect of Al_2O_3 and SiC microparticles on the growth of carbon nanotubes and their application in high dielectric permittivity polymer composites. *Compos. Sci. Technol.,* **74:** 221–227.

Dietrich K. N., Douglas. R. M., Succop. P. A., Berger. O. G. and Bornschein. R. L. (2001). Early exposure to lead and juvenile delinquency. *Neurotoxicology and Teratology*, **23(6):**511–518.

Doshi, J. and Reneker, D.H., 1995: Electrospinning Process of Electrospun Fibers, *J. Electrostatics*. **35 (2-3):** 151-160.

Douben. P. E. T. and Koeman J. H. (1989). Effect of sediment on cadmium and lead in the stone loach (noemacheilus barbatulus L.). *Aquatic Toxicology*. **15(3**): 253-268.

Doye, I. & Duchesne, J. (2003). Neutralisation of acid mine drainage with alkaline industrial residues: laboratory investigation using batch-leaching tests. *Appl. Geochem.* **18:** 1197-1213.

Dubinin. M. M. (1966). chem. *And phys of carbon*. P.L Walker Jr (Ed), Mercel Dekker, New York.

Dubinin. M. M.(1975). *Progress in surface and membrane science.* D. A . Cadenhead *et al*. (Eds). Academic Press NY.

Duffus. J. H. (2002). Heavy metals- A Meaningless Term? IUPAC Technical Report. *Pure Appl. Chem.* **74(5):**793-807.

Edzwald. James K., (2011). *Water Quality and Treatment: A handbook on Drinking Water. 6th Edition.* New York: McGraw- Hill. ISBN 978-0-07-163011-5

Egashira. R., Tanabe. S. & Habaki. H. (2012). Adsorption of heavy metals in mine wastewater by Mongolian natural zeolite. 20th International Congress of Chemical and Process Engineering CHISA 2012 25 – 29 August 2012, Prague, Czech Republic. *Procedia Engineering* **42:** 49 – 57.

Eick. M. J., Peak. J. D., Brady. P. V., Pesek. J. D. (1999). Kinetics of lead absorption/desorption on goethite: residence time effect. *Soil Sci.***164:** 28-/39.

Elliott. H. A. & Huang. C. P., (1981). Adsorption characteristics of some Cu(II) complexes on aluminosilicates. *Water Res.* **15:** 849–855.

Erdem E., Karapinar N., Donat D. (2004). The removal of heavy metal cations by natural zeolites. *J. Colloid Interface Sci.* **280:** 309–314).

Erhayem, M., Al-Tohami, F., Mohamed, R. and Ahmida, K. (2015) Isotherm, Kinetic and Thermodynamic Studies for the Sorption of Mercury (II) onto Activated Carbon from *Rosmarinus officinalis* Leaves. *American Journal of Analytical Chemistry*, **6**: 1-10.

Evarett, D.H. (1954). A General Approach to Hysteresis, Part 4. An Alternative Formulation of the Dimain model. Trans. *Faraday Soc.* **51:** 1551-1557.

Fahmy. A., Wassel. M. A., Shehata. H. A., Youssef. H. F., Elzaref. A. S. (2016). Adsorption of Cadmium Ions onto Zeolite-A prepared from Egyptian Kaolin using microwave Technique. *International Journal of Science and Research (IJSR)*. **391(7)**

Farmer. V. C., Russell. J. D. (1964). The Infra- Red Spectra of layered Silicates. *Spectrochim. Acta* **20:** 1149.

Farmer. V. C., in: V.C. Farmer (Ed.) (1974*). Infrared Spectra of Minerals*, Mineralogical Society, London, UK, pp. 331-358.

Farooq. R. & Yousef. N. S. (2015). Equilibrium and kinetic studies of adsorption of Copper on natural biosorbent. *International Journal of Chemical Engineering and applications.* **6(5):** 319-324

Feng, J.J. (2002). The Stretching of An Electrified Non Newtonian Jet: A Model for Electrospinning. *Physics of Fluids.* **14**: 3912-3926.

Fergusson. D. M., Boden. J. M. & Horwood. L. J. (2008). Dentine lead levels in childhood and criminal behaviour in late adolescence and early adulthood. *Journal of Epidemiology and Community Health*, **62(12):** 1045–1050.

Fischer. H. (2003). Polymer nanocomposites: from fundamental research to specific applications. *Materials Science and Engineering C*. **23(6–8)**: 763–772.

Fischer. S., Thummler. K., Volkert. B., Hettrich. K., Schmidt. I. & Fischer. K. (2008). Properties and applications of Cellulose Acetate. *Macromol. Symp.* **262(1):** 89-96.

Fong, H., Liu, W., Wang, C.S. and Vaia, R.A. (2002). Generation of Electrospun Fibers of Nylon 6 & Nylon 6-Montmorillonite Nanocomposite. *Polymer*. **43**: 775-780.

Foo. K. Y., Hameed. B. H. (2010). Insights into the modeling of adsorption isotherm systems. *Chemical Engineering Journal.* **156:** 2–10.

Friedman, J. R., Ashton, W. B., and Rapoport, R. D. (1993). *A review of the global emissions, transport and effects of heavy metals in the environment. Report PNL-SA- 22394; OrderNo.DE93016817.* Richland, WA.

Freundlich. H. M. F. (1906). Over the adsorption in solution. *J. Phys. Chem.* **57:** 385 –470.

García. R and Báez. A. P. (2012). Atomic Absorption Spectrometry (AAS), Atomic Absorption Spectroscopy, Dr. Muhammad Akhyar Farrukh (Ed.), ISBN: 978-953-307-817-5

Gascon. J., Kapteijn. F., Zornoza. B., Sebasti´an. V., Casado. C. and Coronas. J.(2012). Practical Approach to Zeolitic Membranes and Coatings: State of the Art, Opportunities, Barriers and Future Perspectives. *Chem. Mater*. **24(15):** 2829-2844.

Gates. W. P., Komadel. P., Madejova´ J., Bujda´k. J., Stucki. J. W., Kirkpatrick. R. J. (2000). Electronic and structural properties of reduced-charge montmorillonites. *Appl. Clay Sci*. **16:** 257- 271.

Ghiacci. M., Abbaspur. A., Kia. R., Seyedeyn-Azad. F. (2004). Equilibrium isotherm studies for the sorption of benzene, toluene, and phenol onto organo-zeolites and as-synthesized MCM-41. *Sep. Purif. Technol*. **40:** 217–229.

Giannelis. E. P. (1996). Polymer Layered Silicate Nanocomposites. *Advanced Materials*. **8:** 29-35.

Giannelis. E. P., Krishnamoorti. R., Manias. E. (1999). Polymer-silicate nanocomposites: model systems for confined polymers and polymer brushes. *Adv Polym Sci*. **138:** 107–147.

Gindl, W., & Keckes, J. (2004). Tensile properties of cellulose acetate butyrate composites reinforced with bacterial cellulose. *Composites Science and Technology*. **64:** 2407–2413.

Goel, P. K. (2006). *Water Pollution- Causes, Effects and Control*: New Age International New Delhi. ISBN 978-81-224-1839-2.

Goldberg. S. (2005) *Equations and models describing the adsorption processes in soils.* Soil science Society of America, 677 S. Segoe Road, Madison, WI 53711, USA. Chemical Processes in Soils. SSSA Book Series, No. 8.

Gong. R., Sun. Y., Chen. J.,Liu. H.,Yang. C.(2005). Effect of chemical modification on dye adsorption capacity of peanut hull. *Dyes and Pigments*. **67:** 179.

Gramlich. V and Meier. W. M. (1971). Crystallographic Information File for Linde Type A, Hydrated *Z. Kristallogr.* **133:** 134–149.

Greenlee. L. F., Lawler. D. F., Freeman. B. D., Marrot. B., Moulin. P. (2009). Reverse osmosis desalination: Water sources, technology, and today's challenges. *Water Research* **43**: 2317 – 2348

Guerrero-Ruiz, (1993). Some aspects of reversible chemisorption on supported Platinum catalysts. *Reaction Kinetics and Catalysis Letters,* **49(1):** 53-60.

Gupta, S. S.; Bhattacharyya, K. G., (2008). Immobilization of Pb (II), Cd (II) and Ni (II) ions on kaolinite and montmorillonite surfaces from aqueous medium. *J. Environ. Manage*., **87 (1):** 46-58.

Gunay A., Arslankaya E., Tosun I. (2007). Lead removal from aqueous solution by natural and pre-treated clinoptilolite: adsorption equilibrium and kinetics. *Journal of Hazardous Materials* **146:** 362-371.

Guto, P. Clean Water for Today and tomorrow. (2012). *Int'l Journal of BioChemiPhysics*. **20 (**i).

Ha. M., Kwon. H. J., Lim. M. H., Jee. Y. K., Hong. Y. C., Leem. J. H., Sakong. J., Bae. J. N., Hong. S. J., Roh. Y. M. & Jo. S. J. (2009). Low blood levels of lead and mercury and symptoms of attention deficit hyperactivity in children: a report of the children's health and environment research (CHEER). *Neurotoxicology*. **30(1)**: 31–36.

Hafner, B. (2007). *Scanning Electron Microscopy Primer. Characterization Facility*, University of Minnesota—Twin Cities 4/16/2007.

Hajji, P.; David, L.; Gerard, J. F.; Pascault, J. P.; Vigier, G. (1999). Synthesis, structure, and morphology of polymer–silica hybrid nanocomposites based on hydroxyethyl methacrylate *J. Polym. Sci., Part B: Polym. Phys.* **37(22):** 3172-3187

Halliday. D. & Resnick. Robert. (2013). *Fundamentals of Physics*. Wiley, London. pp 54 - 336

Hamidpour. M, Kalbasi. M, Afyuni. M, and Shariatmadari. H. (2010). Kinetic and isothermal studies of cadmium sorption onto bentonite and zeolite. *Int. Agrophys.*, **24:** 253-259.

Han, D., Yan, L., Chen, W., Li, W., & Bangal, P. R. (2011). Cellulose/ graphite oxide composite films with improved mechanical properties over a wide range of temperature. Carbohydrate Polymers. **83(2):** 966–972.

Hana. R., Zoub. W., Li. H., Li. Y., Shi. J. (2006). Copper (II) and lead(II) removal from aqueous solution in fixed-bed columns by manganese oxide coated zeolite. *Journal of Hazardous Materials B*. **137**: 934–942.

Hasany. S. M., Saeed. M. M., Ahmed. M. (2002). Sorption and Thermodynamic behaviour of Zinc (II)- Thiocyanate Complexes onto Polyurethane Foam from Acidic Solutions. *J. Radioanal. Nucl. Chem*. **252(3):** 477-484.

Hay, R. L., & Sheppard. R. A. (2001). *Occurrence of zeolites in sedimentary rocks: An overview*. In D.L. Bish and D.W. Ming, Editors, Natural zeolites: properties, applications

and uses, **45:** 217-232. Reviews in Mineralogy and Geochemistry, Mineralogical Society of America, Chantilly, Virginia.

Heidari. A, Younessi. H, Mehrabanb. Z and Heikkinen. H. (2013) Selective adsorption of Pb(II), Cd(II) and Ni(II) ions from aqueous solution using Chitosan-MAA Nanoparticles. *International Journal of Biological Macromolecules.* **61:** 251-263

Heller-Kallai. L. (2001). Protonation- Deprotonation of Dioctahedral Smectites. *Appl. Clay Sci*. **20(1-2):** 27-38.

Herdan. J., Feeney. R., Kounaves. S. P., Flannery. A. F., Storment. C. W. & Kovacs. G. T. A. (1998). Field Evaluation of an electrochemical probe for In-Situ screening of heavy metals in groundwater. *Environmental Science & Technology.* **32(1)**: 131-136.

Ho, T. C., Tan, T., Chen, C., and Hopper, J. R. (1991). Characteristics of metal capture during fluidized bed incineration. *AICHE Symp. Ser.* **281(87):** 118–126.

Hodi. M, Polyak. K and Htavay. J. (1995). Removal of pollutants from drinking water by combined Ion-exchange and adsorption methods. *Environmental International.* **25:** 325-331

Hohman, M. M., Shin, M., Rutledge, G.C. and Brenner, M.P., (2001). Electrospinning & electrically Forced Jets, I. Stability Theory. *Physics of Fluids*, **13**, 2201-2220.

Hohman, M. M., Shin, M., Rutledge, G.C. and Brenner, M.P., (2001). Electrospinning and Electrically Forced Jets. II. Applications. *Physics of Fluids.* **13**, 2221-2236.

Hojati, S. and Khademi, H. (2013). Cadmium sorption from aqueous solutions onto an Iranian sepiolite: Kinetics and isotherms. *J. Central-South Univ. Technol.*, **20:** 3627-3632.

Hong, L., Wang, Y. L., Jia, S. R., Huang, Y., Gao, C., & Wan, Y. Z. (2006). Hydroxyapatite-bacterial cellulose composites synthesized via a biomimetic route. *Materials Letters*. **60:** 1710–1713.

Horsfall M, Spiff A. I. & Abia. A. A . (2004). Studies on the influence of mercaptoacetic acid (MAA) modification of cassava (manihot sculenta cranz) waste biomass on the adsorption of Cu^{2+} and Cd^{2+} from aqueous solution. *Korean Chemical Society*. **25**(7): 969-976.

Horsfall, M. & Spiff, A. I. (2004). Studies on the effect of pH on the sorption of Pb^{2+} and Cd^{2+} ions from aqueous solutions by caladium bicolor (wild cocoyam) biomass. *Electronic J. Biotechnol*. **8:** 2.

Horsfall. M. and Spiff. A. I. (2005). Equilibrium sorption study of Al^{3+}, Co^{2+} andAg^{2+} in aqueous solutions by fluted pumpkin (Telfairia occidentalis HOOK) waste biomass, *Acta Chim. Slov*. **52:** 174–181.

Hua. G. & Reckhow. D. A. (2007). Comparison of disinfection byproduct formation from Chlorine and alternative disinfectants. *Water Res.* **41(8)**: 1667-1678

Huang. C. P. & Ostovic. F. B. (1978) Removal of cadmium(II) by activated carbon adsorption. *J. Environ. Eng. ASCE.* **104:** 863–878.

Huang, H. H.; Orler, B.; Wilkes, G. L. (1985). Ceramers: Hybrid materials incorporating polymers/ oligomeric species with inorganic glasses by sol-gel process. *Polym. Bull.* **14(6):** 557- 564.

Huang, S. L., Chin, W.K., & Yang, W.P. (2005). Structural characteristics and properties of silica/poly(2hydroxy ethylmethacrylate) (PHEMA) nanocomposites prepared by mixing colloidal silica or tetraethyloxysilane (TEOS) with PHEMA. *Polymer*. **46:** 1865–1877.

Hutson. N. D., Yang. R. T. (1997). Theoretical basis for the Dubinin-Radushkevitch (D-R) adsorption isotherm equation, *Adsorption.* **3:** 189-195.

IARC. (1993). Cadmium and Cadmium Compounds (Group 1). IARC monographs **Vol. 58**: 1993. International Agency for Research on Cancer, Lyon France.

Ibrahim. M., Nada. A., Kamal. D. E. (2005). Density Functional Theory and FTIR spectroscopy of carboxyl groups. *Indian Journal of Pure and Applied Physics.* **43:** 911-917.

Igwe. J. C & Abia. A. A (2003) Maize cob and husks as adsorbents for the removal of Cadmium, Lead and Zinc ions from wastewater. *The Physical Scientist*. **2:** 210-215.

Inglezakis. V. J., Loizidou. M. D., Grigoropoulou. (2002). H. P. Equilibrium and kinetic ion exchange studies of $Pb^{2+,}$ Cr^{3+}, Fe^{3+} and Cu^{2+} on natural clinoptilolite. *Water Res.* **36:** 2784–2792.

Iguchi, M., Yamanaka, S., & Budhiono, A. (2000). Bacterial cellulose – a masterpiece of nature's arts. *Journal of Materials Science*. **35:** 261–270.

Igwe. J. C., Abia. A. A., Ibeh. C. A. (2008). Adsorption kinetics and intra-particulate diffusivities of Hg, As and Pb ions on unmodified and thiolated coconut fiber. *Int.J. Environ. Sci. Technol.* **5:** 83–92.

Isa, M.H., Ibrahim, N., Abdul Aziz, H., (2008). Removal of Chromium (VI) from aqueous solution using treated oil palm fiber. *J. Hazard. Mater*. **152:** 662.

Itodo. A. U., Happiness. U. O., Obaroh. I. O., Usman. A., Audu. S. S. (2009). Temkin, R-D, Langmuir and Freundlich adsorption Isotherms of industrial dye uptake unto H_3PO_4 catalyzed poultry waste bio-adsorbent. *Journal of Science and Technology research* **8**(1):52- 56.

Itodo. A.U. and Itodo H.U. (2010). Sorption Energies Estimation Using Dubinin-Radushkevich and Temkin Adsorption Isotherms. *Life Science Journal*. **7(4):** 48-50

IUPAC. (1997). *Copendium of chemical terminology, 2nd Ed. (the 'Gold Book').* Compiled by A.D Mc Naught and A. Wilkinson. Blackwell Scientific Publications, Oxford.

Jarup. L, M. Berglund, C G Elinder, G Nordberg and M Vahter. (1998). Health effects of Cadmium exposure- a review of the literature and a risk estimate. *Scand. J . Work. Environ. Health*. **24:**1:51

Ji. F, Li. C.,Tang. B, Xu. J, Lu. G. & Liu. P. (2012). Preparation of cellulose acetate/ zeolite composite fiber and its adsorption behaviour for heavy metals in aqueous solution. *Chemical Engineering Journal 2012.* **209:** 325-333

Jiang, L. Y., Li, Y. B., Wang, X. J., Zhang, L., Wen, J. Q., & Gong, M. (2008). Preparation and properties of nano-hydroxyapatite/chitosan/carboxymethyl cellulose composite scaffold. *Carbohydrate Polymers.* **74:** 680–684.

Karn, B.; Kuiken. T; Otto. M. (2009). "Nanotechnology and in Situ Remediation: A Review of the Benefits and Potential Risks". *Environmental Health Perspectives.* **117 (12):**1823–1831.

Kaya A. and Ören A.H., (2005)**.** Adsorption of zinc from aqueous solutions to the bentonite. *J. Hazard. Mater.*, **125:** 183-189.

Kesraoui-Ouki. S., Cheeseman C. & Perry R. (1993). Effects of conditioning and treatment of chabazite and clinoptilolite prior to Lead and Cadmium Removal. *Environ. Sci. Technol.* **27(6):** 1108-1116.

Kickelbick. G. (2007). In *Hybrid Materials. Synthesis, Characterization, and Applications*; Kickelbick, G., Ed.; Wiley-VCH: Weinheim, Germany; Chapter 1.

Kim. H. S. and Kim. H. J. (2008). Influence of the zeolite type on the mechanical- thermal properties and volatile organic compound emissions of natural flour-filled polypropylene hybrid composites. *J. Appl. Polym. Sci.* **110(5):** 3247- 3255.

Kim. W., Lee. J. S., Bucknall. G., Koros. W. J., Nair. S. (2013). Nanoporous layered silicate AMH-3/cellulose acetate nanocomposite membranes for gas separations. *Journal of Membrane Science* **441:**129–136

Kimani, E., Mbui. D., Kamau. G., W. (2012). Adsorption of Lead (II) and Iron (III) ions from aqueous solutions using Kenyan Zeolite, Kisii soapstone and bentonite clay. *M.Sc. Thesis UoN***.**

Klemm, D., Heublein, B., Fink, H. P., & Bohn, A. (2005). Cellulose: Fascinating biopolymer and sustainable raw material. *Angewandte Chemie International Edition*, **44:** 3358–3393.

Koyama. K & Takeuchi. Y (1977). Clinoptilolite: the distribution of potassium atoms and it's role in thermal stability. *Z. Kristallogr.* **145:** 216–239.

Krishna. B. S, Murty. D. S. R., Jai-Prakash. B. S. (2000). Thermodynamics of Chromium (VI) Anionic Species sorption onto Surfactant- Modified Montmorillonite Clay. *J. Colloid Interf Sci.* **229:** 230- 236.

Krishna. R. H. and Swamy. A. V. V. S. (2012).Investigation on the effect of particle size and adsorption kinetics for the removal of Cr(VI) from the aqueous solutions using low cost sorbent. *Eur. Chem. Bull.* **1(7):** 258-262

Krishnamoorti, R.; Vaia, R. A. (2007). Polymer Nanocomposites. *J. Polym. Sci., Part B: Polym. Phys.* **45(24):** 3252-3256.

Krishnamoorti. R., Vaia. R. A., Giannelis. E. P. (1996). Structure and dynamics of polymer-layered silicate nanocomposites. *Chem Mater* **8:** 1728-1734

Kumar. K. V.&, Sivanesan. S. (2007). Sorption isotherm for safranin onto rice husk: comparison of linear and non-linear methods. *Dyes Pigments*. **72:** 130–133.

Kurama. H., Zimmer. A. & Reschetilowski. T. (2002). Chemical modification effect on the sorption capacities of natural clinoptilolite. *Chemical Engineering & Technology*. **25:** 301–305.

Landrigan. P. J. (1989). Toxicity of lead at low dose. *British Journal of Industrial Medicine*, **46(9**):593–596.

Langmuir. I. (1916). The constitution and fundamental properties of solids and liquids, *J. Am. Chem. Soc.* **38 (11):** 2221–2295.

LeBaron. P. C., Wang. Z. & Pinnavaia. T. J. (1999). Polymer-layered silicate nanocomposites: an overview. *Appl Clay Sci* **15:** 11–29.

Leddy. N. *Surface Area and Porosity*. (2012). Centre for Microscopy Analysis (CMA). Analytical Workshop.

Lee. D. H. and Moon. H. (2001). Adsorption equilibrium of heavy metals onto natural zeolites. *Korean Journal of Chem Engineering.* **18 (2):** 247-256.

Lee. M. G., Cheon. J. K., Kam. S. K. (2003). Heavy metal adsorption characteristics of zeolite synthesized from fly ash. *J. Ind. Chem. Eng*. **9(2):** 174-180.

Legube. B. & Vel Leitner. K. (1999). Catalytic Ozonation: a promising advanced oxidation technology for water treatment. *Catalysis Today.* **53:** 61-72.

Lennard- Jones, J. E. (1924). On the Determination of Molecular Fields. *Proc. R. Soc. Lond. A.* **106 (738):** 463-477.

Li. S. M., Jia. N., Zhu. J. F., Maa. M. G., Sun. R. C. (2010). Synthesis of cellulose–calcium silicate nanocomposites in ethanol/water mixed solvents and their characterization. *Carbohydrate Polymers* **80:** 270–275

Li. Y., Li. X., Chu. J., Dong. C., Qi. J. and Yuan. Y. (2010). Synthesis of core-shell magnetic molecular imprinted polymer by the surface RAFT polymerization for the fast and selective removal of endocrine disrupting chemicals from aqueous solutions *Environ. Pollut.* **158:** 2317–2323.

Li. Y., Dong. C., Chu. J., Qi. J. and Li. X. (2011). Surface molecular imprinting onto fluorescein-coated magnetic nanoparticles *via* reversible addition fragmentation chain transfer polymerization: A facile three-in-one system for recognition and separation of endocrine disrupting chemicals *Nanoscale.* **3:** 280–287.

Limousin. G., Gaudet. J. P, Charlet. L., Szenknect. S., Barthes. V., Krimissa. M. (2007). Sorption isotherms: a review on physical bases, modeling and measurement. *Appl. Geochem.* **22:** 249–275.

Lin. C. Y. & Yang. D. H. (2002). Removal of pollutants from wastewater by coal bottom ash, *J. Environ. Sci. Health, Part A: Toxic/Hazard. Subst. Environ. Eng.* **37**: 1509–1522.

Lindqvist, O. (1995). Environmental impact of mercury and other heavy metals. *J. Power Sources* **57:** 3–7.

Liu. B., Han. M., Guan. G., Wang. S., Liu. R. and Zhang. Z. (2011). Highly- Controllable Molecular Imprinting at Superparamagnetic Iron Oxide Nanoparticles for Ultrafast Enrichment and Separation. Z. *J. Phys. Chem. C.* **115(35):** 17320–17327.

Liu, S. L., Zhang, L. N., Zhou, J. P., & Wu, R. X. (2008). Structure and properties of

cellulose/Fe_2O_3 nanocomposite fibers spun via an effective pathway. *The Journal of Physical Chemistry C*. **112:** 4538–4544.

Lopez, O. D. (2009). Green technologies for sulphate and metal removal in mining and metallurgical effluents. *Environmine*, **1:** 9.

Lottermoser, B. (2003). *Mine wastes Characterization, Treatment and Environmental Impacts;* Springer: Berlin, Germany.

Lowe. E. F., Battoe. L. E., Stites. D. & Coveney. M. (1992). Particulate phosphorus removal via wetland filtration : An examination of the potential for hypertropic Lake restoration. *Env. Mgmt.* **16(1):** 67-74

Luna-Xavier, J. L.; Bourgeat-Lami, E.; Guyot, A. (2001). The role of initiation in the synthesis of silica/ poly(methyl methacrylate) nanocomposite latex particles through emulsion polymerization. *Colloid Polym. Sci.* **279:** 947-958.

Luo. X., Deng. F., Min. L., Luo. S., Guo. B., Zeng. G. and Au. C. (2013). Facile one-step synthesis of inorganic-framework molecularly imprinted TiO_2/WO_3 nanocomposite and its molecular recognitive photocatalytic degradation of target contaminant. *Environ. Sci. Technol.*, **47(13):** 7404–7412.

Ma, H., Zhou, B., Li, H.-S., Li, Y.-Q. & Ou, S.-Y. (2011). Green composite films composed of nanocrystalline cellulose and a cellulose matrix regenerated from functionalized ionic liquid solution. *Carbohydrate Polymers*. **84(1):** 383–389.

Macias-Perez. M. C., Salinas-Martinez de Lecea., Muiloz- Guillena. C. M. and Linares-Solano. (1996). *A. Low Temperature SO_2 Capture by Calcium-Based Sorbents: Characterization of the Active Calcium*. Inorganic Chemistry Department, Alicante University, Alicante, Spain.

Madejova. J. (2003). FTIR techniques in clay mineral studies. Review. *Vibrational Spectroscopy*. **31:**1-10

Malakootian. M., Nouri. J. and Hossaini. H. (2009) Removal of Heavy Metals from paint industry's Wastewater using Leca as an available adsorbent. *Int J Environ Sci Tech* **6(2):** 183-190. ISSN: 1735-1472.

Marques, P. A. A., Trindade, T., & Neto, C. P. (2006). Titanium dioxide/cellulose nanocomposites prepared by a controlled hydrolysis method. *Composites Science and Technology*, **66:** 1038–1044.

Maurer. M. & Boller. M. (1999). Modelling of phosphorus precipitation in wastewater treatment plants with Enhanced Biological Phosphorus Removal. *Water Science and Tech.* **39(1):** 147-163

Mäurer. T. and Czarnetzki. B. (2001). Effect of Electrolyte Addition on the Colloidal Stability of Aqueous Zeolite Sols. *Helvetica Chimica Acta*, **84(9):** 2550-2556

Mahmoudian, S., Wahit, M. U., Imran, M., Ismail, A. F., & Balakrishnan, H. (2012). A facile approach to prepare regenerated cellulose/graphene nanoplatelets nanocomposite using room-temperature ionic liquid. *Journal of Nanoscience and Nanotechnology*. **12(7):** 5233–5239.

Mahmoudian, S., Wahit, M. U., Ismail, A. F., & Yussuf, A. A. (2012). Preparation of regenerated cellulose/montmorillonite nanocomposite films via ionic liquids. Carbohydrate Polymers. **88(4):** 1251–1257.

Marsalek. R. (2012). Zeta Potential – Applications**.** *2012 2nd International Conference on Environment and Industrial Innovation IPCBEE.* vol.35 IACSIT Press, Singapore.

McCaughey, B.; Hampsey, J. E.; Wang, D. H.; Lu, Y. F. (2004). In *Encyclopedia of Nanoscience and Nanotechnology*; Nalwa, H. S., Ed.; American Scientific Publishers: Stevenson Ranch, CA, 2004. **9**: 529-559.

McFarlane. J. W., Tesh. S. J., Crane. R. A., Hallam. K. R., Scott. T. B. (2014). Synthesis of nanocomposite surfaces via the co-deposition of metallic salts and nano particles. *Mater. Sci. Eng. B.* **182:** 59 .

McNaught. A. D. and Blackwell. A. W. (IUPAC). (1997). *Definition of electrokinetic potential in "IUPAC. Compendium of Chemical Terminology", 2nd ed. (the "Gold Book"*). Compiled by Scientific Publications, Oxford (1997). ISBN 0-9678550-9-doi:10.1351/goldbook

Mehizadeh. S., Sadjadi. S., Ahmadi. S. J. & Outokesh. M. (2014). Removal of heavy metals from aqueous solution using platinum nanoparticles/ zeolite-4A. *Journ. Of Env. Health. Sci. & Eng.* **12:** 7.

Merkel, T. C.; Freeman, B. D.; Spontak, R. J.; He, Z.; Pinnau, I.; Meakin, P.; Hill, A. J.(2002). Sorption, transport, and structural evidence for enhanced free volume in poly (4-methyl-2-pentyne)/fumed silica nanocomposite membranes. *Chem. Mater.* **15(1):** 109-123

Merkel, T. C.; He, Z. J.; Pinnau, I.; Freeman, B. D.; Meakin, P.; Hill, A. J. (2003). Sorption and transport in poly(2,2-bis(trifluoromethyl)-4,5-difluoro-1,3-dioxole-co-tetrafluoroeth ylene) containing nanoscale fumed silica. *Macromolecules.* **36:** 8406-8414.

Milan Z., Sanchez E., Weiland P., de Las Pozas C., Borja R., Mayari R. and Rovirosa N. (1997). Ammonia removal from anaerobically treated piggery manure by ion exchange in columns packed with homoionic zeolite. *J. Chem. Eng.* **66(1):** 65-71.

Millennium Ecosystem Assessment (MA). (2005). *Ecosystems and Human Well-being: Synthesis*. Island Press, Washington, DC.

Miller-Chou, B.A. & Koenig, J. L. (2003). A Review of Polymer Dissolution. Progress in *Polymer Science*, **28(8):** 1223-1270.

Mishra. A. K., Mishra. S. B., Mamba. B. B., Dlamini. D. S. & Mthombo. T. S. (2013) Fabrication and Characterization of HCl-Treated Clinoptilolite Filled Ethylene Vinyl Acetate Composite Films. *J. Appl. Polym. Sci*, DOI: **10**.1002/APP.38021.

Mishra. A. M. (2015). *Nanocomposites for wastewater treatment.* Published by Pan Stanford Publishing Pte. Ltd. Penthouse Level, Suntec Tower 3 8 Temasek Boulevard Singapore 038988.

Mohan. S., Sreelakshmi. G. (2008). Fixed bed column study for heavy metal removal using phosphate treated rice husk. *J. Hazard. Mater*. **153:** 75–82.

Mohapatra S. P. (1988). Distribution of heavy metals in polluted creek sediment. *Environmental Monitoring and Assessment.* **10(2):** 157-163.

Moms. R. D., Audet. A. M, Angelillo. I. F., Chalmers. T. C. and Mosteller. F. (1992). Chlorination, Chlorination By-products, and Cancer: A Meta-analysis. *American Journal of Public Health*. **82(7):** 955-963.

Morel F. M. M. and Hering J. G. (1993). Principles *and Applications of Aquatic Chemistry.* Wiley, New York, NY.

Moreno, N.; Querol, X.; Ayora, C.; Ferna´ndez-Pereira, C.; Janssen- Jurkovicova´, M. (2001). Utilization of zeolites synthesized from coal fly ash for the purification of acid mine waters. *Environ. Sci. Technol.* **35:** 3526-3534.

Mozgawa. W., Jastrzebski, Handke. M. (2005). Vibrational Spectra of D4R and D6R structural Units. *Journal of molecular structure*. **744-747:** 663-670.

Mozgawa. W., Krol. M., Barczyk. (2011). K. FTIR studies of zeolites from different structural groups. *Chemik*. **65 (7):** 667-674.

Mthombo. S. T., Mishra. A. K., Mishra. S. B. & Mamba. B. B**.** (2009) Synthesis and characterization of polymer-zeolite composites for the removal of heavy metals from water – Poster Presentation. *1st BIOMATASA Conference, 23rd – 25th September 2009*, CSIR, Pretoria, South Africa.

Mthombo. T. S., Mishra. A. K., Mishra. S. B. and Mamba. B. B. (2011). The adsorption behavior of Cu(II), Pb(II), and Co(II) of ethylene vinyl acetate-clinoptilolite nanocomposites. *Journal of Applied Polymer Science*, **121:** 3414–3424.

MuRoz- Guillena, M. J., Linares-Solano, A. and Salinas-Martinez, de Lecea, C. (1995). A new Parameter to characterize limestones as SO_2 sorbents. *Appl. Surf. Sci*.. **89:** 197- 203.

Musarrat. J., Zaidi. A., Khan. M. S., Siddiqui. M. A. and Al-Khedhairy. A. A. (2011). Genotoxicity assessment of heavy metal-contaminated soils. *Environ.Pollut.* **20:** 323–342.

Nagajyoti, P.C., Lee. K. D. and Sreekanth, T. V. M. (2010). Heavy metals, occurrence and toxicity for plants: a review. *Environ.Chem.Lett.* **8:** 199–216.

Naidu. D. A., King. P, Narayana Saibaba. K. V & Prasad. V. S. R. K. (2013) Equilibrium, kinetic and thermodynamic studies on lead removal From aqueous solution by *Tectona grandis l.f. International Journal of Research in Engineering & Technology (IJRET)* **1(2):** 35-48.

Nameni, M., Moghadam. M. R. A and Arami. M. (2008). Adsorption of hexavalent chromium from aqueous solutions by wheat bran. *M. Int. J. Environ. Sci. Tech* **5(2):** 161-168.

National Research Council (1992). *Environmental neurotoxicology*. Washington, DC, National Academy Press (http://www.nap.edu/openbook.php?record_id=1801, accessed 24 November 2009).

Ndeda. L. A., Manohar. S. (2014). Determination of Heavy Metals in Nairobi Dam Water, (Kenya). *IOSR Journal of Environmental Science, Toxicology and Food Technology (IOSR-JESTFT)* **8(5-IV)**: 68-73

Nechifor. G., Pascu. D. E., Pascu. M., Traistaru. G. A. and Albu. P. C. (2015). Comparative study of Tempkin and Flory-Huggins Isotherms for adsorption of Phosphate anion on membranes. *U.P.B. Sci. Bull., Series B*, **77(2):**1454 – 2331.

Needleman. H. L., Gunnoe. C., Leviton. A., Reed. R., Peresie. H. & Maher. C. (1979). Deficits in psychologic and classroom performance of children with elevated dentine lead levels. *New Engl J Med.* **300**: 689-695

Needleman. H. L., Schell. A., Bellinger. D., Leviton. D. & Allred. E. N. (1990). The long-term effects of exposure to low doses of lead in childhood. An 11-year follow-up report. *New England Journal of Medicine*. **322(2):** 83–88.

Needleman. H. L., Reiss. J. A., Tobin. M. J., Biesecker. G. E. & Greenhouse J. B. (1996). Bone lead levels and delinquent behavior. *Journal of the American Medical Association*. **275(5):** 363–369.

Needleman. H. L. McFarland. C., Ness. R. B., Fienberg. S. E. & Tobin. M. J. (2002). Bone lead levels in adjudicated delinquents. A case control study. *Neurotoxicology and Teratology*. **24(6):** 711–717.

Nevin. R. (2000). How lead exposure relates to temporal changes in IQ, violent crime and unwed pregnancy. *Environmental Research*. **89:**1–22.

Newbury D. E., Fiori. C. E., Marinenko. R. B., Myklebust. R. L., Swyt. C. R., Bright. D. S. (1990). Compositional mapping with the electron probe microanalyzer: Part I. *Anal. Chem*. **62:** 1159A- 1166A

Nigg. J. T., Casey. B. J. (2005). An integrative theory of attention-deficit/ hyperactivity disorder based on the cognitive and affective neurosciences. *Development and Psychopathology*, **17(3):** 785–806.

Nigg. J. T., Knottnerus. M. G., Martel. M. M., Nikolas. M., Cavanagh. K., Karmaus. W. & Rappley. D. M. (2008). Low blood lead levels associated with clinically diagnosed attention-deficit/hyperactivity disorder and mediated by weak cognitive control. *Biological Psychiatry*. **63(3)**: 325–331.

Ning P, Bart H. J., Li B, Lu. X., Zhang. Y. (2008). Phosphate removal from wastewater by model-La(III) zeolite adsorbents. *Journal of Environmental Sciences* **20:** 670–674.

Nordic Council of Ministers. (2003). *Cadmium Review*. Report **No. 1** Issue No. 04.

Nguyen. C. & Do. D. D. (2001). The Dubinin–Radushkevich equation and the underlying microscopic adsorption description. *Carbon* **39:** 1327–1336.

Nguyen. Q. T. & Baird. D. G**.** (2006). Preparation of Polymer–Clay Nanocomposites and Their Properties. *Advances in Polymer Technology*. **25(4):** 270–285.

Nriagu. J. O. (1989). A global assessment of natural sources of atmospheric trace metals. *Nature*. **338:** 47-48

Nurmi. J. T., Tratnyek. P. G., Sarathy. V., Baer. B. R., Amonette. J. E., Pecher. K., Wang. C., Linehan. J. C., Matson. D. W., Penn. R. L., Driessen. M. D.(2004). *Environ. Sci. & Technol.* **39:** 1221.

Obare, S.O. and Meyer, G.J. (2004). Nanostructured materials for environmental remediation of organic contaminants in water. *J. Environ. Sci. Health, Pt. A: Toxic/Hazard. Subst. Environ. Eng,*. **30 (10):** 2549-2582.

Obiri-Nyarko. F., Malina. J. K., Malina. G. & Kasela, T. (2014). Removal of Lead and Benzene from Groundwater by Zeolite and Brown Coal: Isotherm and Kinetic Studies. *Proceedings of the 4th International Conference on Environmental Pollution and Remediation Prague, Czech Republic, August 11-13, 2014 Paper No. 83.*

Ogoyi, D. O., Mwita, C. J., Nguu, E. K. & Shiundu, P. M. (2011). Determination of heavy metal content in water, sediment and microalgae from Lake Victoria, East Africa. *The Open Environmental Engineering Journal,* **4:** 156-161.

Okada A., Kawasumi M, Usuki A, Kojima Y, Kurauchi T, Kamigaito O. (1990). *Synthesis and properties of nylon-6/clay hybrids.* In: Schaefer DW, Mark JE, editors. Polymer based molecular composites. MRS Symposium Proceedings, Pittsburgh. **171:** 45–50.

Oke. I. A., Olarinoye. N. O. and Adewusi. S. R. A. (2008). Adsorption Kinetics for Arsenic Removal from aqueous solutions by untreated powdered eggshells. *Adsorption* **14:**73-83.

Oliveira. S. C. B., Corduneanu. O., Oliveira-Brett. M. A. (2008). In situ evaluation of heavy metal–DNA interactions using an electrochemical DNA biosensor. *Bioelectrochemistry* **72:** 53–58

Olsson. C. and Westman. G. (2013). Direct Dissolution of Cellulose: Background, Means and Applications. *Intechopen Journal.* DOI: 10. 5772/52144.

Oriakhi. C. O. (1998). Nano Sandwiches. *Chemistry in Britain (Chem. Br.)* **34:** 59-62.

OSPAR. (2002). Cadmium. Hazardous Substances Series. OSPAR Commission. ISBN 0946956936.

Ouki. S. K. & Kavannagh M. (1999), Treatment of metals contaminated wastewaters by use of natural zeolites. *Water Science and Technology*. **39:** 115-122.

Oyoo-Okoth. E., Admiraal. W.,Osano. O., Ngure. V., Kraak. M. H. S., Omutange. E. S. (2010). Monitoring exposure to heavy metals among children in Lake Victoria, Kenya: Environmental and fish matrix. *Ecotoxicology and Environmental Safety* **73:** 1797–1803.

Panayotova, M. I. (2001). Kinetics and thermodynamics of copper ions removal from wastewater by use of zeolite. *Waste Management* **21(7)**: 671-676.

Panayotova, M. & Velikov, B. (2002) Kinetics of heavy metal ions removal by use of natural zeolite. *Journal of Environmental Science and Health.* **37(2):** 139–147.

Pandey, P. K., Sharma, S. K., Sambi, S. S. (2010). Kinetics and equilibrium study of chromium adsorption on zeolite NaX. *Int. J. Environ. Sci. Tech.* **7 (2):** 395-404.

Panuccio, M. R.; Sorgonà, A.; Rizzo, M.; Cacco, G., (2009). Cadmium adsorption on vermiculite, zeolite and pumice: Batch experimental studies. *J. Environ. Manage*., **90 (1):** 364-374

Patel. H. A., Somani. R. S., Bajaj. H. C. and Jasra. R. V. (2006). Nanoclays for polymer nanocomposites, paints, inks, greases and cosmetics formulations, drug delivery vehicle and waste water treatment. *Bull. mater. sci*.. **29(2):** 133–145

Pehlivan, H., Balkose, D., Ulku, S., Tihminlioglu, F. (2005). Characterization of pure and silver exchanged natural zeolite filled polypropylene composite films. *Comp. Sci. Technol*. **65:**2049-2058.

Perkin-Elmer Corporation. (1996). Analytical Methods for Atomic Absorption Spectroscopy. 0303-0152

Petit. S., Decarreau. A., Mosser. C. Ehret. G., Grauby. O. (1995). Hydrothermal Synthesis (250°C) of Copper-Substituted Kaolinites. *Clays Clay Mineral*. **43:** 482-494.

Pitcher. S. K., Slade R.C.T., Ward N.I. (2004). Heavy metal removal from motorway storm-water using zeolites. *Science of the Total Environment* **334– 335**: 161–166.

Prabhakar, S., Singh, A. K., and Pooni, D. S. (2012).Effect of environmental pollution on animal and human health: a review. *Ind.J.Anim.Sci***. 82:** 244–255.

Prasetyoko. D, Ramli. Z, Endud. S, Hamdan. H, Sulikowski. B. (2006) Conversion of rice husk ash to zeolite beta. *Waste Management* **26: 1173–1179**

Ramadan. A. R., Esawi. A. M. K., El Badawi. N., Mahmoud. M. (2015). Cellulose Acetate Nanocomposite Membranes for Water Desalination Applications. *Advanced materials for engineering applications.* Chapter **7**, *462-464.* The American University of Cairo, Egypt.

Rao. K. S., Anand. S., Venkateswarlu. P.(2010). Adsorption of cadmium(II) ions from aqueous solutions by tectona grandis L.F. (Teak Leaves Powder). *Bioresources*. **5:** 438–454.

Rashed. M. N. (2013). Adsorption Technique for the Removal of Organic Pollutants from Water and Wastewater. Intech. Aswan University, Egypt.

Ray, S. S. & Okamoto, M. (2003). Polymer/ Layered Silicate Nanocomposites: A review from preparation to processing. *Prog. Polym. Sci.* **28:** 1539.

Reischl. M., Stana-Kleinschek. K., Ribitsch. V. (2006). Electrokinetic Investigations of Oriented Cellulose Polymers. *Macromol. Symp.* **244:** 31–47.

Reculusa, S.; Mingotaud, C.; Bourgeat-Lami, E.; Duguet, E.; Ravaine, S. (2004). Synthesis of Daisy- Shaped and Multipod- like Silica/ polystyrene Nanocomposites. *Nano Lett.* **4 (9):**1677- 1682.

Reneker, D.H., Yarin, A.L., Fong, H. and Koombhongse, S. (2000) Bending Instability of Electrically Charged Liquid Jets of Polymer Solutions in Electrospinning. *J. of Appl. Phys.* **87:** 4531-4547.

Reynolds Research Group. (2012).*Shimadzu IRAffinity-1- User Guide and Tutorial for Taking IR Measurements in the 2nd Edition*: April 2012.

Rhodes. C. (2007). Zeolites: Physical Aspects and environmental applications. *Annu. Rep. Prog. Chem., Sect. C.* **103:** 287–325

Robati. D. (2013) Pseudo-second-order kinetic equations for modeling adsorption systems for removal of lead ions using multi-walled carbon nanotube. *Journal of Nanostructure in Chemistry.* **3:**55

Roberts. J. R. (1999). *Metal toxicity in children. In: Training Manual on Pediatric Environmental Health*. *Putting it into practice.* Children's Environmental Health: Emeryville, CA.

Rosa. G. and Clasen. T. (2010). Estimating the Scope of Household Water Treatment in Low and Medium Income Countries. *Am. J. Trop. Med. Hyg.* **82(2)**: 289-300

Roy. S. P. (2010). Overview of heavy metals and aquatic environment with notes on their recovery. *Ecoscan* .**4:** 235–240.

Rozic M., Cerjan-Stefanovic S., Kurajika S., Vanica V., Hodzic E. (2000). Ammoniacal nitrogen removal from water by treatment with clays and zeolites. *Water Res.* **34(14):** 3675-3681.

Russell. J. D., Fraser. A. R., in: Wilson. M. J. (Ed.). (1994). *Clay Mineralogy: Spectroscopic and Chemical Determinative Methods*, Chapman & Hall, London, UK. pp. 11.

Sabriye D. and Ali C. (2006). Pb(II) and Cd(II) Removal from Aqueous Solutions by Olive Cake. *J. Hazard. Mater.*, **138:** 22-28.

Saha, U. K., Taniguuchi, S., & Sakurai, K. (2002). Simultaneous sorption of cadmium, zinc, and lead on hydroxyaluminumand hydroxyaluminosilicate–montmorillonite complexes. *Soil Science Society of America Journal*. **66:** 117–128

Saifuddin N, Nian C Y, Zhan L W, Ning K X. (2011). Chitosan- Silver nanoparticles composites as Point of Use drinking water filtration system for household removal of pesticides in water. *Asian Journal of Biochemistry*. **6(2):** 142- 159.

Sanaeepur. H., Nasernejad. B. & Kargari. A. (2014). Cellulose Acetate/ nanoporous zeolite mixed matrix membrane for CO_2 separation. Greenhouse gases. *Science & Technology* **5 (3):** 291-304.

Sankar. M. U., Aigal. S., Maliyekkal. S. M., Chaudhary. A., Anshup., Kumar. A. A., Chaudhari. K. & Pradeep. T. (2013). Biopolymer- reinforced synthetic granular nanocomposites for affordable point-of-use water purification. *Proceedings of the National Academy of Sciences (PNAS).* **110(21):** 8459-8464 .

Santasnachok. C., Kurniawana. W. & Hinodea. H. (2015). Kinetic and Thermodynamic Studies of Removal of Cadmium Ion onto Synthetic Pure Zeolite from Rice Husk Ash, Thailand. *Global Journal of Research in Engineering.* **15(2)** Version I.

Sari, A., Tuzen, M., Citak, D. and Soylak, M. (2007). Equilibrium, kinetic and thermodynamic studies of adsorption of Pb (II) from aqueous solution onto Turkish kaolinite clay. *J. Hazard. Mater.*, **149:** 283-291.

Saswati. G and Ghosh. U. C.. (2005). Studies on the Adsorption Behavior of Cu (II) and Cr (VI) on Synthetic Hydroxyl Stannic Oxide. *Water SA*. **11 (4):** 597-602.

Savage, N. and Diallo, M. S. (2005). Nanomaterials and water purification: Opportunities and challenges., *Journal of Nanoparticle Research* **7**: 331–342.

Savina. I. N., English. C. J., Whitby. R. Zheng. L. Y., Leistner. A., Mikhalovsky. S. V., Cundy. A. B. (2011). High Efficiency removal of dissolved As (III) using iron nanoparticle-embedded macroporous polymer composites. *J. Hazard. Mater*. **192(3):** 1002-1008.

Schadler, L. S. (2003). *Nanocomposite Science and Technology*; Wiley- VCH: Weinheim, Germany. Chapter 2.

Schadler, L. S.; Kumar, S. K.; Benicewicz, B. C.; Lewis, S. L.; Harton, S. E. (2007). Designed Interfaces in Polymer Nanocomposites: A Fundamental Viewpoint. *MRSBull.* **32(4):** 335.

Schadler, L. S.; Brinson, L. C.; Sawyer, W. G. (2007). Polymer Nanocomposites - A Small Part of the Story. *Journal Of Materials*. **25(3):** 53-61.

Schaefer, D. W.; Justice, R. S. (2007). How nano are nanocomposites? *Macromolecules*, **40(24):** 8501- 8517.

Semmens, M. J.; Martin, W. P. (1988). Influence of pretreatment on the capacity and selectivity of clinoptilolite for metal ions. *Water Res.* **22:** 537–542.

Shaheen. S. M. (2009). Sorption and lability of cadmium and lead in different soils from Egypt and Greece. *Geoderma.* **153:** 61- 68.

Shaheen. S. M., Derbalah. A. S, and Moghanm. F. S. (2012). Removal of Heavy Metals from Aqueous Solution by Zeolite in Competitive Sorption System. *International Journal of Environmental Science and Development*, **3:** 4.

Sharifipour, F., Hojati, S., Landi, A. and Faz Cano, A. (2014). Kinetics and Thermodynamics of Lead Adsorption from Aqueous Solutions Onto Iranian Sepiolite and Zeolite. *Int. J. Environ. Res*., **9(3):**1001-1010.

Shoda. M. & Sugano. Y. (2005). Recent advances in bacterial cellulose Production. *Biotech. And Bioproc. Eng.* **10(1):** 1-8.

Shyaa. A , Hasan. O. A. & Abbas. A. M (2015) Synthesis and characterization of polyaniline/ zeolite nanocomposite for the removal of chromium(VI) from aqueous solution. *Journal of Saudi Chemical Society*. **19:**101–107.

Soheilmoghaddam, M., Wahit, M. U., & Ibrahim Akos, N.(2013). Regenerated cellulose/ epoxidized natural rubber blend film. *Materials Letters.* **111:** 221–224.

Soheilmoghaddam, M., Wahit, M. U., Mahmoudian, S.,& Hanid, N. A. (2013). Regenerated cellulose/halloysite nanotube nanocomposite films prepared with an ionic liquid. *Materials Chemistry and Physics.* **141(2–3):** 936–943.

Sokolova. I. M. & Lannig. G. (2008). Interactive effects of metal pollution and temperature on metabolism in aquatic ectotherms: implications of global climate change. *Climate Research*. **37:** 181–201.

Soloukhin, V. A.; Posthumus, W.; Brokken-Zijp, J. C. M.; Loos, J.; de With, G. (2002). Mechanical properties of silica–(meth) acrylate hybrid coatings on polycarbonate substrate. *Polymer.* **43:** 6169- 6181.

Somasundaran. P., Mehta. S. C., Yu. X., and Krishnakumar. S. (2008). *Handbook of Surface and Colloid Chemistry*, Third Edition. CRC Press, Taylor & Francis Group. Boca Raton/

London/ New York.- *Colloid Systems and Interfaces Stability of Dispersions through Polymer and Surfactant Adsorption,* **Chapter 6.**

Sparks. D. L. (2003). *Environmental Soil Chemistry*, III rd ed., Academic press, New York, USA.

Spicer, P. T.; Pratsinis, S. E.; Raper, J.; Amal, R.; Bushell, G.; Meesters, G., (1998). Effect of shear schedule on particle size, density and structure during flocculation in stirred tanks. *Powder Tech.*. **97 (1):** 26-34

Srivastava. S., Goyal. P. (2010). Novel Biomaterials Decontamination of Toxic Metals from Wastewater. Environmental Science & Engineering. Springer-Verlag, Berlin Heidelberg.

Stohs. S. J. & Bagchi. D.(1995). Oxidative mechanisms in the toxicity of metal ions. *Free radical biology and medicine* **18(2):** 321-336.

Su, Y. L. (2006). Preparation of polydiacetylene/ Silica nanocomposite for use as a chemosensor. *React. Funct. Polym.* **66 (9):** 967- 973.

Supraka. S. R., Pralay. M., Masami. O., Yamada. K & Ueda. K. (2002). New Polylactide/ Layered Silicate Nanocomposites: 1. Preparation, Characterization and properties. *Macromolecules* **35(8):** 3104-3110.

Taha. A. A., Wu. Yi., Wang. H. & Li. F. (2012). Preparation and application of functionalized cellulose acetate/silica composite nanofibrous membrane via electrospinning for Cr(VI) ion removal from aqueous solution. *Journal of Environmental Management* **112:** 10-16

Tashauoei, H. R., Movahedian A. H., Amin, M. M., Kamali, M., Nikaeen, M., Vahid Dastjerdi, M. (2010). Removal of cadmium and humic acid from aqueous solutions using surface modified nanozeolite A. *Int. J. Environ. Sci. Tech*., **7(3):** 497-508.

Teixeira. C. R., Arruda. M. A. Z. (2004). Biosorption of heavy metals using rice milling by-products. Characterisation and application for removal of metals from aqueous effluents. *Chemosphere* **54:** 987–995.

Tempkin. M. I., Pyzhev. V. (1940). Kinetics of ammonia synthesis on promoted iron catalyst, *Acta Phys. Chim.* USSR **12:** 327–356.

Terdkiatburana. T., Wang. S., Tad´e. M. O. (2008). Competition and complexation of heavy metal ions and humic acid on zeolitic MCM-22 and activated carbon. *Chemical Engineering Journal* **139:** 437–444

Tesh. S. J. and Scott. T. B. (2014). Nano-Composites for Water Remediation: A Review. *Adv. Mater.* **26:** 6056–6068

Theng. B. K. G. (1974). *The Chemistry of Clay-Organic Reactions*, Wiley Publishers., New York.

Tiarks, F.; Landfester, K.; Antonietti, M. (2001). Silica Nanoparticles as surfactants and fillers for latexes made by miniemulsion polymerization. *Langmuir*. **17(19):** 5775- 5780.

Tiwari, R. P., Ramudu. B.P., Srivastava. R. K., Gupta. M. K. (2007). Sorption And Desorption Studies Of Metallic Zinc On An Alluvial Soil. *Iranian J Environ. Health Sci Eng* **4:** 139.

Tobin. J. M., Cooper. D. G. Neufeld. R. J. (1984). Uptake of Metal Ions by *Rhizopus arrhizus* Biomass *Appl. Environ. Microbiol*, **47 (4):** 821-824.

Tosheva, L., & Valtchev, V. P. (2005). Nanozeolites: Synthesis, crystallization mechanism, and applications. *Chemistry of Materials*. **17(10):** 2494–2513.

Treacy. M. M & Higgins. J. B. (2001). Collection of simulated XRD Powder Patterns for Zeolites. *Published on behalf of the structure Commission of the International Zeolite Association* (4th Revised Edition). New York/ Amsterdam: Elsevier.

Tsibranska. I., Hristova. E. (2011). Comparison of different kinetic models for adsorption of heavy metals onto activated carbon from apricot stones. *Bulgarian Chemical Communications.* **43(3):** 370 – 377).

Tsioptsias, C., & Panayiotou, C. (2000). Preparation of cellulose–nanohydroxyapatite composite scaffolds from ionic liquid solutions. *Carbohydrate Polymers*. **74:** 99–105.

Tsitsishvili G. V., Andronikashvili T. G., Kirov G. N., Filizova L. D. (1992). *Natural Zeolites*, Ellis Horwood, New York 158.

Ulosoy. U. and Simsek. S. (2005). Lead removal by polyacrylamide- bentonite and zeolite composites: effect of phytic acid immobilization. *J. Hazard. Mater. B.* **127:** 163-171.

Unalan. I. U., Cerri. G., Marcuzzo. E., Cozzolino. C. and Farris. S. (2014). Nanocomposite films and coatings using inorganic nano-building blocks (NBB): current applications and future opportunities in the food packaging sector. *RSC Adv.* **4**: 29393

UNEP. (2010). *Clearing the Water: A focus on water quality solutions.* UNON Publishing Services Section, Nairobi. ISBN: 978-92-807-3074-6

Usuki A, Kojima Y, Kawasumi M, Okada A, Fukushima Y, Kurauchi T, Kamigaito O. (1993). Synthesis of nylon-6–clay hybrid. *J Mater Res*. **8:**1179–83.

Vaca-Mier. M., Callejas. R. L. P., Gehr. R., Cisneros. B. J. and Alvarez. P. J. J. (2001). Heavy metal removal with Mexican clinoptilolite: multi-component ionic exchange. Wat. Res. **35 (2)**: 373-378.

Vaia. R. A., Giannelis. E. P. (1997). Lattice of polymer melt intercalation in organically-modified layered silicates. *Macromolecules.* **30:** 7990–7999.

Vaia. R. A., Vasudevan. S., Krawiec. W., Scanlon. L. G., Giannelis. E. P. (1995). New polymer electrolyte nanocomposites: melt intercalation of poly(ethylene oxide) in mica-type silicates, *Adv. Mater.* **7:** 154-156.

Vaia. R. A., Price. G., Ruth. P. N., Nguyen. H. T., Lichtenhan. J. (1999). Polymer/layered silicate nanocomposites as high performance ablative materials. *Appl Clay Sci* **15:** 67–92.

Vassilis. J.I., Marinos. A.S., Despoina. G., and Maria. D.L. (2007). Removal of Pb(II) from Aqueous Solutions by Using Clinoptilolite and Bentonite as Adsorbents, *Desalination*. **210:**248-256.

Vermeulan. T. H., Vermeulan. K. R. and Hall. L. C. (1966). Fundamental. *Ind. Eng. Chem.* **5:** 212–223.

Vijayaraghavan. K., Padmesh. T.V.N., Palanivelu. K., Velan. M. (2006). Biosorption of Nickel(II) ions onto *Sargassum wightii*: application of two-parameter and three parameter isotherm models, J. *Hazard. Mater.* **B133**: 304– 308.

Vinod. G. K., Rastogi. A., Diwivedi. M. K., and Mohan. D. (1997). Process development for the removal of Zinc and Cadmium from wastewater using slag—A blast furnace waste material. *Sep. Sci. Technol*. **32:** 2883- 2912.

Viswanadham. N., Raviraj. K., Madhulika. S., Kumar. M. & Dhar. M. (2009). Catalytic properties of nano-sized ZSM-5 aggregates. *Catalysis Today.* **141:** 182-186

Voudrias. E., Fytianos. F. and Bozani. E. (2002). Sorption Description isotherms of Dyes from aqueous solutions and Waste Waters with Different Sorbent materials. *Global Nest, The Int.J.* **4(1):**75-83 .

Waalkes, M. P. (2000). Cadmium Carcinogenesis in review. *Jour. Inorganic Biochemistry*. **79:** 240-244.

Wallace. M. A., Aderval. S. L, Christine. A. H. and Antonio. C. A. (2003) An Evaluation of Copper Biosorptions by brown seaweed under optimized conditions. *Electronic Journal of Biotechnology*. **6 (3):** 5, ISSN: 0717-3458.

Wang. H. L., Chen. X. T., Yang. B., Ma. F. L., Wang. S., Tang. M. L., Hao. M. G. & Ruan. D. Y. (2008). Case-control study of blood lead levels and attention deficit hyperactivity disorder in Chinese children. *Environmental Health Perspectives*. **116(10):** 1401–1406.

Wang. M. & Rutledge. G. C. & Hsieh. A. J. (2004). Electrospinning of Poly (MMA-co-MAA) copolymers and their layered silicate nanocomposites for improved thermal properties. Dept. of Chemical Engineering Massachusetts Institute of Technology Cambridge, MA 02139; U.S. Army Research Laboratory AMSRD-ARL-WM-MD Aberdeen Proving Ground, MD 21005-5069.

Wang, M., Singh, H., Hatton, A. and Rutledge, G.C. (2004) Field-Responsive Superparamagnetic Composite Nanofibers by Electrospinning. *Polymer*. **45**, 5505-5514.

Wang, S., & Peng, Y. (2010). Natural zeolites as effective adsorbents in water and wastewater treatment. *Chemical Engineering Journal*. **156(1):** 11–24.

Wang, Y. Y.; Hsieh, T. E. (2007). Effect of UV Curing on Electrical Properties of a UV curable co-Polyacrylate/ Silica Nanocomposite as a Transparent Encapsulation Resin for Device Packaging. *Macromol. Chem. Phys.* **208:** 2396- 2402.

Webb. **P.** (2003). *Introduction to Chemical Adsorption Analytical Techniques and their Applications to Catalysis.* MIC Technical Publications. Micromeritics Instrument Corp., Norcross, Georgia 30093.

Weber. T. N. and Chakravarti. R. K. (1974) Pore and Solid Diffusion Models for fixed Bed Adsorbers . *J Am Inst Chem Eng* **20**:228-238.

Weller. M. T. & Dann. S. E. (1998). Hydrothermal Synthesis of Zeolites. *ChemInform.* **29(41):** no. doi:10.1002/chin.199841269

WHO. (1992) Cadmium- environmental aspects. Environmental Health Criteria 135. World Health Organisation, *International Program on Chemical Safety* (IPCS), Geneva, Switzerland.

WHO. (1993). Guidelines for Drinking Water Quality, Vol 1. WHO, Geneva. http://www.who.int/water_sanitation_health/GDW/Chemicals/Chemlist.html.

WHO. (2008). *Guidelines for drinking-water quality.* Third Edition. Incorporation the first and second agenda. Volume 1- Recommendations. ISBN 978924154761 1 (WEB version) (NLM classification: WA 675).

WHO. (2010). *Childhood Lead Poisoning.* WHO Press, World Health Organization, 20 Avenue Appia, 1211 Geneva 27, Switzerland ISBN 978 92 4 150033 3.

WHO. (2011). *Guidelines for drinking-water quality*. Fourth edition, Malta: Gutenberg. ISBN 978 92 4 154815 1.

Wijmans. J. G., Nakao. S. and Smolders. C. (1984). A. Flux limitation in ultrafiltration: osmotic pressure model and gel layer model. *Journal of membrane science.* **20:** 115-124

Winey, K. I.; Vaia, R. A. (2007). Polymer Nanocomposites. *MRS Bull.* **32:** 314-322.

Wingenfelder. U., Hansen. C., Furrer. G. and Schulin. R. (2005). Removal of Heavy Metals from Mine Waters by Natural Zeolites. *Environ. Sci. Technol.* **39:** 4606-4613.

Wingenfelder. U., Nowack B., Furrer G., and Schulin R., (2005). Adsorption of Pb and Cd by amine-modified zeolite. *Water Res*., **39:** 3287-3297.

Worch. **E.** (2012). *Adsorption Technology in Water Treatment. Fundamentals, processes and modeling.* Walter De Guyter GmbH & Co, KG, Publishers. Berlin/ Boston.Germany/ USA. ISBN 978-3-11-024022-1.

Wright. J. P., Dietrich. K. N., Ris. M. D., Hornung. R. W., Wessel. S. D., Lanphear. B. P., Ho. M., Rae. M. N. (2008). Association of prenatal and childhood blood lead concentrations with criminal arrests in early adulthood. *PLoS Medicine*, **5(5):** 101.

Xiangfeng. Z., Chen. X., Zhuang. J. (2015). Review: The positive relationship between ocean acidification and pollution. *Marine Pollution Bulletin*.**91:** 14–21

Xiaolei. Q., Alvarez. P. J. J., Li. Q. (2013). Applications of nanotechnology in water and wastewater treatment. *Water Research* **47**: 3931 -3946

Xu. J, Bhattacharyya. D. (2008). Modelling of Fe/Pd Nanoparticle- Based Functionalized Membrane Reactor for PCB Dechlorination at Room Temperature. *J. Phys. Chem., C.* **112 (25):** 9133- 9144.

Yakout. S. M and Ali. M. M. S. (2011). Sorption of cationic dyes onto activated carbon derived from agro-residues *J. At. Mol. Sci.*, **2(2**): 117-128

Yang. C. H. and Goodwin, Jr. J. G. (1982). Reversible Chemisorption on highly dispersed Ruthenium Catalysts. *Journal of Catalysis* **78(1)**: 182-187A.

Yao-Jen. T., Chen-Feng. Y. & Chien-Kuei. C. (2012). Kinetics and thermodynamics of adsorption for Cd on green manufactured nano-particles. *Journal of Hazardous Materials* **235– 236:** 116– 122.

Yarin, L., Koombhongse, S. and Reneker, D.H. (2001) Taylor Cone and Jetting From Liquid Droplets in Electrospinning of Nanofibers. *J. Appl. Phys.*, **90**: 4836- 4846.

Yu. J. H., Fridrikh, S. V. and Rutledge. G. C. (2004) Production of Submicron Diameter Fibers by Two- Fluid Electrospinning. *Advanced Materials*. **16:** 1562-1566.

Yu, L., Gong, J., Zeng, C., & Zhang, L. (2013). Preparation of zeolite-A/chitosan hybrid composites and their bioactivities and antimicrobial activities. *Materials Science and Engineering: C*, **33(7):** 3652–3660.

Zagorodni, A. A. (2007). *Ion exchange materials: Properties and applications*. Elsevier. Oxford, pp. 477. ISBN: 978-0-08-044552-6.

Zamzow. M. J., Eichbaum. B. R., Sandgren. K. R. and Shanks. D. E. (1990). Removal of heavy metals and other cations from wastewater using zeolites. *Sep. Sci*. *Technol*. **25:** 13–15: 1555.

Zhang, H., Wang, Z. G., Zhang, Z. N., Wu, J., Zhang, J., & He, J. S. (2007). Regenerated cellulose/ multi-walled carbon nanotube (MWCNT) composite fibers with enhanced mechanical properties prepared with an ionic liquid 1-allyl-3-methylimidazolium chloride (AmimCl). *Advanced Materials*, **19:** 698–704.

Zhang, M. Q.; Rong, M. Z.; Friedrich, K. (2003). In *Handbook of Organic- Inorganic Hybrid Materials and Nanocomposites*; Nalwa, H. S., Ed.; American Scientific Publishers: Stevenson Ranch, CA. **2:** 113-150.

Zhang. Q., Du. D., Jiao. T., Zhang. Z, Wang. S., Sun. Q. and Gao. F. (2013). Rationally designed porous polystyrene encapsulated zirconium phosphate nanocomposite for highly efficient fluoride uptake in waters. *Sci. Rep*. **3:** 2551.

Zhang. S. Q and Hou W.G., (2008) Adsorption behavior of Pb(II) on montmorillonite. *Coll. Surfaces A: Physicochem. Eng. Aspects*. **320:** 92-97.

Zheng, Y. P.; Zheng, Y.; Ning, R. C. (2003). Effects of nanoparticles SiO_2 on the performance of nanocomposites. *Mater. Lett.* **57 (19):** 2940- 2944.

Zhou, D., L. Zhang, J. Zhou and S. Guo. (2004). Cellulose/chitin beads for adsorption of heavy. metals in aqueous solution. *Water Res.* 3**8:** 2643-2650.

Ziemkiewicz, P. F.; Skousen, J. G.; Simmons, J. (2003). Long-term performance of passive acid mine drainage treatment systems. *Mine Wat. Environ.* **22:** 118-129.

Zou. H., Wu. S., and Shen. J. (2008). Polymer/Silica Nanocomposites: Preparation, Characterization, Properties, and Applications. *Chem. Rev.* **108:** 3893–3957.

Internet references

http://monographs.iarc.fr/ENG/Classification/List_of_Classifications.pdf. Retrieved on the 27th April, 2017 at 1324hrs.

http://iopscience.iop.org/article/10.1088/0143-0807/34/6/S123. Retrieved on the 7th Feb 2017 at 1738hrs

http://www.worldwildlife.org/threats/water-scarcity. Retrieved on the 17.06.2015 1048hrs.

https://www.slideshare.net/DrPriyBratDwivedi/kinetics-modeling-of-adsorption-processpptx Retrieved on the 18th April 2017 at 4.21pm

http://www.slideshare.net/sharmasuriti/atomic-absorption-spectroscopy-15185397. Retrieved on the 7th of Feb 2017 at 1727hrs.

http://www.sssj.org/ejssnt/duan-small.jpg. Retrieved on the 2nd Feb 2017 at 1626hrs.

http://www.ncbi.nlm.nih.gov/pmc/articles/PMC2689675/?tool=pubmed, accessed 19 November 2009.

http://www.cambridge.org/ Retrieved on the 27th April 2017 at 1331hrs.

www.thermo.com/eThermo/CMA/PDFs/Product/productPDF_11602.pdf. Retrieved on the 10.06.16 4.11pm

http://water.epa.gov/drink/contaminants/basicinformation/nitrate.cfm#four. Retrieved on the 17.06.15 1307hrs

https://commons.wikimedia.org/wiki/File:Cellulose_Acetate.png. Retrived on the 10th Feb 2017 at 1111hrs.

https://www.sciencetopia.net/physics/braggs-law. Retrieved on the 7th Feb 2017 at 1753hrs

http://www.nobelprize.org/nobel_prizes/chemistry/laureates/1901/hoff-bio.html retrieved on 24.01.2017 at 1455hrs

http://archive.cnx.org/contents/f5c058e0-41f2-4ef6-878b-2fdc07760129@1/bet-surface-area-analysis-of-nanoparticles. Retrieved on the 7th Feb 2017 at 1811hrs

http://www.nanocomposix.com- downloaded on the 5th December 2016

http://www.beilstein-journals.org/bjnano/single/articleFullText.htm?publicId=2190-4286-6-157. Retrieved on the 2nd Feb 2017 at 1513Hrs

http://www.epa.gov/dwreginfo . Retrieved on the 28th April, 2017 at 1117hrs.

https://www.osha.gov/SLTC/metalsheavy/index.html. Retrieved on the 28th April 2017 at 1228hrs.

http://www.fisica.unige.it Retrieved on the 28th April 2017 at 1445hrs.

http://heienv.com/hydroxide-precipitation-of-metals/ Retrieved on the 6th of July 2018 at 1200 hrs

APPENDICES

Appendix 1: Effect of varying zeolite ratios on adsorption

	Zeolite Ratio (%)	Ions adsorbed in mg/l	Ions adsorbed in mg/L	Ions adsorbed in mg/L	Ions adsorbed in mg/L	Std. Deviation	% adsorption
Lead (Initial Conc of 15 mg/L)	-	1st reading	2nd reading	3rd reading	mean		
	10.00	13.2000	13.0800	13.2500	13.1800	0.0875	87.87%
	20.00	14.6100	14.6300	14.4900	14.5800	0.0758	97.20%
	30.00	14.5200	14.5100	14.4600	14.5000	0.0324	96.70%
	40.00	14.3500	14.4000	14.3700	14.3700	0.0254	95.80%
	50.00	14.2300	14.2100	14.1700	14.2000	0.0308	94.67%

	Zeolite Ratio (%)	Ions adsorbed in mg/L	Ions adsorbed in mg/L	Ions adsorbed in mg/L	Ions adsorbed in mg/L	Std Deviation	% adsorption
Cadmium (Initial Conc of 15 mg/L)	-	1st reading	2nd reading	3rd reading	mean		
	10.00	4.1100	4.2800	4.2600	4.2200	0.0930	28.10%
	20.00	10.8500	10.8300	10.8600	10.8500	0.0158	72.30%
	30.00	11.9700	11.9500	11.9700	11.9600	0.0122	79.73%
	40.00	12.7600	12.7700	12.7500	12.7600	0.0100	85.06%
	50.00	11.2500	11.1600	11.1800	11.2000	0.0474	74.67%

Anova: Two-Factor Without Replication

SUMMARY	*Count*	*Sum*	*Average*	*Variance*
Row 1	2	17.4	8.7	40.1408
Row 2	2	25.43	12.715	6.95645
Row 3	2	26.46	13.23	3.2258
Row 4	2	27.13	13.565	1.29605
Row 5	2	25.4	12.7	4.5
Column 1	5	50.99	10.198	11.70852
Column 2	5	70.83	14.166	0.32448

ANOVA

Source of Variation	*SS*	*df*	*MS*	*F*	*P-value*	*F crit*
Rows	31.37546	4	7.843865	1.872431	0.27921	6.388233
Columns	39.36256	1	39.36256	9.396346	0.037463	7.708647
Error	16.75654	4	4.189135			
Total	87.49456	9				

Appendix 2: Effect of contact time on adsorption

	Time (Mins)	Ions adsorbed in mg/L	Ions adsorbed in mg/L	Ions adsorbed in mg/L	Ions adsorbed in mg/L	Std Deviation	% Adsorption
Cadmium Ion Conc. (15mg/L)		**1st reading**	**2nd reading**	**3rd reading**	**Mean**		
	0	0.0000	0.0000	0.0000	0.0000	0.0000	0.00%
	5	7.7700	7.7000	7.8100	7.7700	0.0557	51.80%
	10	8.2800	8.3900	8.3000	8.3200	0.0587	55.47%
	20	9.0000	8.9300	8.9900	8.9700	0.0381	59.80%
	40	10.6200	10.8100	10.7300	10.7200	0.0954	71.47%
	75	12.6700	12.8200	12.8800	12.7900	0.1082	85.27%
	Time (Mins)	**Ions adsorbed in mg/L**	**Ions adsorbed in mg/L**	**Ions adsorbed in mg/L**	**Ions adsorbed in mg/L**	**Std Deviation**	**% Adsorption**
		1st reading	2nd reading	3rd reading	Mean		
Lead Ion Conc. (15mg/L)	0	0.0000	0.0000	0.0000	0.0000	0.0000	0.00%
	5	13.4000	13.3200	13.3500	13.3600	0.0406	89.10%
	10	14.3300	14.3400	14.3300	14.3300	0.0071	95.53%
	20	14.7500	14.7400	14.7500	14.7500	0.0071	98.33%
	40	14.7800	14.7600	14.7500	14.7600	0.0159	98.40%
	75	14.8300	14.8400	14.8100	14.8300	0.0158	98.87%

Anova: Two-Factor Without Replication

SUMMARY	*Count*	*Sum*	*Average*	*Variance*
Row 1	2	0	0	0
Row 2	2	21.13	10.565	15.62405
Row 3	2	22.65	11.325	18.06005
Row 4	2	23.72	11.86	16.7042
Row 5	2	25.48	12.74	8.1608
Row 6	2	27.62	13.81	2.0808
Column 1	6	48.57	8.095	19.07691
Column 2	6	72.03	12.005	34.89347

ANOVA

Source of Variation	*SS*	*df*	*MS*	*F*	*P-value*	*F crit*
Rows	255.0863	5	51.01726	17.27572	0.003584	5.050329
Columns	45.8643	1	45.8643	15.53079	0.01095	6.607891
Error	14.7656	5	2.95312			
Total	315.7162	11				

Appendix 3: Kinetic data for adsorption experiments

$$q_e = \frac{\{(C_i - C_e)mgl^{-1} * 0.11\}}{0.04g} = \frac{15mgl^{-1} * 0.11}{0.04g} = 37.5\ mgg^{-1} Max\ adsorption\ capacity$$

$$q_t = \frac{\{(C_i - C_t)mgl^{-1} * 0.11\}}{0.04g}$$

C_i is the initial concentration of the metal ions (15mg/l); C_e is the equilibrium concentration after maximum adsorption; C_t is the concentration after time t.

Linear form of pseudo first order kinetic equation:

$\ln(q_e - q_t) = \ln q_e - k_1 t$

q_e is the maximum equilibrium adsorption capacity; q_t is the adsorption capacity at time t; k_1 is the 1st order kinetic constant.

Pseudo first order data for cadmium adsorption onto nanocomposites

Time (min)	**q_e (max adsorption capacity in mg/g)**	**q_t (adsorption capacity at time t in mg/g)**	**$q_e - q_t$ (mg/g)**	**$\ln(q_e - q_t)$**
0	37.500	0.000	37.500	3.624
5	37.500	19.425	18.075	2.895
10	37.500	20.800	16.700	2.815
20	37.500	22.425	15.075	2.713
40	37.500	26.800	10.700	2.370
75	37.500	31.975	5.525	1.709

Pseudo first order data for lead adsorption onto nanocomposites

Time (min)	**q_e (max adsorption capacity in mg/g)**	**q_t (adsorption capacity at time t in mg/g)**	**$q_e - q_t$ (mg/g)**	**$\ln(q_e - q_t)$**
0	37.500	0.000	37.500	3.624
5	37.500	33.400	4.100	1.411
10	37.500	35.825	1.675	0.516
20	37.500	36.875	0.625	-0.470
40	37.500	36.900	0.600	-0.511
75	37.500	37.075	0.425	-0.856

Linear form of pseudo second order kinetic equation:

$$\frac{t}{q} = \frac{1}{k_2 q_e^2} + \frac{t}{q_e}$$

Where:

k_2 is the rate constant of adsorption; q_e the amount of ions adsorbed at equilibrium (mg/g); q is the amount of ions adsorbed on the surface of the adsorbent at any time t (mg/g).

Pseudo second order data for Cadmium adsorption onto nanocomposites

Time (t in min)	**q (amount adsorbed at time t in mg/l)**	**t/q**
0	0.000	0.000
5	19.425	0.257
10	20.800	0.481
20	22.425	0.892
40	26.800	1.493
75	31.975	2.346

Pseudo second order data for lead adsorption onto nanocomposites

Time (t in min)	**q (amount adsorbed at time t in mg/l)**	**t/q**
0	0.000	0.000
5	33.400	0.150
10	35.825	0.279
20	36.875	0.542
40	36.900	1.084
75	37.075	2.023

Appendix 4: Effect of nanocomposite mass on adsorption

Cadmium (Initial Conc of 27mg/L)	Adsorbent mass (g)	Ions adsorbed in mg/L	Ions adsorbed in mg/L	Ions adsorbed in mg/L	Ions adsorbed in mg/L	Std. Deviation	% adsorption
	-	1st reading	2nd reading	3rd reading	Mean		
	0.02	7.0800	7.0600	7.0100	7.0500	0.0361	26.11%
	0.04	17.5900	17.6400	17.6200	17.6200	0.0255	65.26%
	0.05	20.4500	20.4500	20.4100	20.4400	0.0234	75.70%
	0.06	23.4100	23.4200	23.3400	23.3900	0.0436	86.63%

Lead (Initial Conc of 27mg/L)	Adsorbent mass (g)	Ions adsorbed in mg/L	Ions adsorbed in mg/L	Ions adsorbed in mg/L	Ions adsorbed in mg/L	Std. Deviation	% adsorption
	-	1st reading	2nd reading	3rd reading	Mean		
	0.02	13.0100	12.9900	12.9800	12.9900	0.0158	48.00%
	0.04	20.5300	20.5400	20.5100	20.5300	0.0158	76.00%
	0.05	24.4500	24.5200	24.4600	24.4800	0.0381	90.67%
	0.06	26.1200	26.1600	26.1400	26.1400	0.0200	96.81%

Anova: Two-Factor Without Replication

SUMMARY	*Count*	*Sum*	*Average*	*Variance*
Row 1	2	20.04	10.02	17.6418
Row 2	2	38.15	19.075	4.23405
Row 3	2	44.92	22.46	8.1608
Row 4	2	49.53	24.765	3.78125
Column 1	4	68.5	17.125	50.66337
Column 2	4	84.14	21.035	34.30203

ANOVA

Source of Variation	*SS*	*df*	*MS*	*F*	*P-value*	*F crit*
Rows	251.6545	3	83.88483	77.63041	0.002425	9.276628
Columns	30.5762	1	30.5762	28.29645	0.012978	10.12796
Error	3.2417	3	1.080567			
Total	285.4724	7				

Appendix 5: Effect of metal ion concentration on adsorption

	Original Conc in mg/L	Ions adsorbed In mg/L	Ions adsorbed in mg/L	Ions adsorbed in mg/L	Ions adsorbed in mg/L	Std. Deviation	% adsorption
	-	1st reading	2nd reading	3rd reading	Mean		
Cadmium	15	13.7600	13.7500	13.8300	13.7800	0.0436	91.87%
	30	20.2700	20.3400	20.3200	20.3100	0.0361	67.70%
	45	20.1700	20.6100	20.5700	20.4500	0.2433	45.44%
	60	10.2500	10.2600	10.4000	10.3000	0.0839	17.17%
	75	17.5300	17.5800	17.5400	17.5500	0.0264	23.40%

	Original Conc in mg/L	Ions Adsorbed in mg/L	Ions adsorbed in mg/L	Ions Adsorbed in mg/L	Ions adsorbed in mg/L	Std. Deviation	% adsorption
	-	1st reading	2nd reading	3rd reading	mean		
Lead	15	14.8500	14.8400	14.8000	14.8300	0.0264	98.87%
	30	27.4000	27.4600	27.4700	27.4400	0.0381	91.47%
	45	26.2400	26.2500	26.2400	26.2400	0.0071	58.31%
	60	31.3500	31.2800	31.2700	31.3000	0.0436	52.66%
	75	29.4400	29.4300	29.4500	29.4400	0.0100	39.25%

Anova: Two-Factor Without Replication

SUMMARY	*Count*	*Sum*	*Average*	*Variance*
Row 1	2	28.61	14.305	0.55125
Row 2	2	47.75	23.875	25.41845
Row 3	2	46.69	23.345	16.76205
Row 4	2	41.6	20.8	220.5
Row 5	2	46.99	23.495	70.68605
Column 1	5	82.39	16.478	19.26427
Column 2	5	129.25	25.85	41.6778

ANOVA

Source of Variation	*SS*	*df*	*MS*	*F*	*P-value*	*F crit*
Rows	129.43644	4	32.35911	1.132112	0.453587	6.388233
Columns	219.58596	1	219.586	7.682408	0.050243	7.708647
Error	114.33184	4	28.58296			
Total	463.35424	9				

Appendix 6: Effect of pH on the adsorption

	pH	Ions adsorbed in mg/L	Ions adsorbed in mg/L	Ions adsorbed in mg/L	Ions adsorbed in mg/L	Std. Deviation	% adsorption
Cadmium Initial (Conc. of 18mg/L)		1st reading	2nd reading	3rd reading	Mean		
	3.02	1.1400	1.1500	1.1900	1.1600	0.0265	6.40%
	4.00	1.8000	1.5000	2.0100	1.7700	0.2563	9.80%
	6.06	15.7100	15.6800	15.7100	15.7000	0.0173	87.20%
	9.08	16.7900	16.8500	16.8800	16.8400	0.0458	93.60%
	10.08	ND	ND	ND	18.0000	N/A	100.00%

	pH	Ions adsorbed in mg/L	Ions adsorbed in mg/L	Ions adsorbed in mg/L	Ions adsorbed in mg/L	Std. Deviation	% adsorption
Lead Initial (Conc. Of 18mg/L)		1st reading	2nd reading	3rd reading	Mean		
	3.02	0.1100	0.1100	0.1000	0.1100	0.0071	0.60%
	4.00	9.8400	9.8900	9.8200	9.8500	0.0361	57.72%
	6.06	ND	ND	ND	18.0000	N/A	100.00%
	9.08	ND	ND	ND	18.0000	N/A	100.00%
	10.08	15.8100	15.8500	15.8300	15.8300	0.0200	87.94%

Anova: Two-Factor Without Replication

SUMMARY	*Count*	*Sum*	*Average*	*Variance*
Row 1	2	1.27	0.635	0.55125
Row 2	2	11.62	5.81	32.6432
Row 3	2	33.7	16.85	2.645
Row 4	2	34.84	17.42	0.6728
Row 5	2	33.83	16.915	2.35445
Column 1	5	53.47	10.694	71.68648
Column 2	5	61.79	12.358	58.00567

ANOVA

Source of Variation	*SS*	*df*	*MS*	*F*	*P-value*	*F crit*
Rows	486.82414	4	121.706	15.2397	0.010908	6.388233
Columns	6.92224	1	6.92224	0.866784	0.404549	7.708647
Error	31.94446	4	7.986115			
Total	525.69084	9				

Appendix 7: Effect of temperature on metal ion adsorption

Initial Pb Conc of 15mg/l	Temp (K)	Ions adsorbed in mg/L 1st	Ions adsorbed in mg/L 2nd	Ions adsorbed in mg/L 3rd	Ions adsorbed in mg/L mean	Std. Deviation	%Adsorption
	298K	13.3200	13.4000	13.3000	13.3700	0.0608	89.10%
	323K	14.8000	14.7200	14.8200	14.7800	0.0529	98.50%
	343K	14.7900	14.8900	14.7500	14.8100	0.0721	98.70%

Initial Cd Conc of 15mg/l	Temp (K)	Ions adsorbed in mg/L 1st	Ions adsorbed in mg/L 2nd	Ions adsorbed in mg/L 3rd	Ions adsorbed in mg/L mean	Std. Deviation	%Adsorption
	298K	7.7100	7.7800	7.8200	7.7700	0.0557	51.80%
	323K	13.2400	13.1000	13.2000	13.1800	0.0721	87.87%
	343K	13.2700	13.3200	13.2800	13.2900	0.0264	88.60%

Van't Hoff temperature plots for lead and cadmium

Lead ions	Temp (K)	C_e (Ratio of ions in Soln. at eq.)	q_e (Ratio of ions adsorbed at eq.)	k_d (q_e/ C_e)	1/T	In k_d
	298	0.1090	0.8910	8.1743	0.0034	2.1010
	323	0.0150	0.9850	65.6667	0.0031	4.1846
	343	0.0130	0.9870	75.9230	0.0029	4.3297

	Temp (K)	C_e (Ratio of ions in Soln. at eq.)	q_e (Ratio of ions adsorbed at eq.)	k_d (q_e/ C_e)	1/T	In k_d
Cadmium ions.	298	0.4820	0.5180	1.0750	0.0034	0.0723
	323	0.1213	0.8787	7.2420	0.0031	1.9798
	343	0.1140	0.8860	7.7720	0.0029	2.0505

Anova: Two-Factor Without Replication

SUMMARY	*Count*	*Sum*	*Average*	*Variance*
Row 1	2	21.14	10.57	15.68
Row 2	2	27.96	13.98	1.28
Row 3	2	28.1	14.05	1.1552
Column 1	3	34.24	11.41333	9.958433
Column 2	3	42.96	14.32	0.6771

ANOVA

Source of Variation	*SS*	*df*	*MS*	*F*	*P-value*	*F crit*
Rows	15.82893333	2	7.914467	2.90859	0.255847	19
Columns	12.67306667	1	12.67307	4.657389	0.16359	18.51282
Error	5.442133333	2	2.721067			
Total	33.94413333	5				

Appendix 8: Effect of Acid conditioning in regeneration of nanocomposites for reuse

Lead (Initial Conc. of 30 mg/l)	Ions adsorbed in mg/L	Ions adsorbed in mg/L	Ions adsorbed in mg/L	Ions adsorbed in mg/L	Std. Deviation	% adsorption
	1st reading	2nd reading	3rd reading	mean		
1st Cycle	27.40	27.46	27.47	27.44	0.0309	91.47%
2nd Cycle	14.01	13.97	14.04	14.01	0.0287	46.67%
3rd Cycle	7.56	8.01	7.83	7.80	0.1850	25.98%

Cadmium (Initial Conc. of 30mg/l)	Ions adsorbed in mg/L	Ions adsorbed in mg/L	Ions adsorbed in mg/L	Ions adsorbed in mg/L	Std. Deviation	% adsorption
	1st reading	2nd reading	3rd reading	mean		
1st Cycle	20.27	20.34	20.32	20.31	0.0294	67.70%
2nd Cycle	10.67	10.66	10.62	10.65	0.0216	35.50%
3rd Cycle	5.89	6.88	6.52	6.43	0.4091	21.43%

Anova: Two-Factor Without Replication

SUMMARY	*Count*	*Sum*	*Average*	*Variance*
Row 1	2	47.75	23.875	25.41845
Row 2	2	24.66	12.33	5.6448
Row 3	2	14.23	7.115	0.93845
Column 1	3	37.39	12.46333	50.62973
Column 2	3	49.25	16.41667	100.7764

ANOVA

Source of Variation	*SS*	*df*	*MS*	*F*	*P-value*	*F crit*
Rows	294.2539	2	147.127	34.38175	0.028263	19
Columns	23.44326667	1	23.44327	5.478401	0.144101	18.51282
Error	8.558433333	2	4.279217			
Total	326.2556	5				